FORCE SHARING IN HIGH-POWER PARALLEL SERVO-ACTUATORS

MR - E - 1905

JUNE 1, 1974

FINAL REPORT PREPARED FOR:

National Aeronautics and Space Administration
George C. Marshall Space Flight Center
Huntsville, Alabama
Contract Number NAS 8-27803

MOOG INC., CONTROLS DIVISION, PRONER AIRPORT, EAST YORK 14052 716/652-2000 TWX-710 264 1442
Cheltenham, England — Böblingen, West Germany — Hiratsuka, Japan — Rungis, France

FORCE SHARING IN HIGH-POWER PARALLEL SERVO-ACTUATORS

MR - E - 1905

JUNE 1, 1974

FINAL REPORT PREPARED FOR :

National Aeronautics and Space Administration
George C. Marshall Space Flight Center
Huntsville, Alabama
Contract Number NAS 8-27803

Prepared By:

T. Peter Neal
Manager, Control Systems
Engineering Department

MOOG INC.
Controls Division
East Aurora, New York

TABLE OF CONTENTS

LIST OF FIGURES

LIST OF FIGURES (CONT'D)

LIST OF FIGURES (CONT'D)

1.0 INTRODUCTION

The advent of the Space Shuttle program has resulted in a considerable amount of new thinking on the subject of redundant electro-hydraulic servo-actuators. Probably the most critical applications on the Space Shuttle, from a reliability standpoint, are the primary aerodynamic control surfaces. Because of the massive structural loads involved, it is imperative that a high degree of force sharing be maintained between multiple actuators driving a common surface.

Under the sponsor ship of NASA's George C. Marshall Space Flight Center, Moog has conducted a sudy of the force-sharing problem in high-power parallel actuators. The cognizant technical group at Marshall was the Control Mechanisms Branch of the Guidance and Control Division of the Astrionics Laboratory. Paul Golley was the NASA Progect Engineer. Although the program was necessarily slanted toward the Space Shuttle, it was desired that the study be conducted in such a manner that the results would be as generally applicable as possible.

The first step in the study was to examine the various existing force-sharing schemes by conducting a literature survey (Section 3.0). A list of potentially applicable concepts was compiled from this survey, and schemes previously developed at Moog were added to it. A brief analysis was then made of each concept, which resulted in two competing schemes being selected for in-depth evaluation. Next, a functional design of the equalization logic for the two schemes was undertaken (Section 4.0). Then a specific Space Shuttle application was chosen for experimental evaluation (Section 5.0). This application was scaled down so that existing hardware could be utilized. Next, an analog computer study was conducted to evaluate the more important characteristics of the two competing force-sharing schemes (Section 6.0). On the basis of the computer study, a final configuration was selected. A load simulator was then designed to evaluate this configuration on actual hardware (Section 7.0).

Following the body of the report are two appendices, which contain detailed information not essential to understanding the basic force-sharing study. Appendix A discusses the problems of closing high-gain pressure-feedback loops. Appendix B contains operating instructions for the simulator. The simulator itself will be shipped to NASA for further evaluations.

One parting remark is in order. This report represents a reasonably thorough documentation of the entire force-sharing program. For the reader who is not interested in all the gory details of how the final force-sharing configuration evolved, it is probably sufficient to first read through Section 4. Then, recognizing that the final configuration employs the mid-value equalization (MVE) concept, proceed directly to Section 7 and 8 for the final results. Refer to Subsection 5.1 for symbols and definitions, as needed, and to 5.3 for the scaled system parameters used on the simulator.

2.0 DEFINITION OF THE PROBLEM

The ultimate in redundant electrohydraulic servo-actuators is to have multiple channels which are completely separate from each other, electrically, hydraulically, and mechanically. However, to ensure good positioning accuracy under load, it is necessary to maintain high static stiffness within each channel. This creates the kind of problem illustrated in Figure 2.1.

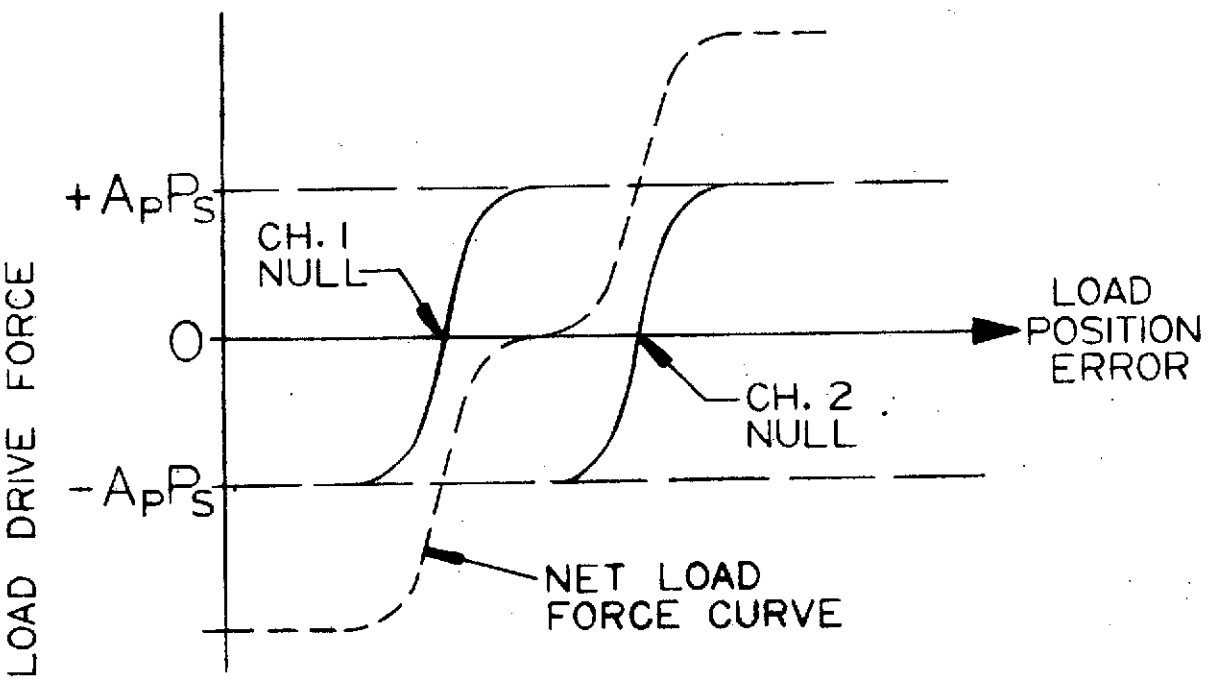

FIGURE 2.1 LOAD DRIVE FORCE vs POSITION ERROR -PARALLEL POSITION SERVOS

This figure shows the actuator force output of two parallel position servos as functions of load position error. The load position error is the difference between the average position command signal and the actual load position. When a position error exists, each servovalve develops a differential pressure across the piston to move the load and zero the error. But in general, some mismatch will exist in the null between the channels. This could be due to such things as mismatched electrical command signals, mismatched feedback signals, or null shifts in the servovalves themselves. Figure 2.1 shows that any significant null difference causes the servos to be hard over

MOOG
MOOG INC., EAST AURORA, NEW YORK

Another disadvantage of self-equalization is that the actuator pistons must be oversized so that the equalization threshold can be set substantially above the load pressures required to handle the maximum anticipated load forces. The major problems of self-equalization can be overcome by employing a multi- channel secondary actuator package, whose output drives a shaft which is then used to position the power spools on the main rams. (Of course, this could be considered to be a form of cross equalization.) The power spools can then be mechanically adjusted to achieve synchronization of the multiple rams. The self-equalization provides good positioning accuracy at the secondary actuator output, and the force fight which occurs at this point involves relatively small forces. A recent application of this principal is on the ill-fated Boeing SST. (Section 6.8 of Reference 1, References 2 and 3, and Section 4.4.2.1 of Reference 4). Some of the more obvious advantages and disadvantages of this scheme are:

Advantages:

- Reliability should be excellent because the channels can be completely independent, except for the synchronizer shaft connecting the power spools.
- Since all the rams remain active as channels are shut down, full force output capability is maintained (assuming that a failure has not occurred in the power stage itself).

Disadvantages:

- The apparent reliability of the scheme is realized only if it can be assumed that the probability of a mechanical failure in the synchronizer shaft or power spools is negligible. For example, all redundancy is lost if the shaft jams.
- There is little flexibility in the physical placement of the channels; they must be close together.
- The scheme is complex, both hydraulically and mechanically.
- Substantial reduction of force-fight by mechanical adjustment of the power spools is difficult. On the SST, it was also necessary to reduce the overall output stiffness of the actuators; and even then, the degree of force sharing actually achieved was apparently only about 70%.

For the Space Shuttle, it would be desirable to achieve a higher degree of force sharing than seems practical with the secondary actuator scheme. It would also be useful to retain more flexibility in the physical placement of the channels and to reduce complexity. In addition, there is no need to mix in mechanical inputs on the Space Shuttle, because it is completely fly-by-wire. With these considerations in mind, it was decided that the basic groundrules for the subject program would be as follows:

- The main rams would be directly controlled by electrohydraulic servovalves - no secondary actuators.
- Active cross equalization would be used to achieve a high degree of force sharing (95%), without degrading output stiffness.
- The equalization would be mechanized electronically - no interchannel mechanical or hydraulic connections.
- An additional requirement for dual-fail-operate (DFO) capability led to the decision to use four channels in the study.
- Because of the large size of the actuators, the system must be all active; active/standby schemes would not be considered.

The primary disadvantage of this approach, compared to the secondary actuator scheme, is that the main pistons must be oversized unless reduced force output capability is acceptable when channels are shut down. However, the potential advantages of the scheme make it worthy of further investigation. In spite of the fact that interchannel electrical connections are required, proper design should be able to make these connections almost as reliable as the synchronization shaft required by the secondary actuator approach. Also, if a failure in the interchannel connections does occur, the results are less likely to be catastrophic with the proposed approach.

One last groundrule which is needed for the program is a precise definition of the desired force sharing performance. First, the maximum likely interchannel mismatch was defined. Considering all the possible sources of interchannel mismatch, it was felt the mismatch between the nulls of any two channels would not likely exceed 10% of total actuator stroke. Therefore, the nominal offset condition was established with the nulls of two channels offset 10% (of total stroke) from the other two. Under these circumstances, the desired degree of force sharing is 95%, meaning that the load pressure of each channel can differ from the average load pressure by no more than 5% of supply pressure. For a supply pressure of 3000 psi, this would represent a 150 psi deviation from the average.

3.0 SELECTION OF PROMISING FORCE-SHARING CONCEPTS

Having set the basic groundrules for the force-sharing program, the study was begun by conducting a search of the available literature on redundant electrohydraulic servo-actuators. The reports studied are References 1 through 15. The majority of the redundant schemes reported employ flow summing or secondary force summing to position the main power spools, which are mechanically linked together. Force sharing at the main pistons is then achieved by mechanical synchronization of the power spools. Other schemes employ the active/standby concept. While all of these approaches are valid in certain applications, they do not satisfy the groundrules established for this program in Section 2.0. Although the schemes using secondary actuators are not directly applicable, some of the secondary actuators themselves do employ cross equalization techniques which are of interest.

All of the concepts from References 1 through 15 which satisfy the groundrules of Section 2.0 were analyzed in enough detail to determine their major advantages and disadvantages. Also analyzed were some new ideas generated within Moog. The following subsections summarize the evaluations of the most applicable concepts.

3.1 Average - Value Equalization

One fairly straightforward idea for cross-channel equalization was presented in the Moog proposal for the subject program. The concept was to adjust the null of each channel so as to drive its load pressure toward the average load pressure of all the channels. This is accomplished by comparing a channel's load pressure with the computed average pressure and feeding back the difference with high gain, as shown in Figure 3.1. If necessary, various operations can be performed on the equalization signal before feeding back. For example, the feedback can be integrated or lagged to make it a slow-acting correction.

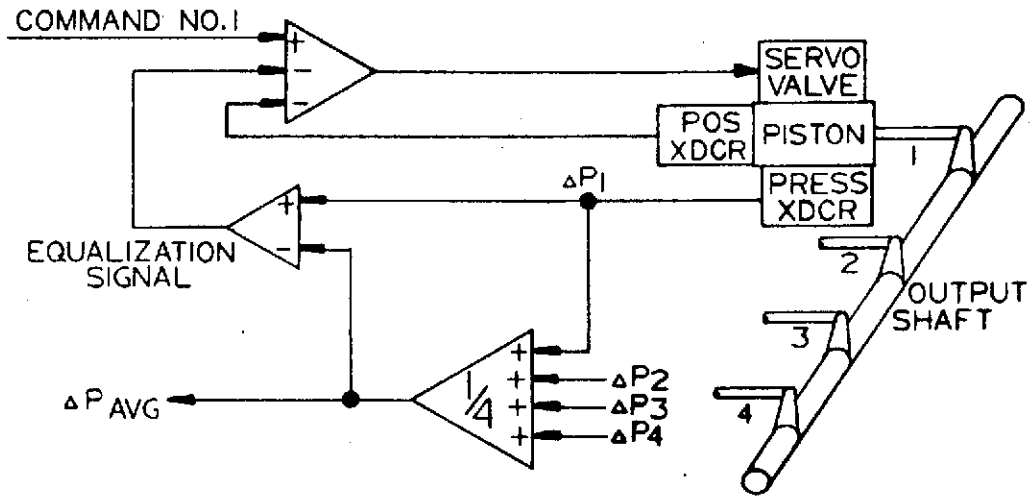

FIGURE 3.1 AVERAGE-VALUE EQUALIZATION

If a channel should become significantly out of synchronization with the others (e. g. due to mismatched position feedback or command signals or due to servovalve null shift), the channel's load pressure will tend to go hard over. As the load pressure begins to change, the equalization will generate a bias signal to the position loop, which will tend to cancel the original mismatch in the loop. If the equalization loop gain is high enough, only a small difference between a channel's load pressure and the average pressure will be needed to offset gross mismatch between channels. This scheme has two major advantages. First, the equalization logic is fairly simple. Secondly, whenever the channels are perfectly synchronized, the load pressure signal within each channel is cancelled by the average signal, so that no equalization signal is generated. Thus, it would appear that this approach can provide force sharing without reducing output stiffness or affecting overall system performance. In addition, the equalization signal itself can be monitored to detect failures.

3.2 Mid-Value Equalization

A prototype fly-by-wire control system was designed by Sperry under an Air Force contract, and was tested on a B-47 airplane (References 7 and 8). The system employs secondary actuators; and therefore, is not directly applicable. However, cross equalization is employed in the secondary actuator package, and the technique used is very interesting. As applied to the subject program, this scheme would look functionally identical to the average value scheme depicted in Figure 3.1, except that the reference pressure used in the equalization is the mid value rather than the average value. The B-47 system had three channels. For four channels, a separate fixed signal must be added to the mid-value logic, so that the logic selects the mid value of five load pressures.

The brief initial study did not indicate whether the mid-value or average-value scheme was superior. It appeared that the most significant differences would occur in the failure logic and in switching transients.

3.3 F-111 Yaw Damper Equalization

The yaw-damper servo for the F-111 airplane was designed by Moog, using a free-floating piston concept for equalization (Section 6.4 of Reference 1). Any load-pressure difference between the two channels causes a free-floating piston between the channels to move at a proportional rate. The movement of this piston is fed back mechanically to both servovalves, thereby driving the load pressures toward each other. Although the scheme is clearly not directly applicable because of the hydromechanical mechanization, the technique was functionally examined for possible new ideas.

Analysis showed that the F-111 technique is functionally very similar to the average value concept discussed in Section 3.1, with the equalization signal being operated upon by combined integral and proportional functions. Because the technique is of no interest to the subject study from a mechanization standpoint and because it is functionally similar to the average value concept, it was not pursued further.

3.4 Bendix Synchronization Concept

Bendix performed a study of synchronization techniques for a 3-channel redundant actuator (Reference 10). Three variations of the same basic technique were evaluated in the study. In the most promising version

("configuration A"), the equalization signal was generated by comparing the channel's own load pressure with that of the adjacent channel, as shown in Figure 3.2.

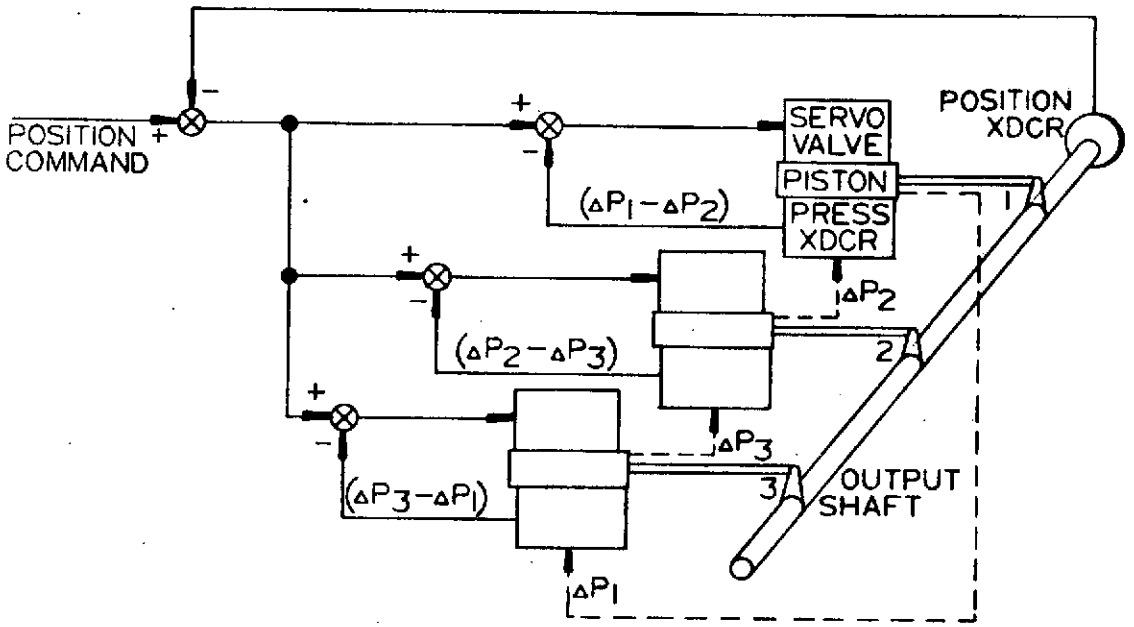

FIGURE 3.2 BENDIX SYNCHRONIZATION CONCEPT

As far as normal operation is concerned, the equalization is functionally very similar to the average value equalization of Section 3.1. In fact, for a 2 channel system, the two schemes are functionally identical. As more channels are added, however, the Bendix approach appears to be inferior to the average value concept, with regard to failures. For example, in a hardover failure, the Bendix equalization will cause the operating channels to follow the hardover channel with considerable gusto. This tendency will also be present with the average value system, but the magnitude of the failure transient should be considerably smaller. The reason for this is that the operating channels equalize toward the average value, which is more heavily weighted by the operating channels than the failed one.

In spite of the fact that the equalization concept of Reference 10 appears inferior to a similar approach already under consideration, Appendix A of the referenced report presents an interesting analysis of the equalization loops. This analysis shows that positive feedback was present in some cases, which could lead to instabilities. Basically, the analysis involved juggling the system block diagram with blocked load (i. e. load position held fixed at zero). This technique was applied to both the average-value and mid-value concepts previously discussed, to check for positive feedback loops and their possible consequences. The analysis showed that the mid-value system has no positive feedback loops. The average-value system does have positive feedback loops present, but they are cancelled by corresponding negative ones.

3. 5 Master /Slave Concept

During the initial study of the various available force-sharing concepts, it was suggested that a load sharing technique be investigated that is used when regulated electrical power supplies are placed in parallel. The hydraulic analogy would be to designate one channel as the master, giving it high position stiffness. The other channels would then be made pressure-control servos by using high-gain pressure feedback and opening their position feedback loops. These servos would then be slaved to a load pressure signal from the master channel, as illustrated in Figure 3. 3.

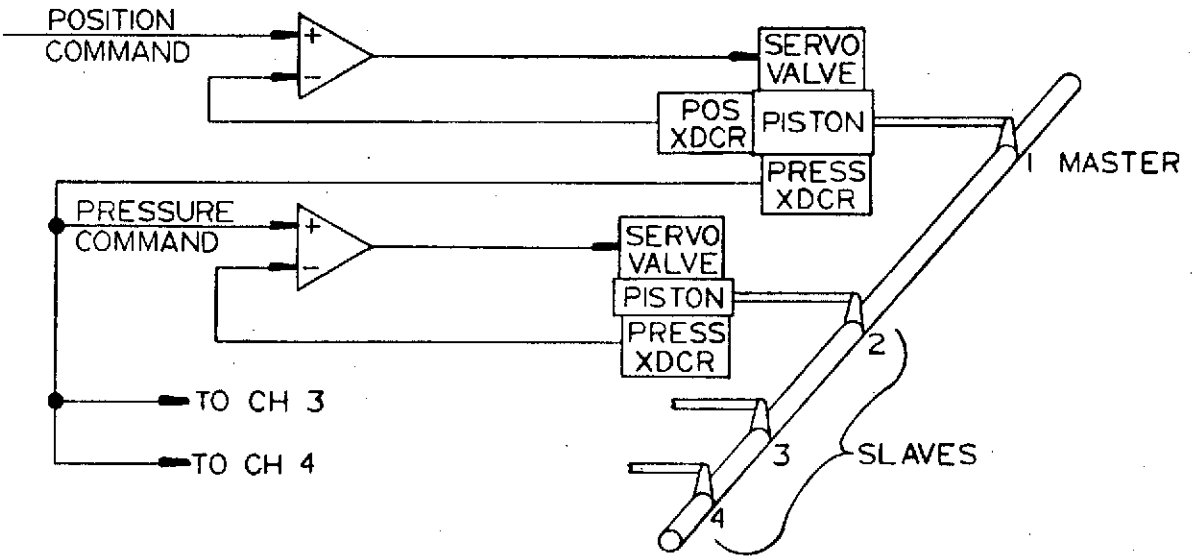

FIGURE 3. 3 MASTER /SLAVE CONCEPT

For normal operation, the master/slave system should provide very good force-sharing at pressure loop gains far below those needed in any of the systems previously studied. The reason for this is that no position loops are present in the slave channels. However, this advantage for normal operation quickly becomes a disadvantage when failures are considered. For example, a hardover failure in the master channel would cause the operating slave channels to happily follow the master; there are no operating position loops to fight this tendency. Therefore, the master/slave system would be required to have very fast and foolproof failure detection/correction logic to select a new master and perform the rather complicated switching. Even then, the transient caused by a hardover failure would probably be quite large. Thus, with regard to failures, the master/slave concept is grossly inferior to the other concepts under consideration, and will not be considered further.

3.6 Concepts Selected for Further Study

On the basis of the study described in the foregoing subsections, the mid-value and average-value equalization schemes appeared to be the most promising for the subject program. It is not so obvious which of these two schemes is superior overall. For this reason, it was decided to investigate both concepts in more detail.

4.0 MECHANIZATION OF SELECTED CONCEPTS

With regard to mechanization of the average-value and mid-value concepts, an overriding consideration is to avoid compromising the fail-safe features inherent in all-active force-summed servo-actuators. With no equalization or failure detection/correction logic, a hard-over in one channel will be automatically offset by the remaining channels. The effects of the failure are limited to a small load position transient. To preserve this desirable feature, the following ground rules should be observed.

- The equalization will probably increase the load position transients caused by hardover failures. Steps should be taken to minimize this degradation.
- To achieve dual-fail-operate (DFO) capability, the offending channel must be shut off after each failure. If the equalization logic is to continue operating after two failures, it must be appropriately modified as channels are shut off.
- Since both the equalization and failure detection/correction logic make use of cross-channel comparisons, the mechanization should minimize the chances of a single logic failure fouling up the operation of all the channels. For example, it must not be possible for a single failure to cause all four channels to be shut off.

With these considerations in mind, it was decided to compute the equalization reference signals (average-value or mid-value pressure) separately within each channel. The most straightforward way to detect a failure is to monitor the equalization signal within each channel. When this signal exceeds a preset threshold, a failure is indicated. Mechanization details for each of the two equalization concepts are discussed in the following subsections.

4.1 Average-Value Logic

Considering first the effects of hardover failures, it can be seen that the average-value equalization will cause the good channels to follow the hardover channel. To visualize this problem, consider first what would happen with the position loops open. A hardover in one channel will cause the computed average pressure to change one quarter of the way toward the hardover pressure. As this happens, the equalization in the operating channels will cause the nulls of these channels to move toward the hardover

channel, which causes the average pressure to change even more. The equalization will not be satisfied until the pressures of the operating channels are equal to the average. This can only occur when all the channels are hardover. However, the position loops of the operating channels will fight this tendency, with the magnitude of the failure transient being determined by the relative magnitudes of the equalization loop and position loop gains.

From the above arguments, it can be seen that the equalization loop gain should be no higher than is needed to achieve the desired degree of force sharing. This rules out the use of integral compensation, which gives essentially infinite static gain. To further limit the magnitude of failure transients, it was decided to electrically limit the equalization output signal to a value which is just large enough to equalize the largest expected null offsets.

The biggest problem is how to modify the logic when failures occur. For the average-value, we must add the load pressure signals from each channel and multiply by $\frac{1}{n}$, where n is the number of channels. The most obvious way to account for shutoffs is to change the gain $\frac{1}{n}$ with each shutoff. However, since we are planning to perform the average-value computation separately within each channel, changing $\frac{1}{n}$ would require additional cross-channel signals. To eliminate this hazard, the scheme of Figure 4.1 was devised. When a channel is shut down, a relay would be de-energized within the failed channel, which would connect the pressure output signal from the failed channel to one of the inputs. This will result in a lopsided average being computed after failures have occurred. For example:

$$\Delta P_{av} = \frac{\Delta P_1 + \Delta P_2 + \Delta P_3 + \Delta P_4}{4} \qquad \text{(All Working)}$$

$$\Delta P_{av} = \frac{2\Delta P_2 + \Delta P_3 + \Delta P_4}{4} \qquad \text{(\# 1 Shut Off)}$$

$$\Delta P_{av} = \frac{3\Delta P_3 + \Delta P_4}{4} \qquad \text{(\# 1 and \# 2 Shut Off)}$$

$$\Delta P_{av} = \frac{2\Delta P_2 + 2\Delta P_4}{4} \qquad \text{(\# 1 and \# 3 Shut Off)}$$

However, this appears to be a small penalty to pay for the inherent reliability of performing a simple switching operation entirely within the failed channel.

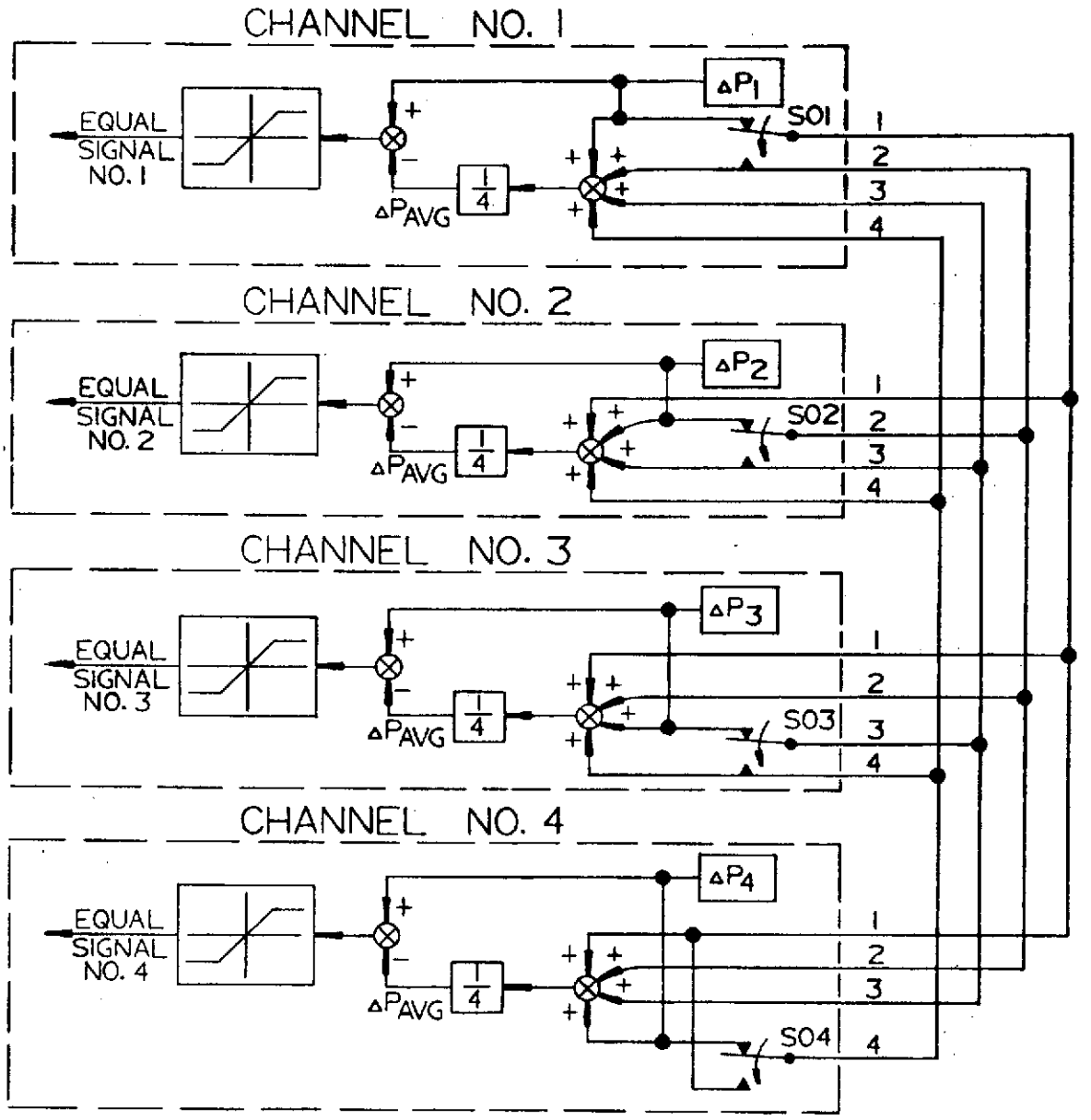

FIGURE 4.1 AVERAGE-VALUE LOGIC

MOOG
MOOG INC., EAST AURORA, NEW YORK

4.2 Mid-Value Logic

A mid-value logic for a four-channel system must use an additional fixed signal so that the logic will select the mid-value of five signals. If the first failure is a hardover, the logic will continue to select one of the good channels, even if the hardover is in the direction of the fixed signal. If the second failure is also hardover in the direction of the fixed signal, however, the logic will pick one of the hardover channels. Thus, we must again change the logic as failures occur. One way to approach the problem is to use the shutoff command to send the failed channel's output signal hardover in the direction opposite to the fixed signal. The mechanization devised to accomplish this is shown in Figure 4.2. A second fixed signal approximately equivalent to system pressure is added to the ΔP_n signal generated by the pressure transducer. Each mid-value computation (MVC) then selects the mid-value of $(\Delta P_1 + P_s)$, $(\Delta P_2 + P_s)$, $(\Delta P_3 + P_s)$, $(\Delta P_4 + P_s)$, and the fixed signal $(2P_s)$. The shutoff signal to a failed channel de-energizes a relay within that channel which grounds its pressure output signal to the other channels. The resulting operation of the logic as failures occur is shown in Figure 4.3. Thus, a fairly simple logic-changing system will ensure that the MVC selects a good channel even after two channels have failed.

Because the equalization logic always selects the load pressure of an operating channel as the mid-value, the operating channels will never equalize toward the hardover channel. Of course, there will still be a failure transient, but the transient will not be aggravated by the equalization. This means that electrical limiting of the equalization output signal is not necessary.

With regard to the mid-value computation itself, there are several mechanization schemes which could be used. One of the simpler ones is shown in Figure 4.4. To understand how this scheme works consider the following example. Suppose that at a given instant, the input signals are ranked in order of decreasing magnitude (channel 1 closest to $2P_s$ and channel 4 closest to zero), and the feedback loop is open. Each forward loop output will then be driven into the $+ 2P_s$ saturation region and the summer output will be $(+ 10P_s)$. Now let's close the feedback loop. Assuming there is some lag in the feedback loop, it will take some finite period of time for the feedback signal to change from zero to $(+10P_s)$.

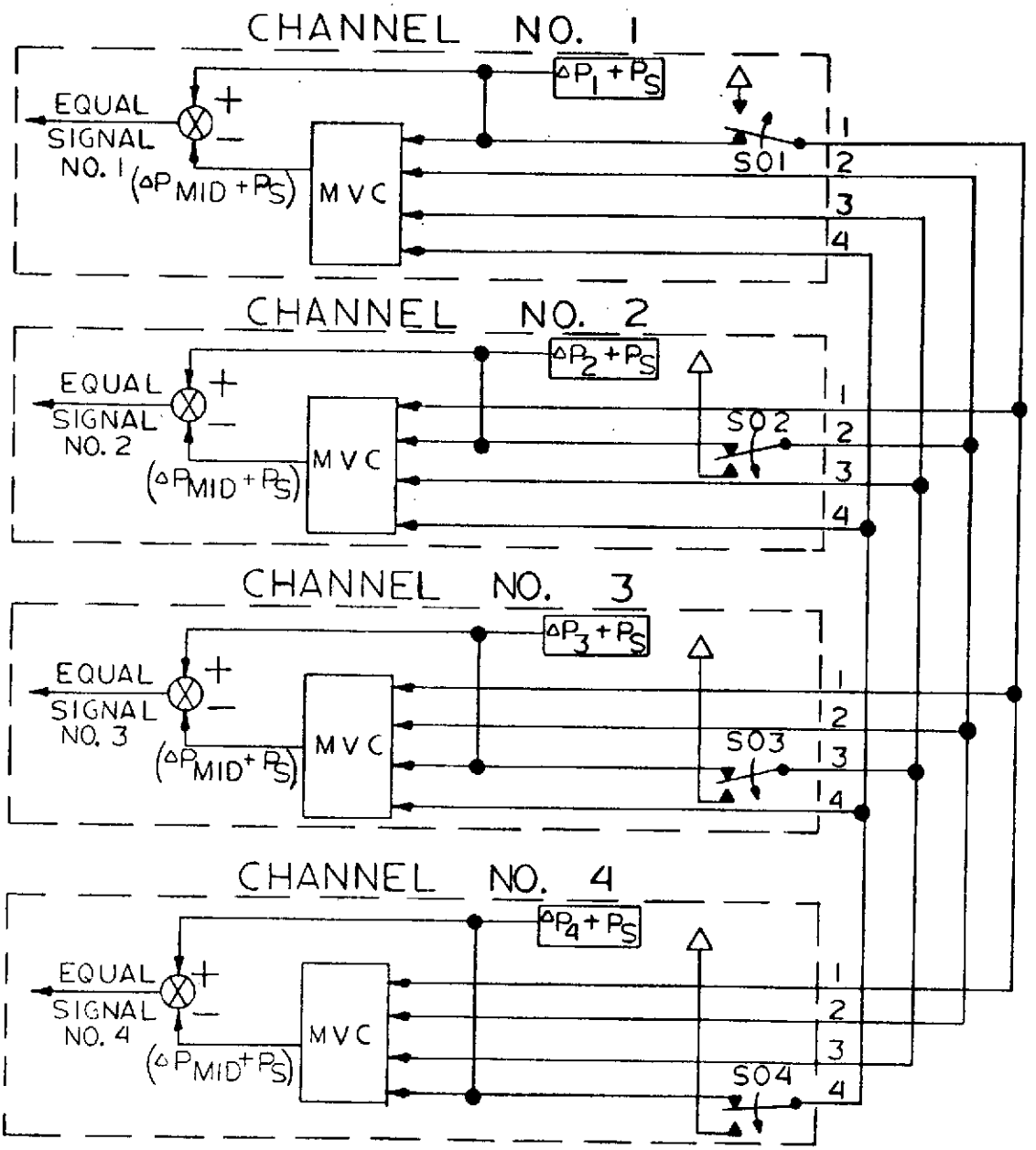

FIGURE 4.2 MID-VALUE LOGIC

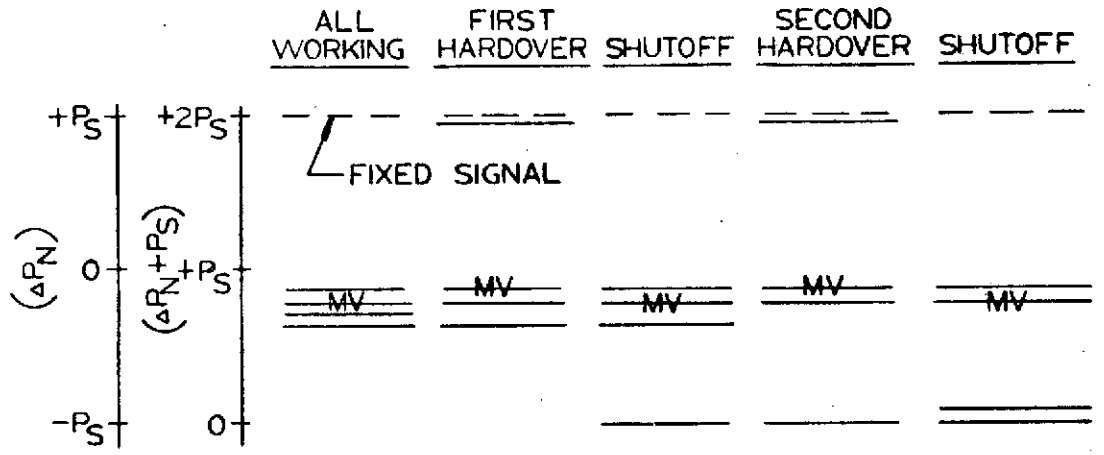

FIGURE 4. 3 FAILURE-UPDATE SEQUENCE OF MID-VALUE LOGIC

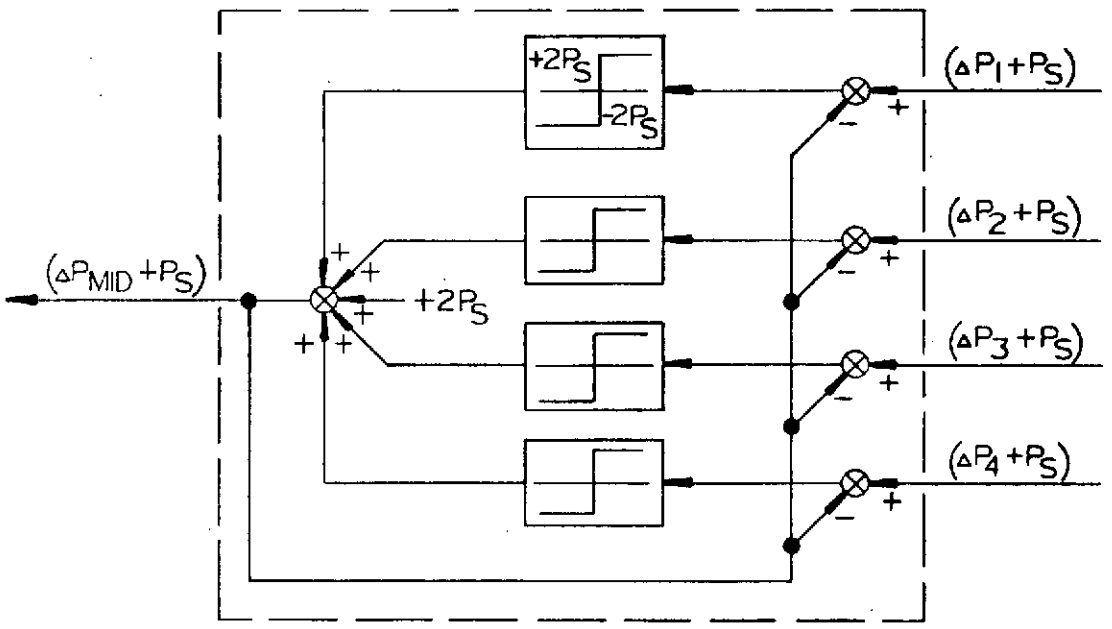

FIGURE 4. 4 MID-VALUE COMPUTATION (MVC)

As the feedback signal passes ($\Delta P_4 + P_s$), channel 4 will receive a negative error signal first, switching its forward loop signal to ($-2P_s$) and reducing the summer output to ($+6P_s$). When the feedback passes ($\Delta P_3 + P_s$), the summer output will be reduced to ($+2P_s$). When the feedback has nearly reached ($\Delta P_2 + P_s$), the channel 2 error signal will become very small and channel 2 will be operating on the near-inifnite gain part of the non-linear gain curve. The system will reach equilibrium when the summer output is just enough below ($\Delta P_2 + P_s$) to generate an error signal in channel 2 which is just large enough that the channel 2 output remains just below ($\Delta P_2 + P_s$). Thus, the summer output follows the mid-value input signal closely (channel 2, in this case), with the outputs of channel 3 and 4 cancelled by channel 1 and the ($+2P_s$) signal.

5.0 DYNAMIC MODEL

To perform a detailed evaluation of the force-sharing concepts, it was necessary to select a specific application. At the beginning of the program, NASA felt that the elevon control surfaces of the Space Shuttle Fly-Back Booster were a good example of the need for force-sharing. Because of the colossal size of the actuators envisioned for the elevons, it was necessary to dynamically scale the problem, so that smaller actuators could be used in the simulator hardware. Both the analog computer study and the simulator then used the scaled down parameters. The remainder of this section derives the dynamic equations used to describe the servo-actuator and shows how the problem was scaled down.

While it is fully realized that the original Fly-Back Booster concept has gone the way of the dinosaur, the subject program was well underway before the Booster's untimely demise. Because the primary purpose of the program was a general study of the force-sharing problem, rather than a detailed design effort for a specific application, it was decided to stick with the original application. This seemed to be a more efficient use of the available time and money than trying to keep up with the latest parameter changes in the Space Shuttle program.

5.1 List Of Symbols

A Piston working area ~ in^2

B_L Equivalent linear damping of load, as seen by actuators, $B_L = H_\delta^* / R^2$ ~ lb-sec/in

e Voltage input to servovalve drive amplifier ~ volts

e_C Position command voltage ~ volts

e_E Equalization feedback voltage ~ volts

F Force output of piston (positive for a push) ~ lb.

F_D Force disturbance applied to load (positive when aiding F) ~ lb.

H Aerodynamic hinge moment of elevon (positive when opposing F) ~ in - lb.

H_δ Aerodynamic spring rate of elevon $(\partial H/\partial \delta) \sim$ in-lb/rad

$H_\delta^\bullet$ Aerodynamic damping of elevon $(\partial H/\partial \dot{\delta}) \sim$ in-lb-sec/rad

I Elevon moment of inertia about hingeline $\sim$ in-lb-sec^2/rad.

i Servovalve current $\sim$ ma

i_R Rated current, i to obtain Q_R $\sim$ ma

K_A Net stiffness of each actuator; includes oil spring $\left(\frac{4\beta A^2}{V} \sim \text{lb/in}\right)$ and mechanical compliance $\sim$ lb/in

K_D Feedback gain of dynamic pressure feedback (DPF) $\sim$ v/psi

K_{DA} Drive amplifier gain $\sim$ ma/v

K_E Equalization feedback gain $\sim$ v/psi

K_L Equivalent linear spring rate of load, as seen by actuator, $K_L = H_\delta / R^2 \sim$ lb/in

K_P Servovalve pressure gain (blocked load) $\sim$ psi/ma

K_{PQ} Servovalve droop, $K_{PQ} = K_Q/K_P \sim$ cis/psi

K_Q Servovalve flow gain (no load) $\sim$ cis/ma

K_S Stiffness of actuator attach structure (per actuator) $\sim$ lb/in

K_T Net drive stiffness of each actuator (includes K_A and K_S) $\sim$ lb/in

K_{VD} Velocity gain of DPF loop $\sim$ sec^{-1}

K_{VE} Velocity gain of equalization loop $\sim$ sec^{-1}

K_{VX} Velocity gain of position loop $\sim$ sec^{-1}

K_X Position feedback gain $\sim$ v/in

M_L Equivalent linear mass of load, as seen by actuators, $M_L = I/R^2 \sim$ lb-sec^2/in

ΔP Differential load pressure across piston, $\Delta P = F/A$ ~psi

ΔP_{av} Average ΔP of the four actuators ~psi

ΔP_{mid} Mid ΔP of the four actuators and an arbitrary fixed ΔP of $+ P_S$ (in effect, ΔP_{mid} is the more positive of the two mid value ΔP's) ~psi

P_S Net supply pressure (pressure minus return) ~psi

Q Flow output of servovalve ~cis

Q_0 Q under no-load conditions ~cis

Q_R Rated value of Q_0 at P_S ~cis

R Length of crank arm between elevon hingeline and centerline of actuators ~in

S Laplace operator ~sec^{-1}

S_P Total stroke of each actuator ~ in

V Total trapped oil volume in each actuator ~ in^3

X Position output of an actuator (load position relative to actuator body), positive for extend ~ in

X_L Position output of actuators relative to ground, $X_L = \delta R$ ($X_L = X$ when K_S is infinite), positive for actuators extending ~in.

β Effective bulk modulus of oil ~psi

δ Elevon angular position relative to ground, positive when actuators extending ~rad.

ζ_L Load resonant damping ratio

$1/\tau_D$ Low-frequency corner of DPF ~ rad/sec

ω_L Load resonant frequency, $\omega_L = \sqrt{n K_T/M_L}$, where n is the number of operating channels ~rad/sec

MOOG
MOOG INC., EAST AURORA, NEW YORK

5.2 Dynamic Equations

Because the load resonant frequency is relatively low (16 to 22 Hz), it was decided not to match the servovalve dynamics of the simulator actuators to the estimated dynamics of the Booster servovalve. Servovalve dynamics were also neglected in the analog study. The static equation used to describe the servovalve function is as follows.

$$Q = \left(K_Q \sqrt{1 - (\text{sign } i) \left(\frac{\Delta P}{P_S} \right)} \right) i - (K_{PQ}) \Delta P$$

When the servovalve output flow exceeds the flow required to move the piston at the desired velocity, the excess flow winds up the "oil spring" (and mechanical compliance of actuator), resulting in increased differential pressure across the piston. This is shown in the following relationships.

$$F = K_A \int \left(\frac{Q}{A} - \frac{dx}{dt} \right) dt = \left(\frac{K_A}{AS} \right) Q - (K_A) X$$

$$\Delta P = \left(\frac{K_A}{A^2 S} \right) Q - \left(\frac{K_A}{A} \right) X$$

The relationships between piston output force and load motions are shown schematically in Figure 5.1, including the effects of structural compliance.

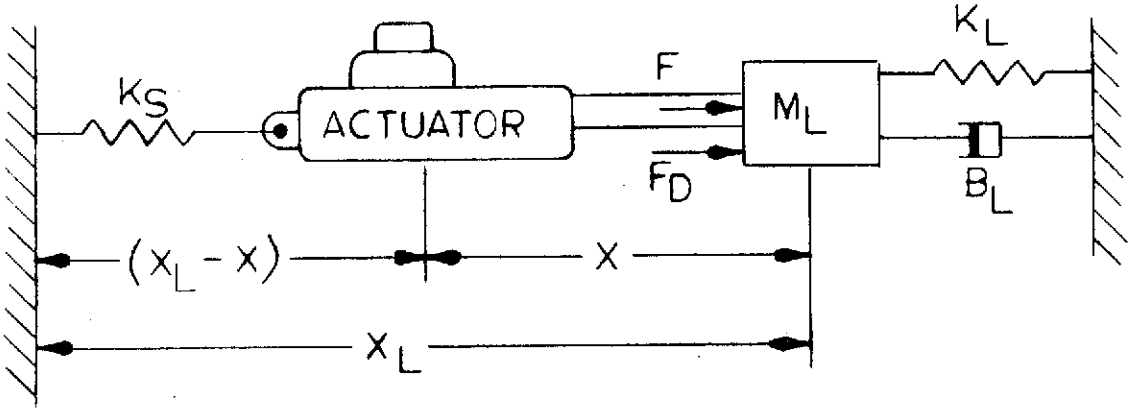

FIGURE 5.1 DYNAMIC MODEL

Note that this figure shows only a single actuator; for multiple actuators, there will be separate actuators and structural springs, all pushing on the same load mass. The piston output force causes the load mass to move relative to ground according to the following equation.

$$(M_L S^2 + B_L S + K_L) X_L = F + F_D$$

While it is recognized that the aerodynamic hinge moments are rather complex functions of elevon deflection, elevon rate, and vehicle angle of attack, it was felt that the important dynamic effects of hinge moment could be adequately approximated by the linear terms H_δ and $H_{\dot{\delta}}$ (K_L and B_L) for a given flight condition. The force F also causes the actuator body to move against the structural spring until force balance is achieved:

$$F = -(X_L - X) K_S$$

$$X = X_L + \left(\frac{A\Delta P}{K_S}\right)$$

As mentioned earlier, the load resonant frequency is relatively low. In addition, the inherent damping contributed by a critical center servovalve and aerodynamic hinge moments are small. Therefore, if any reasonable position loop gains are to be achieved, the load damping must be augmented. Moog often accomplishes damping augmentation by use of Dynamic Pressure Feedback (DPF). The concept uses hydromechanical logic to provide pressure feedback at frequencies near the load resonance, but washes out at low frequencies so that static stiffness is not degraded. The mechanism is basically a high-pass filter. Since a pressure transducer is needed for the equalization logic in the force-sharing system, it is much simpler to mechanize the DPF function electronically in this case. Therefore DPF feedback, consisting of a first-order high-pass filter, was added to the system.

The foregoing relationships were then used to generate a complete functional block diagram of the four-channel force-sharing system. The block diagram for one channel is shown in Figure 5.2. Note that no provisions have been made for torsional deflection of the elevon torque tube between channels. Because a soft torque tube reduces force fight, both the analog study and simulator use rigid torque tubes, as a "worst-case" condition.

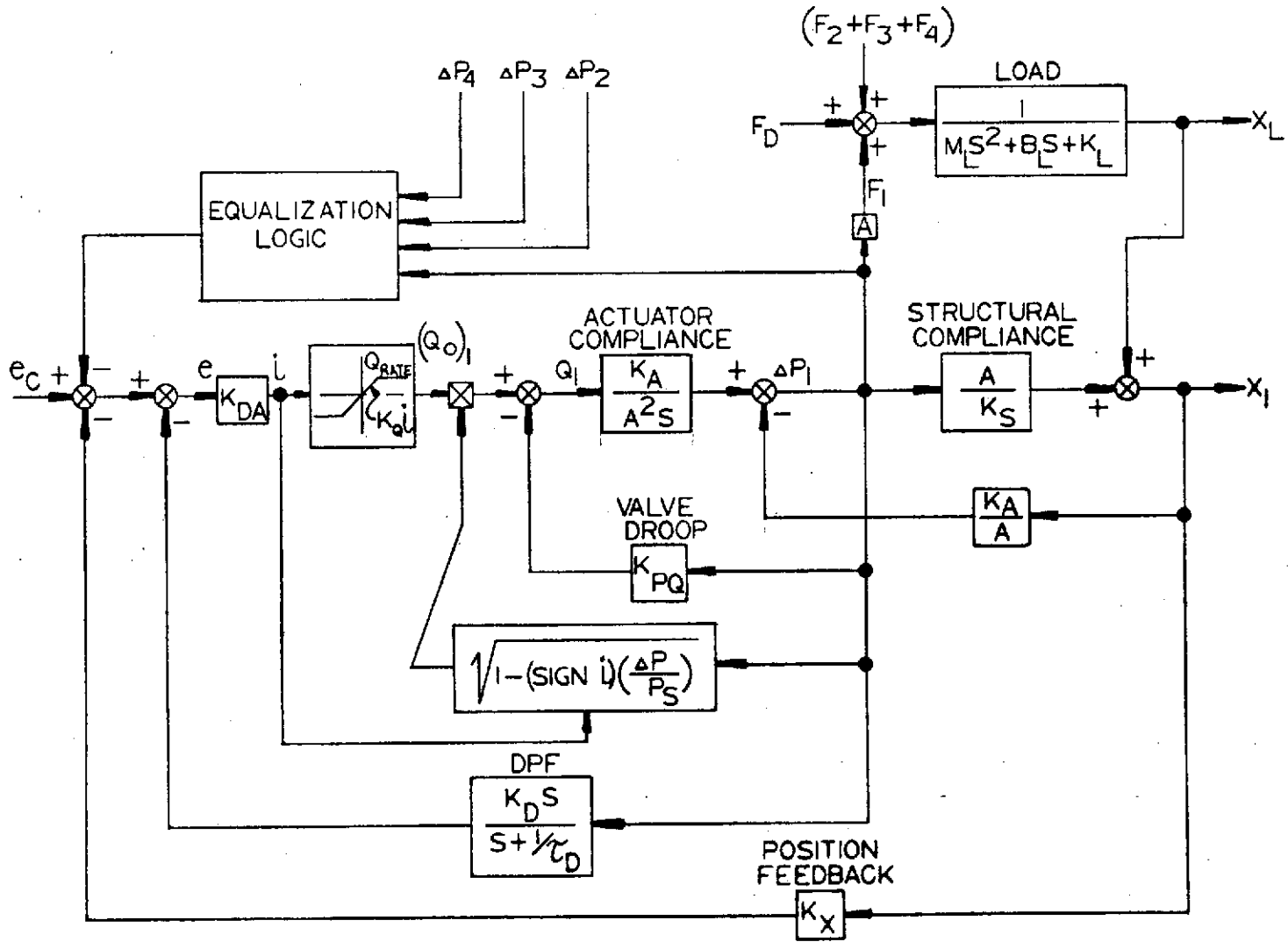

FIGURE 5.2 SYSTEM FUNCTIONAL BLOCK DIAGRAM (ONE CHANNEL SHOWN)

5.3 Scaling Study

The parameter values supplied to Moog by NASA for the Space Shuttle Booster were considered representative of the various competing designs which existed at that time. Some of the parameters were not known, and rough estimates were made. The complete set of parameters used is as follows.

Full-Scale Booster Parameters

$A = 67 \text{ in}^2$

$B_L = 198 \text{ lb-sec/in}$

$H_\delta = 5,730,000 \text{ in-lb/rad.}$

$H_{\dot{\delta}} = 47,500 \text{ in-lb-sec/rad.}$

$I = 9900 \text{ in-lb-sec}^2\text{/rad.}$

$K_A = 1,040,000 \text{ lb/in}$

$K_L = 23,800 \text{ lb/in}$

$K_S = 248,000 \text{ lb/in}$

$K_T = 200,000 \text{ lb/in}$

$M_L = 41.2 \text{ lb-sec}^2\text{/in}$

$P_S = 3000 \text{ psi}$

$R = 15.5 \text{ in}$

$S_P = 18.0 \text{ in}$

$\dot{\delta}_{max} = 30 \text{ deg/sec} = 0.52 \text{ rad/sec (no load)}$

$\omega_L = 140 \text{ rad/sec} = 22.3 \text{ Hz (4 channels active)}$

Although NASA recognized that the simulator hardware must be scaled down considerably from the Booster actuator in the interest of cost and size, they wanted the simulator actuators large enough that the simulation would be realistic. Therefore, NASA provided Moog with four spare Saturn actuators (Moog Model 17-150). These actuators have a piston area of 5 square inches and a total stroke of 7.66 inches.

The design supply pressure of the 17-150 actuators is the same as for the Booster actuators, i.e. 3000 psi. Therefore, if the piston differential pressures on the simulator are comparable to those on the Booster, the simulator force levels will be reduced in proportion to piston area, which is a sizable reduction. To provide a meaningful simulation of full-scale elevon behavior, the simulator hardware should be scaled so that the load responses are preserved. This means that the load angular responses should be essentially the same (angular displacement, rate, and acceleration). Because the 17-150 actuators have a shorter stroke than the Booster actuators, the actuator crank arm must be proportionally reduced to keep the maximum angular deflections the same. Therefore all linear displacements, rates, and accelerations seen by the actuators are also reduced in the ratio of the strokes. In addition, all hinge moments are reduced in proportion to the piston area and to the crank arm length. With these considerations in mind, the following relationships should be preserved (the subscript b denotes Booster values, s denotes scaled simulator values).

$$\delta_s = \delta_b \quad , \quad \dot{\delta}_s = \dot{\delta}_b \quad , \quad \ddot{\delta}_s = \ddot{\delta}_b$$

$$\Delta P_s = \Delta P_b$$

$$\frac{R_s}{R_b} = \frac{(S_P)_s}{(S_P)_b}$$

$$\frac{X_s}{X_b} = \frac{\dot{X}_s}{\dot{X}_b} = \frac{\ddot{X}_s}{\ddot{X}_b} = \frac{R_s}{R_b}$$

$$\frac{F_s}{F_b} = \frac{A_s}{A_b} \quad , \quad \frac{H_s}{H_b} = \frac{A_s R_s}{A_b R_b}$$

Using these relationships, the scaling equations for the various system parameters are as follows.

$$\frac{R_s}{R_b} = \frac{(S_P)_s}{(S_P)_b} = .426$$

$$\frac{(H_\delta)_s}{(H_\delta)_b} = \frac{(H_{\dot{\delta}})_s}{(H_{\dot{\delta}})_b} = \frac{I_s}{I_b} = \frac{A_s R_s}{A_b R_b} = .0318$$

$$\frac{(K_L)_s}{(K_L)_b} = \frac{(B_L)_s}{(B_L)_b} = \frac{(M_L)_s}{(M_L)_b} = \left(\frac{A_s}{A_b}\right)\left(\frac{R_b}{R_s}\right) = .1755$$

$$\frac{(K_S)_s}{(K_S)_b} = \frac{(K_A)_s}{(K_A)_b} = \frac{(K_T)_s}{(K_T)_b} = \left(\frac{A_s}{A_b}\right)\left(\frac{R_b}{R_s}\right) = .1755$$

$$(\dot{\delta}_{max})_s = (\dot{\delta}_{max})_b$$

$$\frac{(\omega_L)_s}{(\omega_L)_b} = \sqrt{\frac{4(K_T)_s / (M_L)_s}{4(K_T)_b / (M_L)_b}} = 1.0$$

These scaling equation yield the final parameter values for the simulator.

Scaled Simulator Parameters

$A = 5 \text{ in}^2$

$B_L = 34.7 \text{ lb-sec/in}$

$H_\delta = 182,000 \text{ in-lb/rad.}$

$H_{\dot{\delta}} = 1510 \text{ in-lb-sec/rad.}$

$I = 315 \text{ in-lb-sec}^2/\text{rad.}$

$K_A = 193,000 \text{ lb/in}$

$K_L = 4180 \text{ lb/in}$

$K_S = 43,600 \text{ lb/in}$

$K_T = 35,500 \text{ lb/in}$

$M_L = 7.23 \text{ lb-sec}^2/\text{in}$

P_S = 3000 psi

R = 6.6 in

S_P = 7.66 in

$\dot{\delta}_{max}$ = 30 deg/sec = 0.52 rad/sec

ω_L = 140 rad/sec = 22.3 Hz (4 channels active)

Note that the values of K_A and K_T are very slightly higher than would be given by the scaling equations. The value of K_A shown is the estimated stiffness of the actual 17-150 actuators. Since this number is only 5% higher than the desired value, it did not make sense to modify the actuators. The value of K_T shown was calculated as the series combination of K_A and K_S (this value of K_T is only 1% higher than desired).

The servovalve used on the 17-150 actuator is a Moog Model 16-120, modified to a conventional flow-control configuration by removing the Dynamic Pressure Feedback (DPF) hardware. This servovalve has the following characteristics at a supply pressure of 3000 psi.

K_Q = 6.0 cis/ma

K_P = 13,000 psi/ma

K_{PQ} = .00046 cis/psi

The servovalve also has a rated flow of about 70 cis and a rated current of 10 ma (parallel coils). Since the flow required to achieve a maximum elevon rate of 30 degrees per second (3.4 inches per second) is only 17.3 cis, the servovalve current must be electrically limited. The simulator values then used are as follows.

i_R = 3 ma

Q_R = 18 cis

MOOG
MOOG INC., EAST AURORA, NEW YORK

6.0 ANALOG COMPUTER STUDY

Evaluation of the relative merits of the two competing force-sharing schemes was accomplished on Moog's EAI TR-48 analog computer. An analog block diagram was developed from the functional diagram of Figure 5.2, and is shown in Figure 6.1. Some of the analog circuits are rather unconventional, making liberal use of external patching. This was done to conserve amplifiers. Note that the parameter values given are in Machine Units (one Machine Unit = 10 volts). The analog diagrams for the average-value and mid-value logic are given in Figures 6.2 and 6.3, respectively. It should be noted that the equalization reference pressure (average or mid-value) is computed only once for all four channels, instead of separately within each channel, as was suggested in Section 4.0. This change was made in the interest of simplicity; the redundant computation approach was left for the simulator electronics.

As explained in Section 4.1, it is necessary to limit the maximum output of the average-value equalization (AVE) to minimize transients due to hardover failures. The zener clamps shown in Figure 6.2 were determined as follows. The design "worst-case" null offset condition for the subject program was defined in Section 2.0; the nulls of two channels are initially offset 10% of total stroke from the other two. Since the measured system gain (4 channels active and serodynamic forces present) was $(X_L/e_C) = 0.106$ in/volt, the effective command offset is $(.10\ S_P/.106) = 7.2$ volts. Since the AVE will try to equalize all four nulls to an average position, the maximum equalization signal needed is 3.6 volts. The maximum output of the circuit of Figure 6.2 should be 0.75 Machine Units or $e_E = 3.8$ volts (measured limit is actually 4.1 volts).

The mid-value equalization (MVE) of Figure 6.3 utilizes ΔP signals instead of the $(\Delta P + P_S)$ signals suggested in Section 4.2. Again, this was done in the interest of simplicity, but channel shut-offs were handled so that the functions described in Section 4.2 were duplicated. The mid-value logic was checked for computational accuracy, and it was able to compute the mid-value as precisely as it could be measured. This accuracy was maintained over the entire range of load pressures, and there was no indication that the MVE became confused when all four channels had virtually identical load pressures.

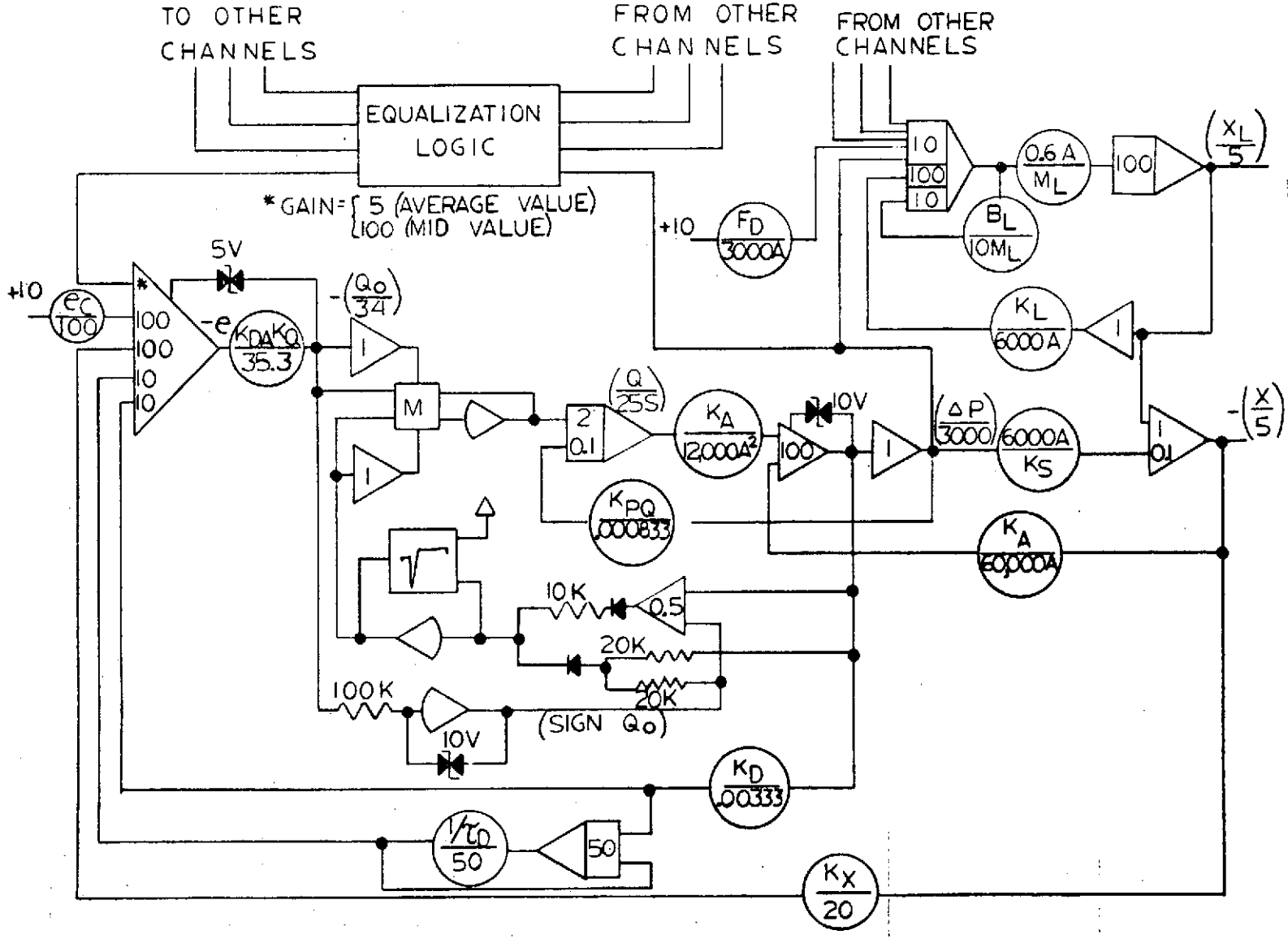

FIGURE 6.1 ANALOG BLOCK DIAGRAM (ONE CHANNEL SHOWN)

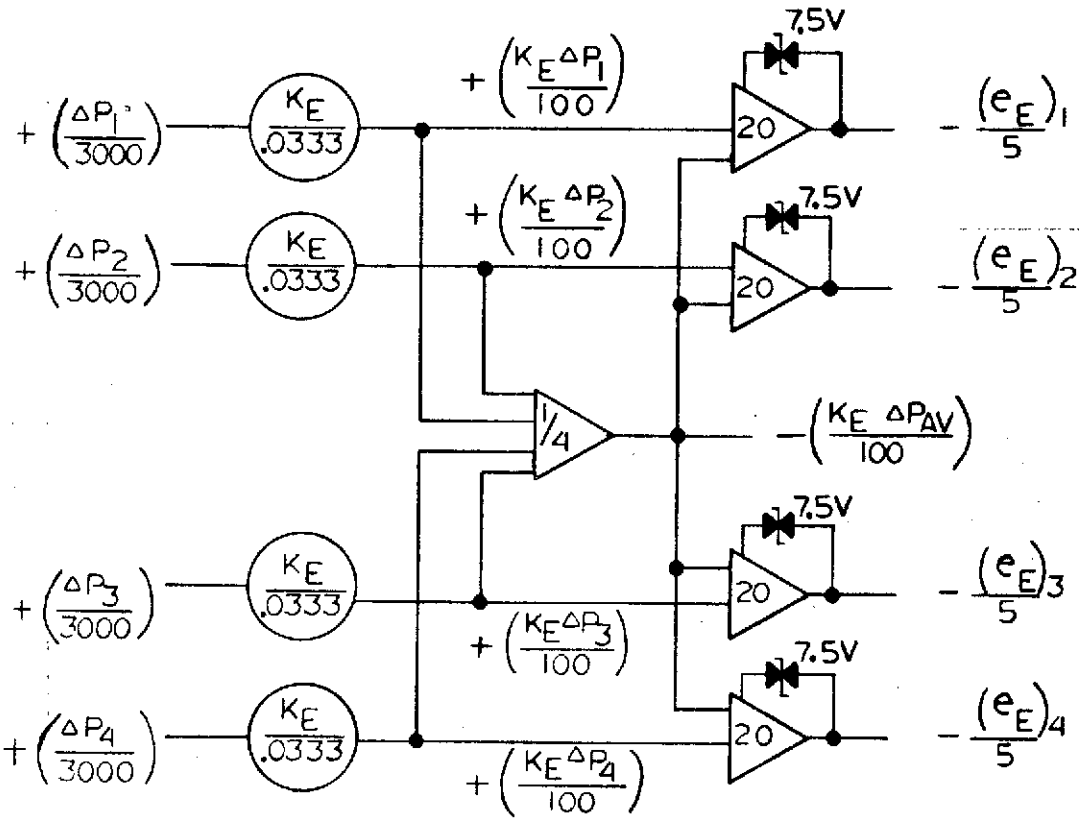

NOTE: ALL EQUALIZATION SIGNALS GO INTO SUMMING AMPLIFIERS WITH A GAIN OF 5.

FIGURE 6.2 ANALOG MECHANIZATION FOR AVERAGE - VALUE LOGIC

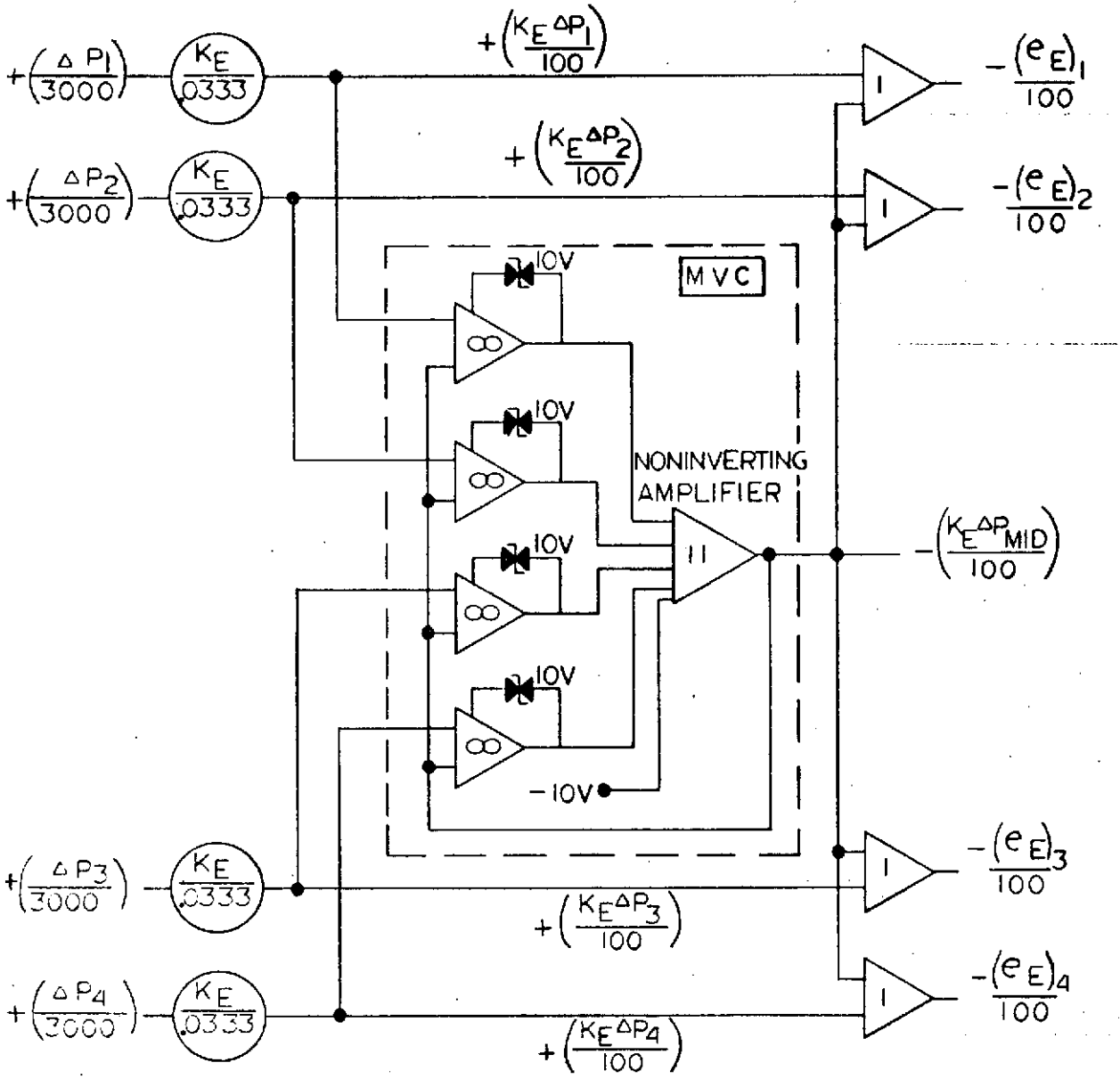

NOTE: ALL EQUALIZATION SIGNALS GO INTO SUMMING AMPLIFIERS WITH A GAIN OF 100.

FIGURE 6.3 ANALOG MECHANIZATION FOR MID-VALUE LOGIC

The parameter values used in the analog study were the scaled simulator values determined in Section 5.3, with one exception. The value of K_{PQ} listed in Section 5.3 is the estimated value for the 16-120 servovalves used on the simulator (.00046 cis/ma). This value is probably not representative because the servovalve is oversized and its output has been electrically limited. A servovalve specifically designed for the desired lower flow would probably have a lower K_{PQ}. A critical-center servovalve will typically achieve pressure saturation at about 3% of rated current ($.03\, i_R\, K_P = P_S$). Using this criterion, the K_{PQ} can be determined as follows.

$$K_P = \frac{P_S}{.03 i_R} = \frac{3000}{.03(3)} = 33,300 \text{ psi/ma}$$

$$K_{PQ} = \frac{K_Q}{K_P} = \frac{6.0}{33,300} = .00018 \text{ cis/ma}$$

Therefore, .00018 cis/ma was used for the analog study, instead of .00046. Actually, the difference in K_{PQ} between the analog computer and simulator is of little importance. The reason for this is that K_{PQ} primarily affects load damping and output stiffness. Roughly 92% of the total load damping comes from the dynamic pressure feedback (DPF), and the closed-loop load stiffness of the actuator position loop is about two orders of magnitude higher than the stiffness of the actuator-attach structure (K_S). Therefore, the primary effects of K_{PQ} are negligible compared to the effects of the DPF and K_S.

The drive amplifier gain and the feedback gains of the various loops are of little importance in themselves; the overall loop gains have the primary influence on system performance. Therefore, K_{DA} was arbitrarily fixed at 3.57 ma/volt ($K_{DA}\, K_Q = 21.4$ cis/volt) so that the various loop gains could be individually changed by adjusting the feedback gains. The following subsections present the results of the analog study. It should be remembered that the analog study does not include servovalve dynamics.

6.1 Basic Servoloop Characteristics

The first step in the analog study was to select appropriate values for the DPF and position feedback parameters. This was done with all active channels perfectly synchronized. Since the load resonant frequency is reduced as channels are shut off, the DPF parameters were optimized for 2-channel operation. This process was accomplished by manipulating

a linearized version of the analog model with a digital servoanalysis program. From a stability standpoint, it is desirable to set the DPF corner frequency as low as possible (approaching proportional pressure feedback). However, low corner frequencies substantially reduce the low-frequency load stiffness. The linear analysis established a good compromise value at about one third of the load resonant frequency (2 channels).

$$1/\tau_D = (1/3)\left(\frac{140}{\sqrt{2}}\right) = 33 \text{ rad/sec}$$

With the corner frequency determined, the DPF loop gain is a compromise between stability and bandwidth. High DPF gain improves load resonant damping, but excessive gain results in large phase lags in the position loop, thereby replacing gain margin problems (low DPF gains) with phase margin problems (high DPF gains). The best balance between position-loop gain margin and phase margin was achieved at $K_D = .0019$ volts/psi. At frequencies above ω_L, the DPF loop looks basically like an integrator. This can be seen from Figure 5.2 by blocking the load (X_L held at zero) and closing the structural compliance loop. The velocity gain of this integrating loop is as follows.

$$K_{VD} = K_D\left(\frac{K_{DA}\,K_Q\,K_T}{A^2}\right) = 58 \text{ sec}^{-1}$$

It is this loop gain which directly determines the improvement in load resonant damping ($2\zeta_L\omega_L = K_{VD}$), and which must therefore be duplicated on the simulator.

With the DPF parameters set into the analog computer, the position feedback gain was increased until the small-signal frequency response to position commands exhibited a load-resonant peak equal to 0 dB, with four channels operating. The value of K_X required to achieve this was 9.0 volts/inch. With only two channels operating, the small-signal response exhibits a + 3 dB peak, but this is not serious. The open-loop characteristic of the position loop (up to the load-resonant frequency) also looks like an integrator. This can be seen from Figure 5.2 by neglecting the load (ΔP held at zero). The velocity gain of this integrating loop is as follows.

$$K_{VX} = K_X\left(\frac{K_{DA}K_Q}{A}\right) = 39 \text{ sec}^{-1}$$

Note that this loop gain is about 10 times the value that can be achieved with no DPF.

With the DPF and position loop parameters set, data was taken to determine the response characteristics of the basic system. The elevon position responses to command inputs are shown in Figures 6.4 and 6.5. These are actually X_L responses with the appropriate conversion factor applied (57.3/R = 8.7 deg/in). From Figure 6.4, it can be seen that the position-loop bandwidth (frequency for 90° phase lag) is 15 Hz (4 channels) and 11 Hz (2 channels). If K_L and B_L are set to zero, the step responses are virtually identical to those of Figure 6.5. This simulates operation in parts of the flight envelope where aerodynamic loads are small. Of course, these responses were all measured with an initial elevon angle of zero. With large initial elevon angles, the responses are more affected by the aerodynamic loads.

To illustrate the effects of rate limiting, Figure 6.6 compares frequency responses for 4° and 2° P-P elevon command inputs with the 1° P-P response of Figure 6.4 (4 channels operating). Notice that the rate limiting does little to reduce the resonant peak. The reason for this is that the servovalve itself is causing the rate limiting; and because the DPF is mechanized electrically, the servovalve is inside the DPF loop. Thus, rate limiting effectively reduces the DPF loop gain, and thereby tends to prevent the DPF from damping the load resonance. Fortunately, the same effect also reduces the position loop gain. The effects of rate limiting on the time response of the actuator are shown in Figure 6.7 (a 2° elevon step). Notice that even though the damping of the load resonant mode is reduced, the residue of this mode is still small. The response is rather lumpy, but is reasonably well behaved.

Figure 6.8 shows the load position response to a small external disturbance force, e.g. to simulate a wind gust hitting the elevon (4 channels operating). Notice that there is considerable amplitude magnification at high frequencies. This is partly due to the load resonance, but is primarily due to the fact that the DPF has reduced the actuator stiffness at high frequencies. If proportional pressure feedback were used instead of DPF or if no pressure feedback were used (necessitating a reduction in position loop gain), the frequency response would be much flatter. However, the flattening would not be due to an increase in high frequency stiffness, but would instead be due to a decrease in low frequency stiffness. Thus DPF is desirable to maintain static stiffness.

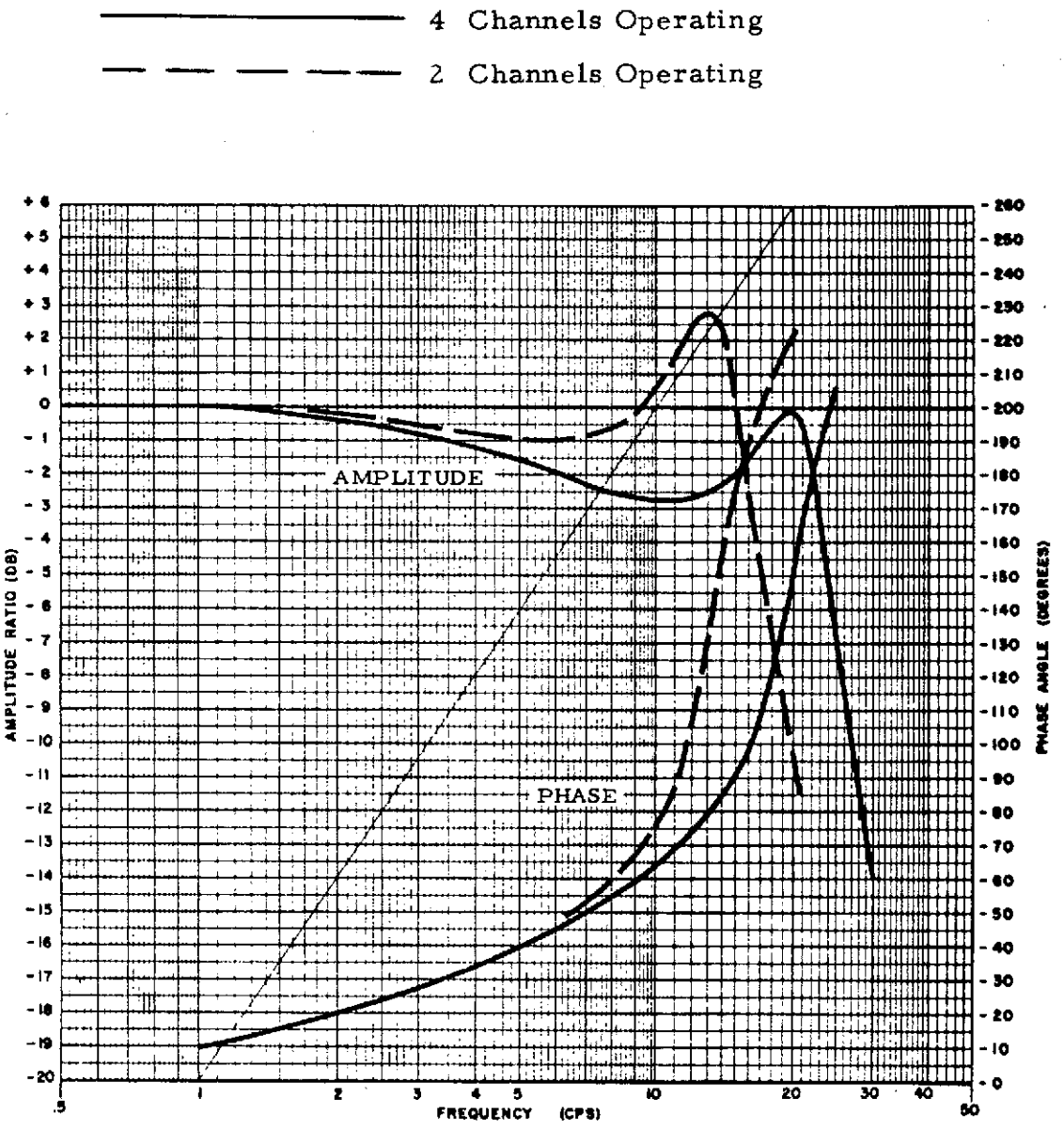

FIGURE 6.4 FREQUENCY RESPONSE OF ELEVON TO 1° P-P COMMAND INPUTS

MOOG
MOOG INC., EAST AURORA, NEW YORK

4 Channels Operating

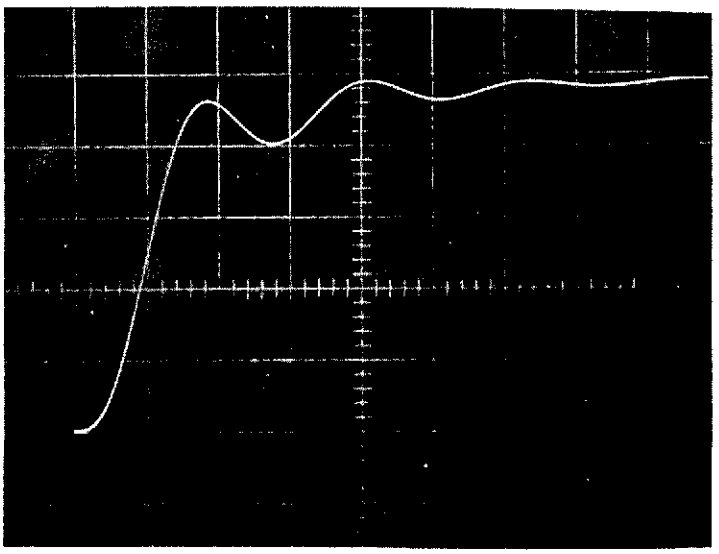

Scales :
0.2 deg/div (vert)
0.02 sec/div (hor)

2 Channels Operating

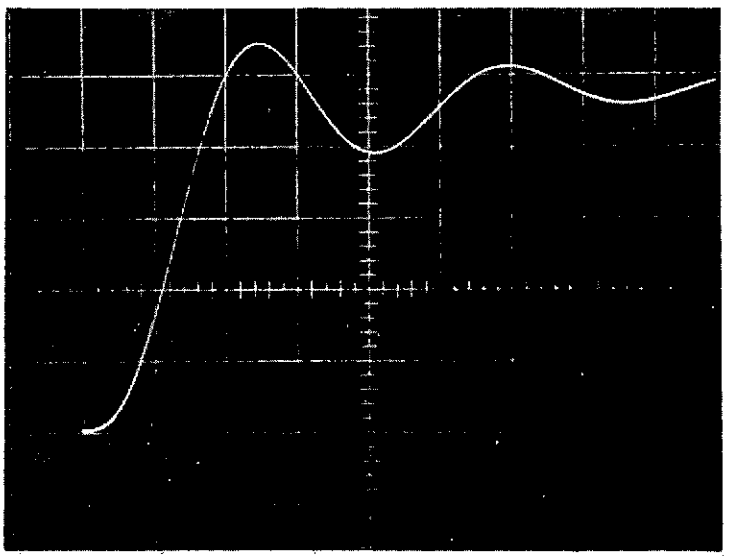

FIGURE 6.5 ELEVON RESPONSE TO + 1° COMMAND STEP

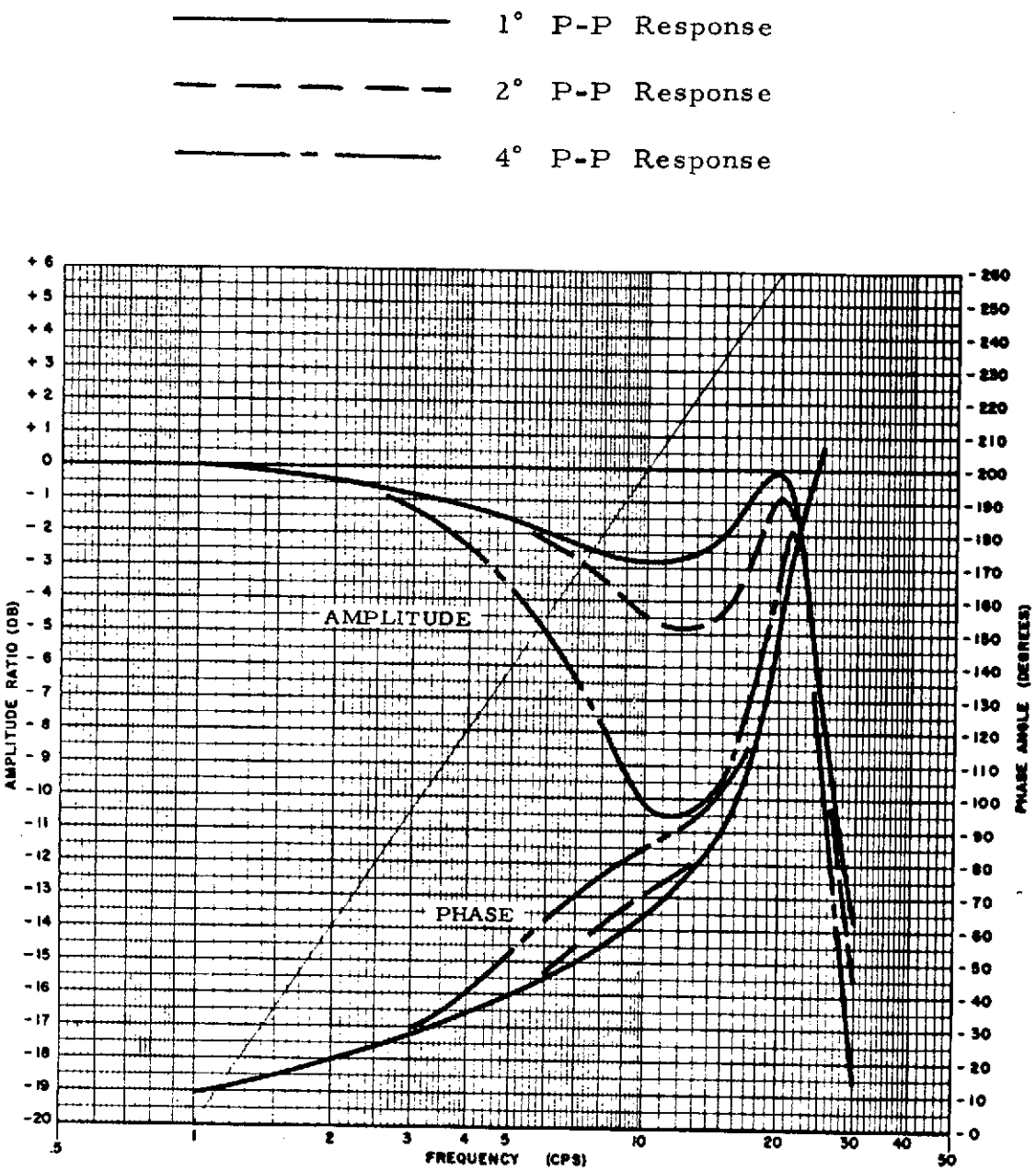

FIGURE 6.6 EFFECTS OF RATE LIMITING ON ELEVON FREQUENCY RESPONSE

Scales :

0. 4 deg/div (vert)

0. 02 sec/div (hor)

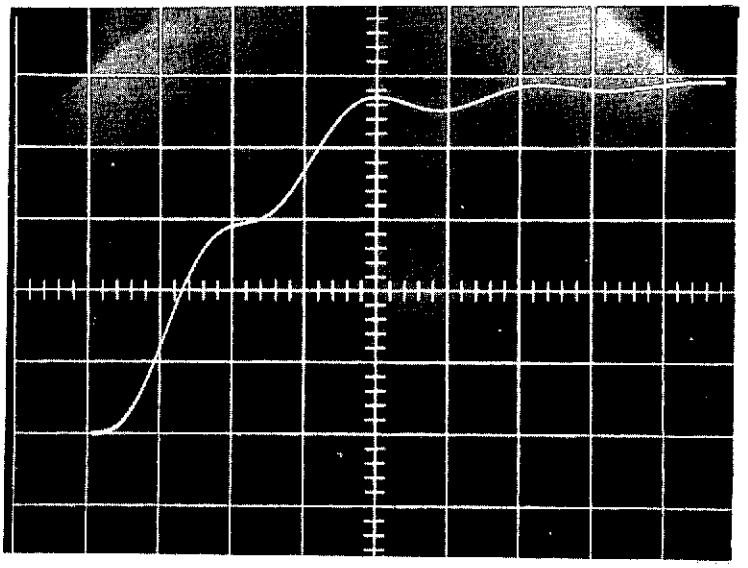

FIGURE 6. 7 ELEVON RESPONSE TO + 2° COMMAND STEP

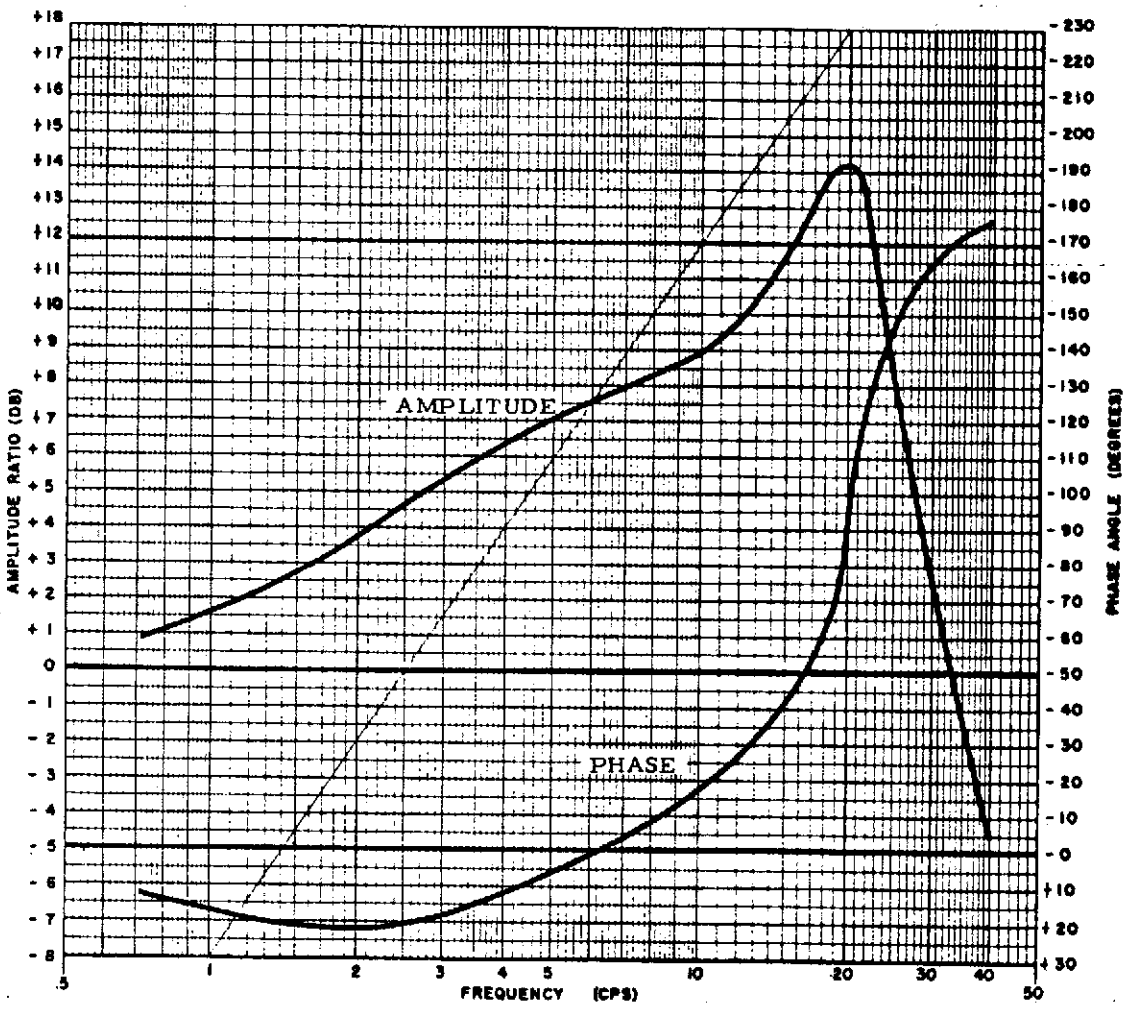

FIGURE 6.8 FREQUENCY RESPONSE OF ELEVON TO 3000 LB. P-P LOAD DISTURBANCES

6.2 Effects of Equalization - Normal Operation

To evaluate the two equalization schemes on the analog computer, the characteristics with all four channels operating were first examined. All evaluations were performed with the "worst-case" offset conditions defined in Section 2.0. The nulls of channels 1 and 2 were offset + 10% of full stroke (command voltages biased $.10\ S_p/.106 = +7.2$ volts), while channels 3 and 4 were not offset. The equalization feedback gain required to achieve the desired degree of force sharing under these conditions was $K_E = .0233$ volts/psi for both the AVE and the MVE. The corresponding loop velocity gain can be computed in the same manner as for the DPF loop (Section 6.1).

$$K_{VE} = K_E \left(\frac{K_{DA}K_Q K_T}{A^2}\right) = 710\ \text{sec}^{-1}$$

Using this equalization gain with the specified offset condition, the following static results were obtained for zero command input and zero load disturbance.

Measured Output	EQUALIZATION		
	None	AVE	MVE
$X_L \sim$ In.	+ .35	+ .40	+ .76
$\delta \sim$ Deg.	+ 3.0	+ 3.5	+ 6.6
$\Delta P_1 \sim$ Psi	+ 3000	+ 230	+ 300
$\Delta P_2 \sim$ Psi	+ 3000	+ 230	+ 300
$\Delta P_3 \sim$ Psi	- 2850	- 67	+ 14
$\Delta P_4 \sim$ Psi	- 2850	- 65	+ 18
$\Delta P_{av} \sim$ Psi	+ 75	+ 82	+ 158
$\text{Max}(\Delta P_n - \Delta P_{av})$	2925	149	144
ΔP_{mid}	--	--	+ 300

Using the definitions of Section 2.0, force fight is the load pressure deviation of the worst active channel from the average load pressure, expressed as a percentage of supply pressure. With this in mind, the bottom row of the table shows that both the AVE and MVE reduce the

force fight from nearly 100% to about 5%. The only apparent difference in the 2 schemes is that the AVE equalizes the channels toward each other, while the MVE equalizes toward the mid-value channel, which in this case is the offset channel 1 (or 2). (Remember that the MVE selects the more positive of the middle two pressures as the mid-value.)

Another primary effect of equalization is improvement of static load stiffness to external disturbances. Figure 6.9 shows the measured stiffness characteristics with zero command input. Note that equalization effectively doubles the average stiffness when interchannel mismatch is present. Equalization also eliminates the flat spot in the stiffness curve near null. In fact, with the high position loop gain being used, the equalization has made the actuators themselves so stiff that the overall system stiffness approaches that of the attachment structure ($4\ K_s$ = 174,400 lb/in, F_D/X_L = 170,000 lb/in for MVE and 160,000 lb/in for AVE).

After studying static characteristics, transient response data was taken for command and disturbance step inputs. Figure 6.10 shows the elevon response to small command steps (channel 1 and 2 nulls again offset + 10%). The AVE and MVE responses are reasonably fast and well behaved. In fact, they are virtually identical to the response with all four channels perfectly synchronized (see Figure 6.5). Without equalization, the step causes the response to be somewhat sluggish. The load pressure responses for the small command steps are shown in Figure 6.11. Notice that equalization not only reduces the steady-state force fight, but also reduces the force transients.

The elevon response to a large load disturbance is shown in Figure 6.12. Equalization has improved not only the static stiffness (as was previously shown in Figure 6.9), but also the dynamic stiffness. Figure 6.12 also shows that equalization reduces the load pressure transients.

On the basis of the foregoing discussion, it would appear that the two equalization schemes provide many benefits with no obvious disavantages as far as normal operation is concerned. The only significant difference in the two schemes is that the AVE equalizes all the channels toward each other, while the MVE equalizes 3 channels toward the mid-value channel, which may have an offset null.

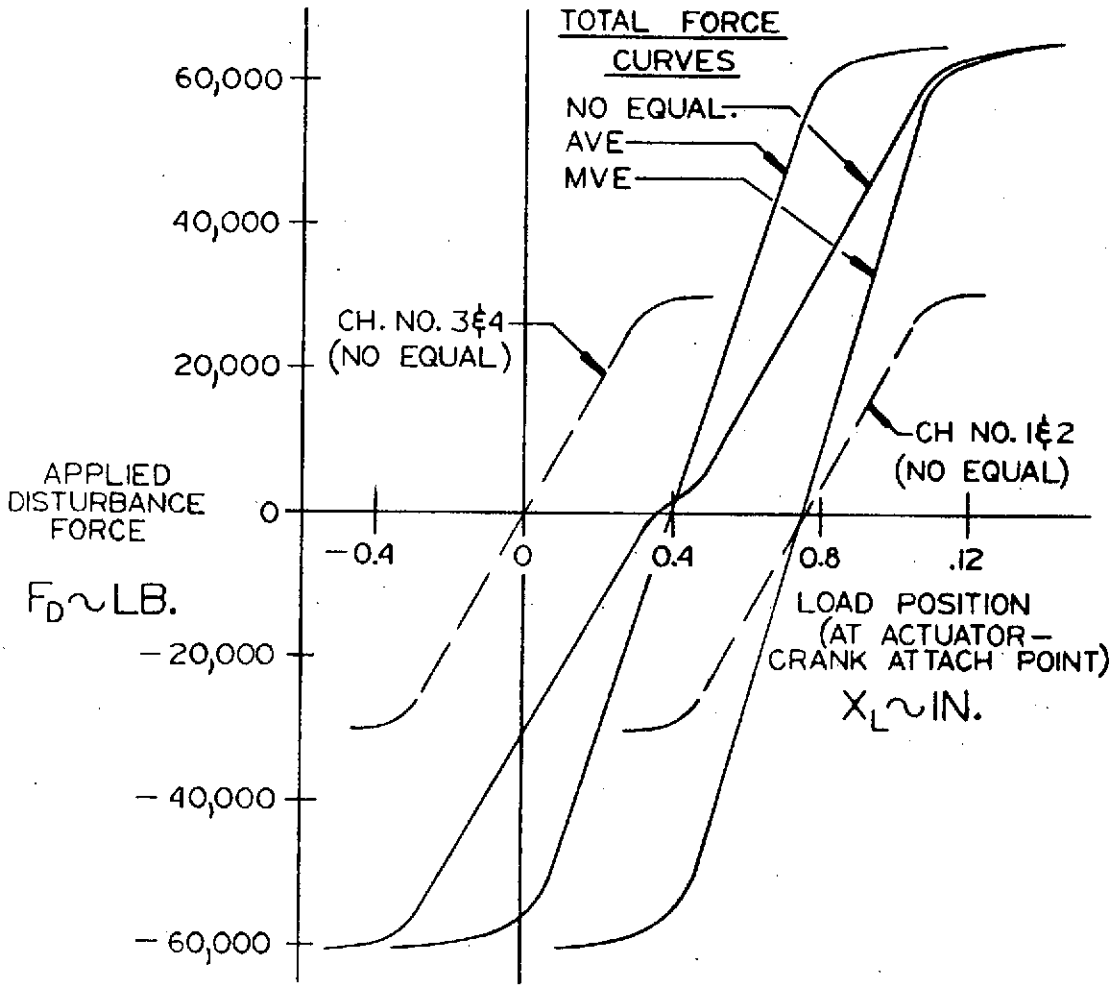

FIGURE 6.9 EFFECT OF EQUALIZATION ON SYSTEM OUTPUT STIFFNESS

MOOG
MOOG INC. EAST AURORA, NEW YORK

With Equalization (AVE or MVE)

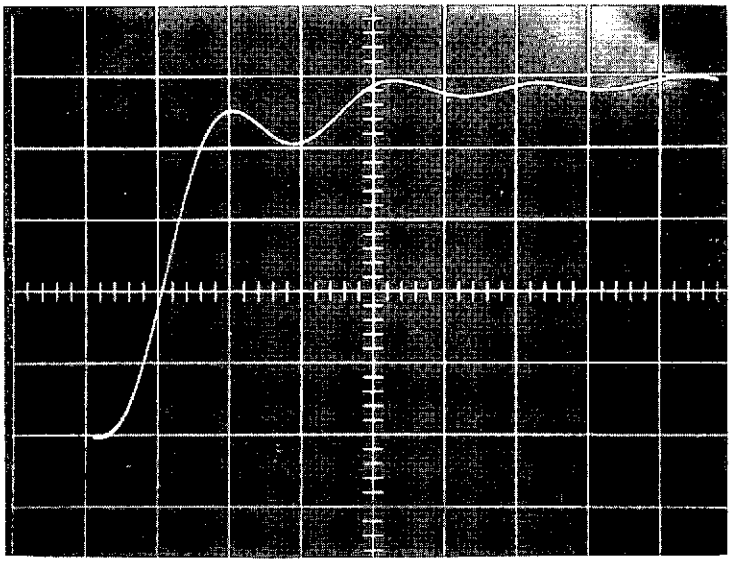

Scales :

0.2 deg/div (vert)

0.02 sec/div (hor)

No Equalization

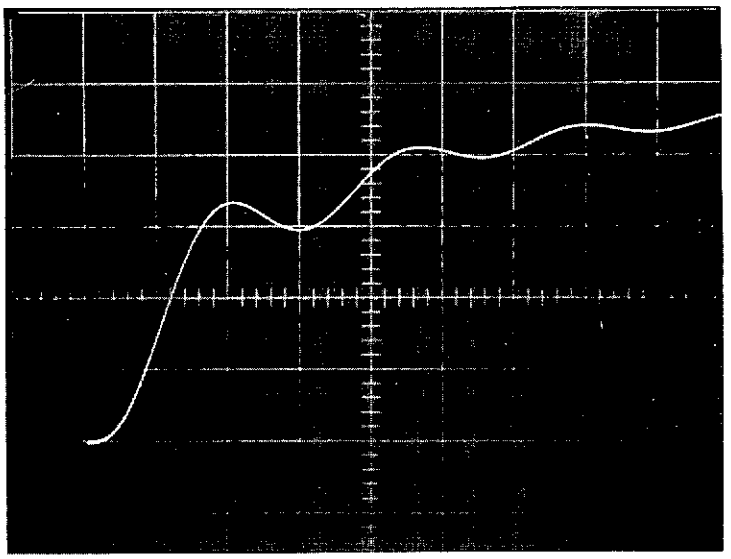

FIGURE 6.10 EFFECT OF EQUALIZATION ON ELEVON RESPONSE TO + 1° STEP COMMAND

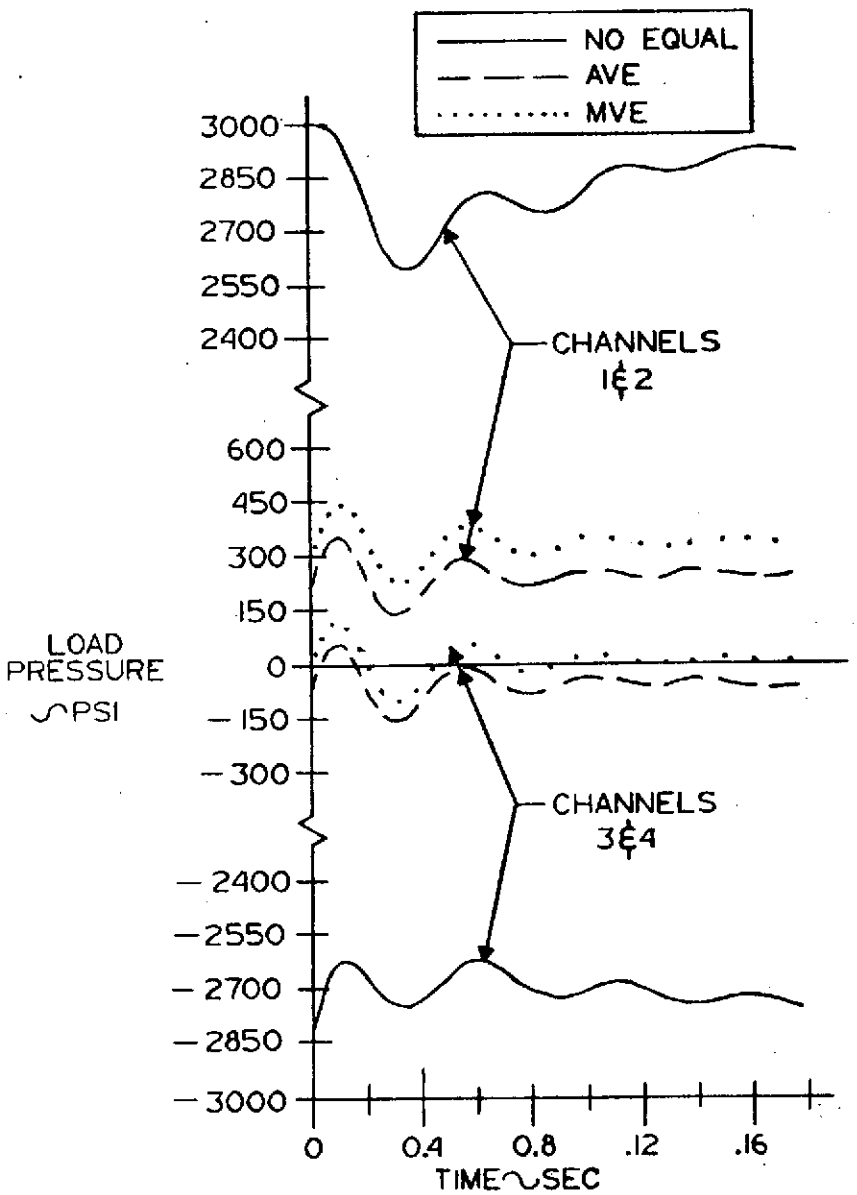

FIGURE 6.11 EFFECT OF EQUALIZATION ON LOAD PRESSURE RESPONSE TO + 1° STEP COMMAND

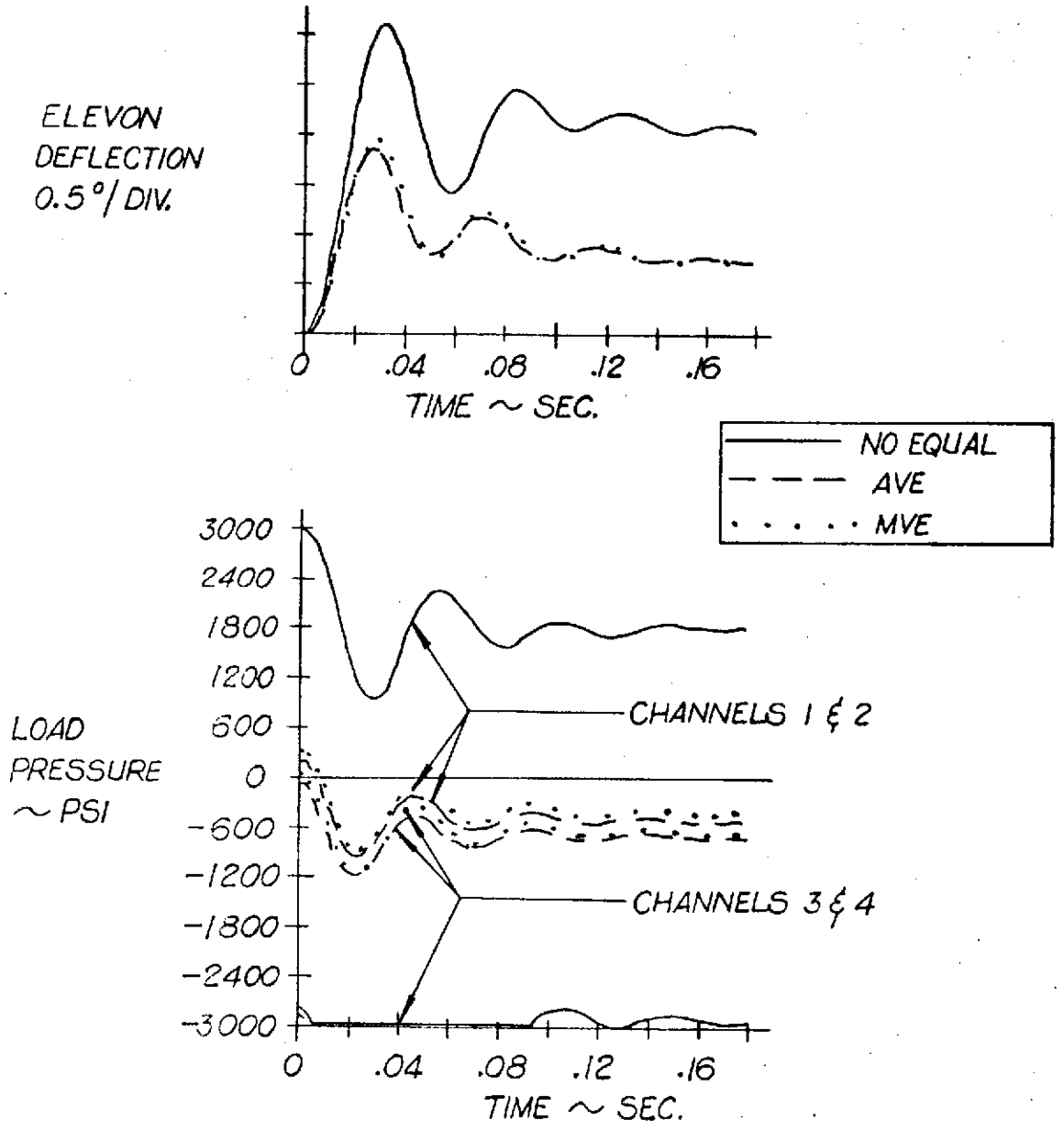

FIGURE 6. 12 EFFECT OF EQUALIZATION ON RESPONSE TO A + 15, 000 LB. LOAD DISTURBANCE

6.3 Effects of Equalization - Hardover Failures

Before discussing the effects of failures and shutdowns, it is first worthwhile to review the logic changes within the equalization as channels are shut down. These changes are explained in detail in Sections 4.1 and 4.2, and can be summarized as follows. When the MVE is used, shutdown of a channel causes that channel's ΔP signal into the MVC to become the equivalent of - 3000 psi. (It is assumed that shutdown always bypasses the piston, so that the channel's actual ΔP to the load goes to zero.) When the AVE is used, shutdown causes the channel's ΔP input line to the averaging amplifier to be disconnected from that channel and shorted to the ΔP input line from another channel. The sequence arbitrarily selected is: channel 1 shorts to channel 2, 2 to 3, 3 to 4, and 4 to 1.

Since the system is supposed to have dual-fail-operate (DFO) capability, it was decided to study the effects of a series of 2 hardover failures followed by shutdowns. To determine the most critical sequence, the steady-state elevon deflections were examined for a large number of sequences. This study determined that the most critical sequence for no equalization and for MVE is : channel No. 1 hardover (-), No. 1 shutdown, No 3 hardover (+), No. 3 shutdown. For the AVE, the most critical sequence is : No. 1 hardover (-), No. 1 shutdown, No. 2 hardover (-), No. 2 shutdown. A comparison of the steady-state elevon deflections is presented in the following table. For ease of comparison, AVE data are presented for two failure sequences.

	Elevon Deflection ~ Deg.				
	Before Failures	$\Delta P_1 \rightarrow$ - 3000	No. 1 Shutoff	$\Delta P_3 \rightarrow$ + 3000	No. 3 Shutoff
No Equal	+ 3.0	+ 0.1	+ 1.5	+ 6.2	+ 2.9
MVE	+ 6.6	0.0	+ 0.8	+ 7.9	+ 0.6
AVE	+ 3.5	- 0.5	+ 3.3	+ 6.4	+ 3.3
				$\Delta P_2 \rightarrow$ - 3000	No. 2 Shutoff
AVE	+ 3.5	- 0.5	+ 3.3	- 5.1	0.0

This table shows several interesting things. First, both equalization schemes increase steady-state elevon movement in almost every case. The AVE is superior to the MVE on the first hardover failure (change in δ is 6.6° for MVE, 4.0° for AVE). On the second failure, the AVE is also superior when the failure is in channel 3 (7.1° for MVE, 3.1° for AVE). When the second failure for the AVE is in channel 2, the change is larger than for the MVE (8.4°). The reason for the larger AVE transient when channel 2 goes hardover, is that the previous shutdown of channel 1 has caused ΔP_2 to be weighted by a factor of 2 in the averaging amplifier:

$$\Delta P_{av} = \frac{2\Delta P_2 + \Delta P_3 + \Delta P_4}{4}$$

Thus, it is not clear which scheme is perferrable, from a failure standpoint.

The steady-state load pressure changes for the failure sequences described above are given in the following table. Note that the values shown are the actual actuator load pressures; the pressure signals sent to the equalization depend upon which channels are shut down.

Change	Equal.	ΔP_1	ΔP_2	ΔP_3	ΔP_4	ΔP_{av}*	ΔP_{mid}*
none	none	+3000	+3000	-2850	-2850	—	—
↓	MVE	+300	+300	+14	+18	—	+300
↓	AVE	+230	+230	-67	-65	+82	—
ΔP_1 → -3000	none	-3000	+3000	-36	-36	—	—
↓	MVE	↓	+1170	+930	+890	—	+930
↓	AVE	↓	+2900	+7	+10	-21	—
No. 1 Shutoff	none	0	+3000	-1430	-1430	—	—
↓	MVE	↓	+192	-46	-66	—	-46
↓	AVE	↓	+303	+7	+9	+156	—
ΔP_3 → +3000	none	↓	+630	+3000	-3000	—	—
↓	MVE	↓	-970	↓	-1260	—	-970
↓	AVE	↓	+218	↓	-2560	+219	—
No. 3 Shutoff	none	↓	+3000	0	-2700	—	—
↓	MVE	↓	+172	↓	-118	—	-118
↓	AVE	↓	+306	↓	+12	+159	—
ΔP_2 → -3000	AVE	0	-3000	+1160	+1300	-885	—
No. 2 Shutoff	AVE	0	0	0	0	0	—

* Computed by AVE or MVE logic

The primary conclusion to be drawn from this table is that equalization continues to hold force fight between active channels to a minimum, even after failed channels are shut down. The MVE provides slightly less force fight after the first shutdown, but the advantage is small (5.5% for MVE, 6.5% for AVE). The effects of equalization on transient response for the failure sequence discussed above are shown in Figure 6.13. This figure shows that equalization generally results in a less abrupt transient with less overshoot, even though the steady-state change is increased. The elevon response to command inputs with two channels shut off is the same as if the channels were perfectly synchronized.

6.4 Failure Detection

Having not yet found any clear-cut reasons for choosing between the two equalization schemes, a brief study was made to determine the best approach to the problem of detecting failures. This study uncovered a major problem: failure detection with the AVE is very difficult, if not completely impractical. This can be seen by referring to the hardover failure data of Section 6.3. The static ΔP data show that failures could be very nicely detected for the MVE by simply monitoring the equalization signal in each channel. For example, a failure signal could be generated whenever $(\Delta P_n - \Delta P_{mid})$ exceeds, say, 500 psi. If this same technique were used with the AVE, however, the detection logic would indicate that two channels had failed when, in fact, only one channel had done so.

The basic problem with the AVE is that the clamp on the output of the equalization amplifier (Figure 6.2) prevents the active channels from working together in opposing the hardover. For example, when channel 1 goes hardover, it is opposed entirely by channel 2 while channels 3 and 4 contribute essentially nothing. The active channels in the MVE work together in opposing the hardover, and the only large equalization signal generated is in the failed channel.

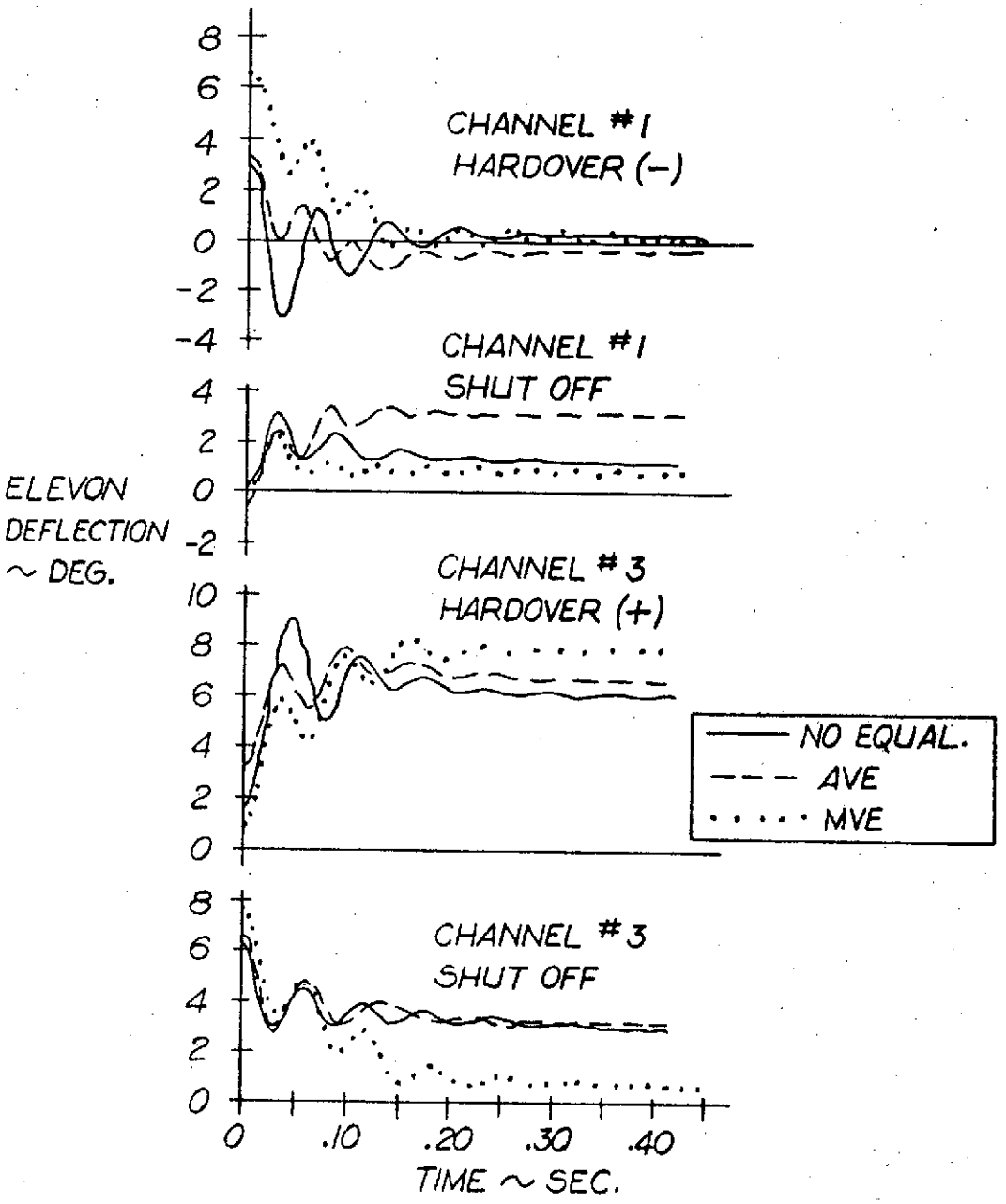

FIGURE 6.13 EFFECT OF EQUALIZATION ON RESPONSE TO A SERIES OF HARDOVER FAILURES AND SHUT DOWNS

Since the basic problem in the AVE is created by the clamp, one obvious fix is to raise the clamping voltage. The effects of opening up the AVE clamp are shown in the following data, for channel 1 going hardover.

Failure State	Clamp Voltage	Elevon Position	ΔP_1	ΔP_2	ΔP_3	ΔP_4	Computed ΔP_{av}
No Failures	Any	+ 3.0°	+230	+230	-67	-65	+82
$\Delta P_1 \rightarrow$ -3000	Normal	- 0.5°	-3000	+2900	+7	+10	-21
↓	Doubled	- 3.6°	↓	+2520	+67	+66	-87
	Clamp Removed	- 17.2°		+620	+320	+320	-435

It can be seen that the effect of opening up the clamp is to allow the active channels to more evenly share the load in opposing the hardover. However, this trend is accompanied by an increase in the magnitude of the failure transient. For example, doubling the clamping voltage roughly doubles the transient, and the improvement in failure detection is not great. Probably the best failure criterion to use would be to sense when ΔP itself exceeds a set limit; but even with the clamp doubled, this threshold would have to be set around 2800 psi to avoid having failure indications on a good channel as well as on the failed one. This is pretty marginal because a drop in supply pressure or a ΔP transient could foul up the works.

Other potential solutions to the failure detection problems of the AVE have been evaluated, but all seem to result in rather marginal detection thresholds. Because failure detection with the AVE seems to be totally impractical, the only alternative is to pursue the MVE scheme. To further investigate the subject of failure detection, various failures in the equalization logic itself were investigated on the analog computer. The data for various failures in the MVE of channel 1 are shown below.

Failure	Elevon Position	ΔP_1	$\Delta P_1 - (\Delta P_{mid})_1$	ΔP_2	ΔP_3	ΔP_4	(ΔP_{mid}) (Ch. 2, 3, 4)
None	+ 6.6°	+300	0	+300	+14	+18	+300
Equal. output open*	- 1.4°	-2780	0	+660	+1020	+970	+970
XDCR output open	+ 6.1°	+1060	0	+41	-260	-250	0
ΔP neg. fdbk. open	+ 6.9°	+1010	-84	+84	-220	-210	+84
ΔP_{mid} output open	+ 3.8°	+140	+140	+275	-26	-18	+140
ΔP_{mid} output hardover	- 0.3°	-2800	+1490	+1090	+850	+815	+850
Equal. output hardover	- 0.5°	-2790	-4190	+1080	+840	+810	+840

Notes:

ΔP_n's are actual, $(\Delta P_{mid})_{234}$ are computed values, and $[\Delta P_1 - (\Delta P_{mid})_1]$ is the computed value seen at the equalization output. Initially, channels 1 and 2 nulls are offset + 10% (except for the case with the * , where the offset is - 10%.

Having decided to use the MVE scheme for the simulator evaluations, the failure-detection logic for each channel can be designed to monitor the output of the equalization, with the detection threshold set at 500 psi. Referring to the above data, it is apparent that there will be no false failure indications ($\Delta P - \Delta P_{mid}$ for channels 2, 3, 4 will be considerably less than 500 psi). In addition, the 2 hardover amplifier failures will be immediately detected. Of the 4 open failures, 3 will be detected as soon as the actuators are asked to develop a significant force output. It is not yet clear whether the transducer-open failure can be detected.

7.0 SIMULATOR EVALUATIONS

The final phase of the force-sharing program was to design and fabricate a load simulator, so that the concepts developed in the foregoing sections could be evaluated with actual hardware. The simulator fixture itself was designed to duplicate the scaled-down Space Shuttle parameters of Section 5.3 as closely as possible. The electronics were designed to implement the mid-value logic of Section 4.2, and to facilitate data gathering and failure simulation. The following subsections briefly describe the simulator hardware, and then present the results of the test program. The reader is referred to Appendix B for a more detailed description of the simulator, together with operating instructions.

7.1 Mechanical and Hydraulic Hardware

The first attempt at designing the simulator resulted in a configuration which placed the four actuators side-by-side, pushing on a common torque tube or crankshaft, much as they would on an actual elevon surface. However, providing sufficient stiffness in the frame and crankshaft proved to be a difficult task, and this approach was therefore abandoned. The final fixture configuration is shown in Figure 7.1. The four Model 17-150 actuators are arranged in opposed pairs, pushing on a short crankshaft. From the center of the crankshaft hangs a pendulum, which simulates the elevon moment of inertia. Between each pair of actuators is a " liquid spring ", manufactured by Taylor Devices Incorporated of North Tonawanda, New York (Taylor Model 4S5451-01). These springs are connected between the frame (ground) and the center of the crankshaft, to simulate the aerodynamic spring rate of the elevon surface. No attempt was made to simulate aerodynamic damping since the analog study showed that this parameter has little effect on the system performance. The bodies of the actuators are connected to individual leaf springs, which are bolted to the ends of the frame. These leaf springs simulate the compliance of the elevon attach structure (K_S).

The liquid springs are basically hydraulic cylinders with the piston head missing, so that the rod itself is the only internal moving part. As the rod is pushed into the cylinder, the silicone fluid is slightly compressed, resulting a modest spring rate for very long strokes. Because the springs can be used in compression only, two opposed springs were necessary. The rods are connected to the crankshaft through sliding collars, so that only one spring is compressed at a time (neither spring is compressed when the crankshaft is centered). The measured spring rate is 3960 lb/in at 74°F, reflected to the actuator crank arm. This is about 5% below the desired value of K_L = 4180 lb/in. Of course, there must be a slight

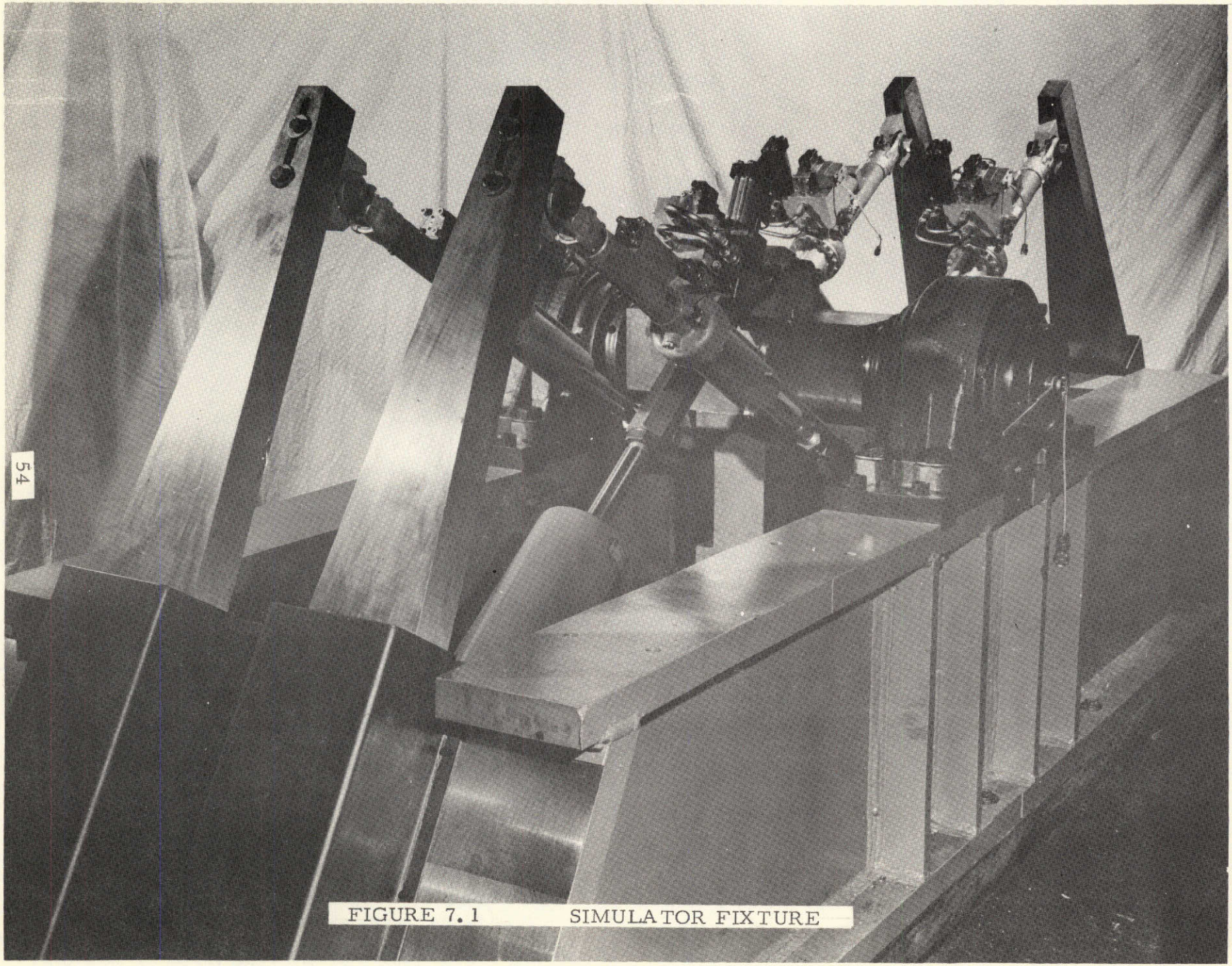

FIGURE 7.1 SIMULATOR FIXTURE

preload in the spring adjustment to ensure positive centering. This preload is highly sensitive to the temperature of the silicone fluid, and should be checked daily. An attempt was made to keep the breakout force at about ± 250 pounds, reflected to the actuator crank arm (load pressure of ± 50 psi for a single actuator to break out the springs).

Measurements of the leaf spring rates were made with the actuator attach fittings at their lowest position and the base attach bolts torqued to 300 foot-pounds. The four springs were reasonably consistent in their behavior, the rate being higher with the actuator pulling than with it pushing. The average rate is 42,600 lb/in, with the largest deviation being 5% high in the actuator-pull direction and 5% low in the actuator-push direction. The average rate is about 2% lower than the desired K_S of 43,600 lb/in. The load inertia cannot be measured directly, but the load resonant frequency was measured with only actuator number 4 connected to the crankshaft (this actuator has K_S virtually identical to the average of 42,600 lb/in). The measured natural frequency was 10.6 Hz, and the frequency calculated from the desired values of K_T and M_L is 11.1 Hz.

Figure 7.2 is a close-up of one of the 17-150 actuators. The actuator has been modified by placing a special manifold block between the servovalve and actuator body. Plumbed into this manifold block are a solenoid bypass valve and a cross-port relief valve. The manifolding is arranged so that both valves interconnect the two sides of the actuator piston, when they are opened. The relief valve prevents excessive load pressures from being generated if the servovalve is suddenly closed when the load is moving at maximum velocity. The valve is a Waterman Model 1518-3-3000, which is a direct-operated spool type. The relief setting is adjusted so that the valve cracks at approximately 3200 psi and reseals at about 2900 psi. The solenoid valve is opened when a channel is shut off, so that the piston can be moved by the remaining active channels with minimum resistance. The solenoid valve is a Waterman Model 1620-3A-110. It is a direct-operated spool type, actuated by a 110 VAC solenoid. The valve is closed when the solenoid is deenergized, so that the coils are not continuously drawing electrical power during normal operation.

Another change to the actuator is that the DPF mechanism was removed from the 16-120 servovalve and a small adaptor manifold attached in its place, so that a differential pressure transducer could be fitted to the servovalve (see Figure 7.3). The transducers used are some spare ones from the Moog Titan actuators (Moog Part Number 062-24924). These transducers are designed so that the output signal is zero when the load pressure is 3500 psi in one direction (port 2 high), 20 mv when the pressure is zero, and 40 mv when the pressure is 3500 psi in the opposite direction (port 1 high).

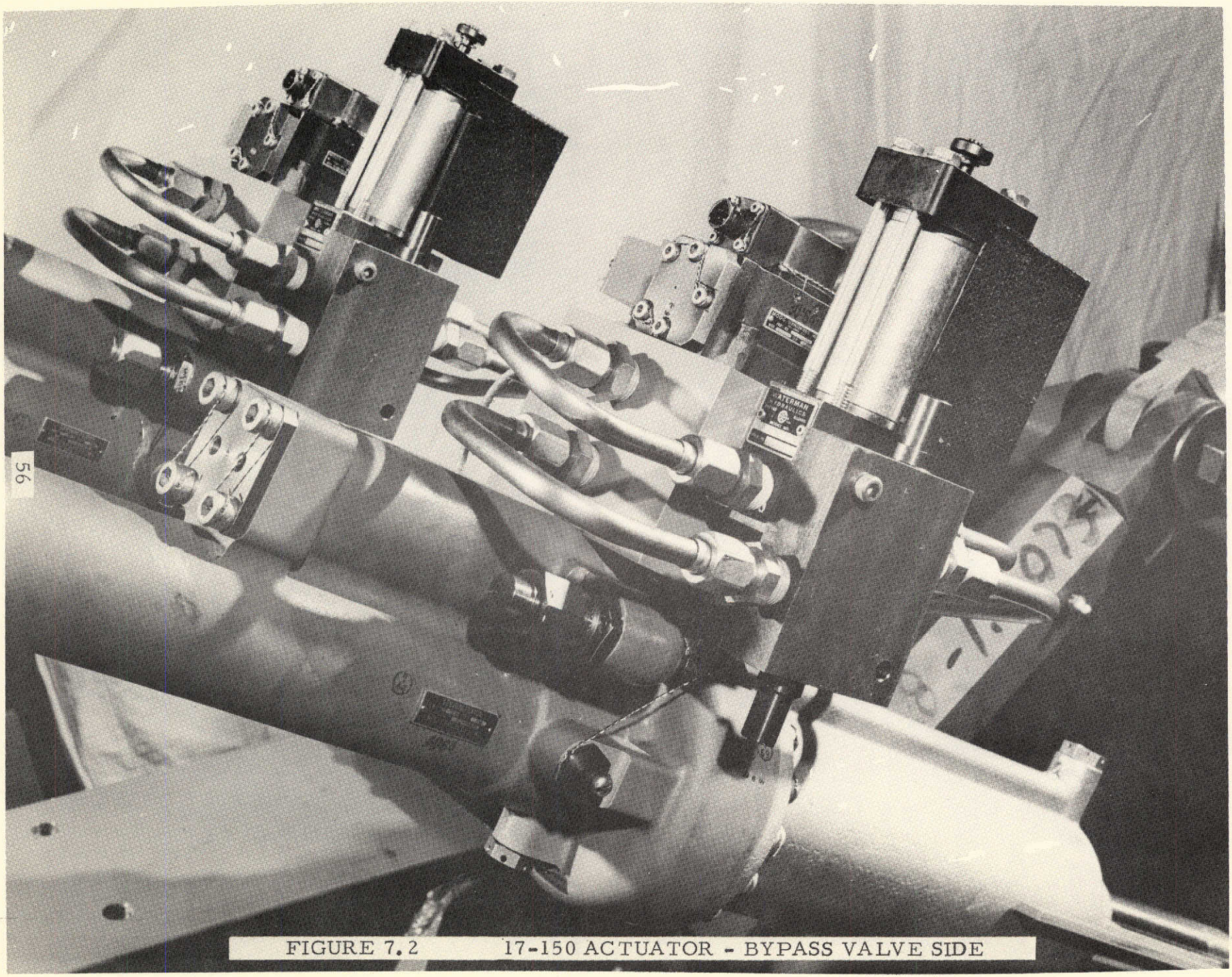

FIGURE 7.2 17-150 ACTUATOR - BYPASS VALVE SIDE

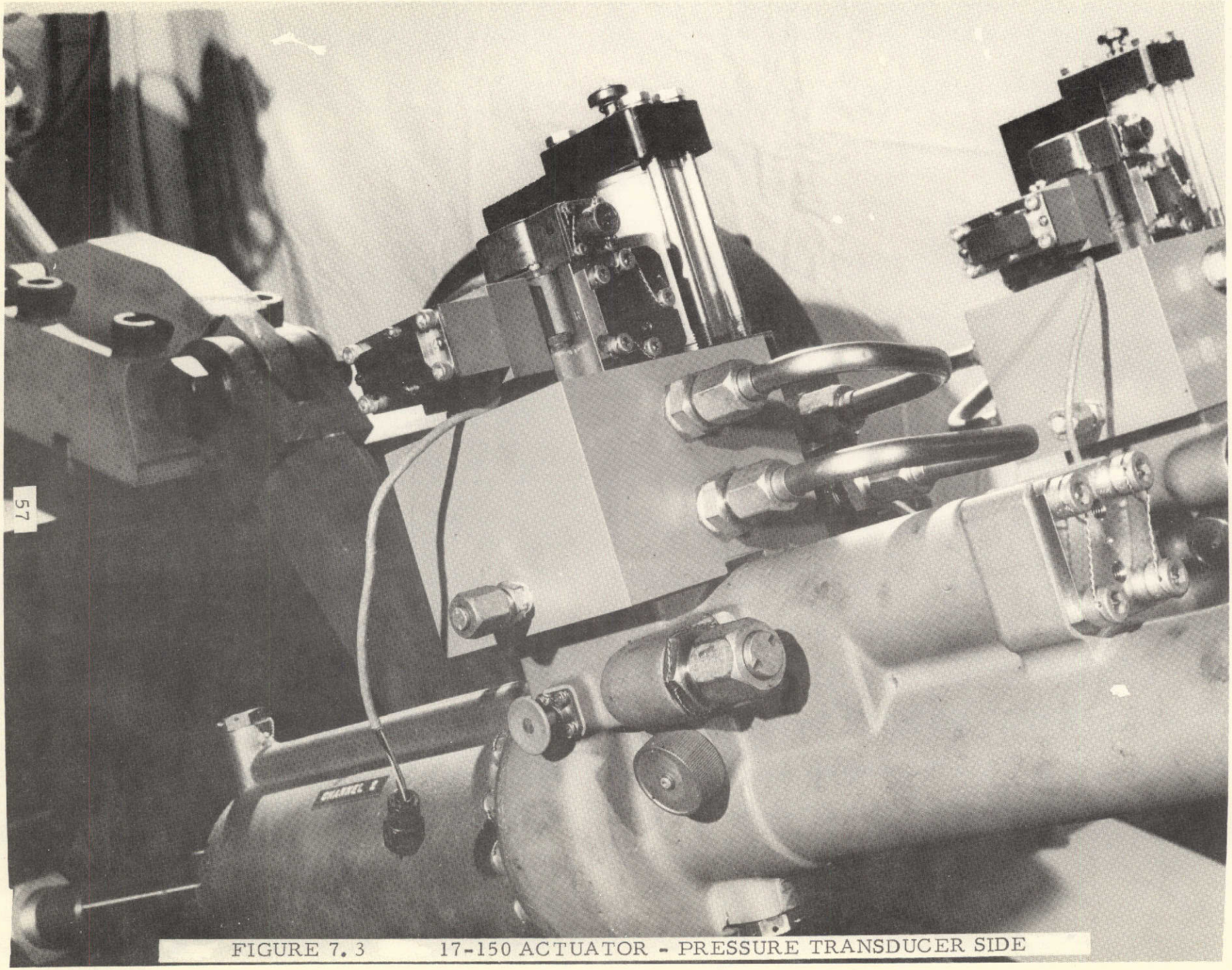

FIGURE 7.3 17-150 ACTUATOR - PRESSURE TRANSDUCER SIDE

Actuator position information (X) is provided by the standard potentiometer for the 17-150 actuator, which is located inside the piston rod. It is a linear film-type device with dual elements and a nominal electrical travel of 11.1 inches. Load position information (X_L and δ) is provided by a small rotary potentiometer mounted directly on one end of the crankshaft (see Figure 7.1). The pot is a film type with a nominal electrical travel of 340 degrees.

The channels are numbered with 1 and 2 opposing each other and 3 and 4 opposing each other. Channels 1 and 3 are on one side of the crankshaft, and 2 and 4 are on the other. The polarities of the excitation voltages for the actuator position and pressure transducers were reversed on channels 2 and 4, as well as the servovalve current. In this way, a positive elevon command signal (actually a negative command voltage) will cause channels 1 and 3 to extend while channels 2 and 4 retract. The actuator positions (X) are all defined as positive in this direction, as are the load pressures (ΔP) required to accelerate in this direction. The transducer outputs all have the same output magnitude and sign. The channels are matched well enough in both directions that nearly perfect force sharing can be obtained without equalization, over a wide range of operating conditions. This means that carefully- controlled amounts of interchannel mismatch can be introduced during the force- sharing experiments.

7.2 Electronic Hardware

An electrical schematic for the electronics of channel number 1 is shown in Figure 7.4. The other three channels are identical, except for the polarity differences noted in the figure. The simulator electronics are somewhat elaborate, to provide maximum flexibility for test purposes. This should not be interpreted as an indication that the force-sharing system is inherently complex; the basic electronics needed for flight hardware could be considerably simpler than shown in Figure 7.4.

It will be noticed that the circuitry for the mid-value computation is somewhat simpler than was used in the analog study (see Figure 6.3). This simplification was based on the design used in Reference 8, and seems to have very adequate accuracy. The reason for lagging the equalization output will be explained in Section 7.4. Another change from the analog circuitry is the addition of failure detection/correction logic. When the equalization output signal exceeds the preset threshold value, relay K1 is pulled in, which lights a failure indicator. If the mode selector (S1) is in the AUTO position, the channel is shut off when K1 pulls in, and

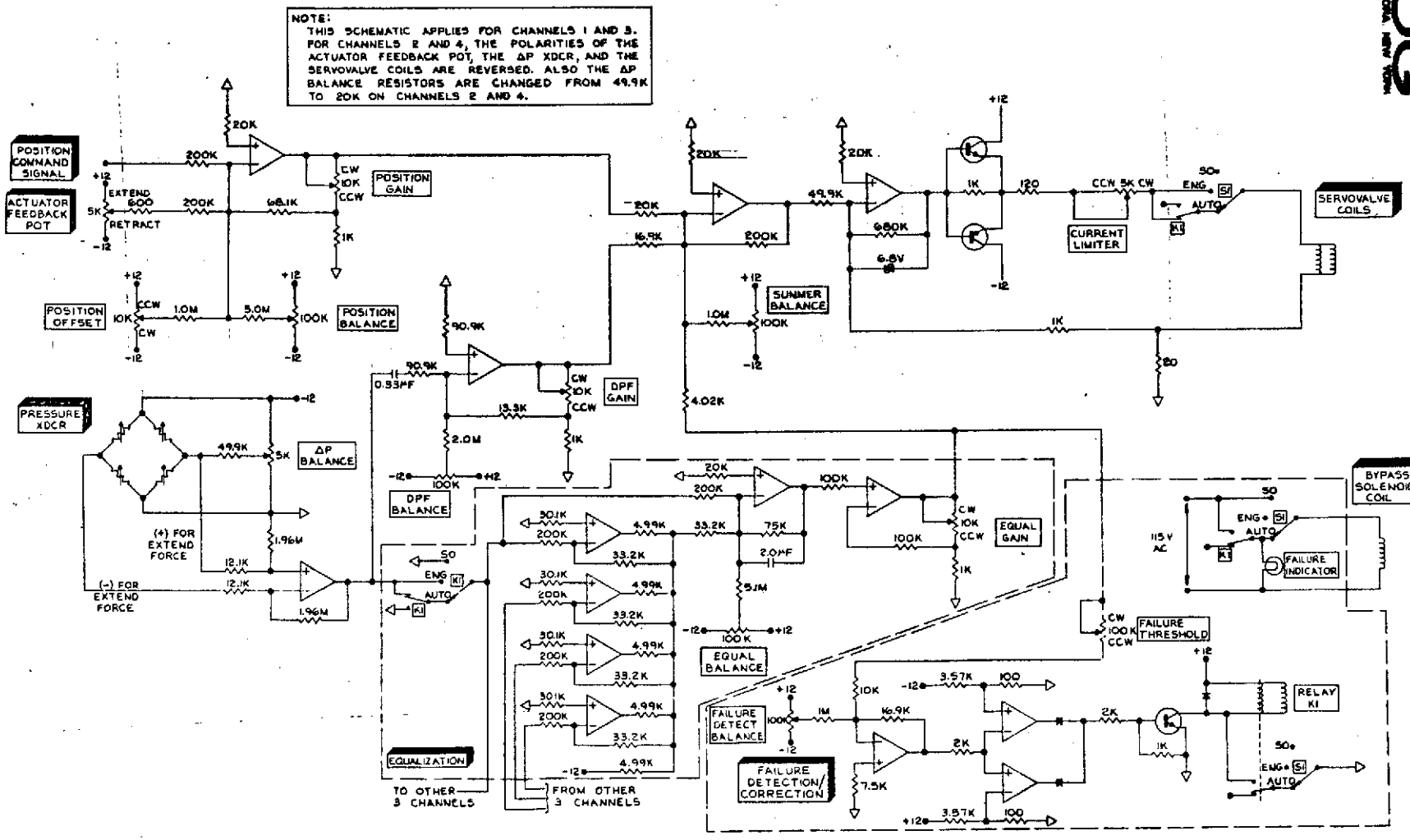

FIGURE 7.4 - SCHEMATIC OF SIMULATOR ELECTRONICS

K1 latches. In shutting off the channel, K1 performs three distinct functions: (1) the bypass solenoid valve is opened, (2) the servovalve coils are opened, and (3) the wire carrying the channel's load pressure signal to the other three channels is grounded. Once such an automatic shutoff has occurred, re-engagement of the channel can only be made by first correcting the source of the failure, and then switching the mode selector to ENGAGE and back to AUTO (this latter action resets the latch). The ENGAGE and SHUTOFF positions of the selector switch provide for manual engage or shutoff of a channel, independent of what the failure detector is doing.

For the simulator hardware, the schematic of Figure 7.4 is mechanized on a series of printed circuit cards. The card rack, power supply, and relays are all mounted in a small 19-inch relay rack. The front panel of the rack is shown in Figure 7.5. The top panel covers the front of the card rack, and the holes are for screwdriver adjustment of various trim pots mounted on the printed circuit cards. Below this are the remaining pots, the switches, and a very elaborate patch panel for each channel. Many of the interconnect wires between the printed circuit cards are brought out to the patch panel and jumpered by 2-pin shorting plugs (plugs removed on channel 1). In this way, the various circuits can be broken in strategic places by simply pulling a plug. This makes it easy to simulate failures, study open-loop characteristics, remove functional elements, calibrate the system, and take data. Appendix B shows schematics of the printed circuit cards and detailed interconnect wiring.

7.3 Basic Simulator Data

After calibration of the actuators, transducers, and electronics, the DPF and position loops were closed. The loop parameters were the same ones used during the analog study, except for K_{VD}, which was inadvertently set too high. (The error was discovered in the process of writing this report. Fortunately, subsequent measurements confirmed that lowering the gain to 58 sec^{-1} had little effect on actuator response.)

$$1/\tau_D = 33 \text{ rad/sec}$$

$$K_{VD} = 72 \text{ sec}^{-1}$$

$$K_{VX} = 40 \text{ sec}^{-1}$$

The elevon frequency responses for small command inputs are shown in Figure 7.6. These responses were measured directly from the potentiometer which senses crankshaft angular deflection, with all operating channels synchronized. By comparing these responses with the corresponding analog data (Figure 6.4), several differences are apparent. First, the position-loop bandwidths (frequency for 90° phase lag) are lower on the simulator.

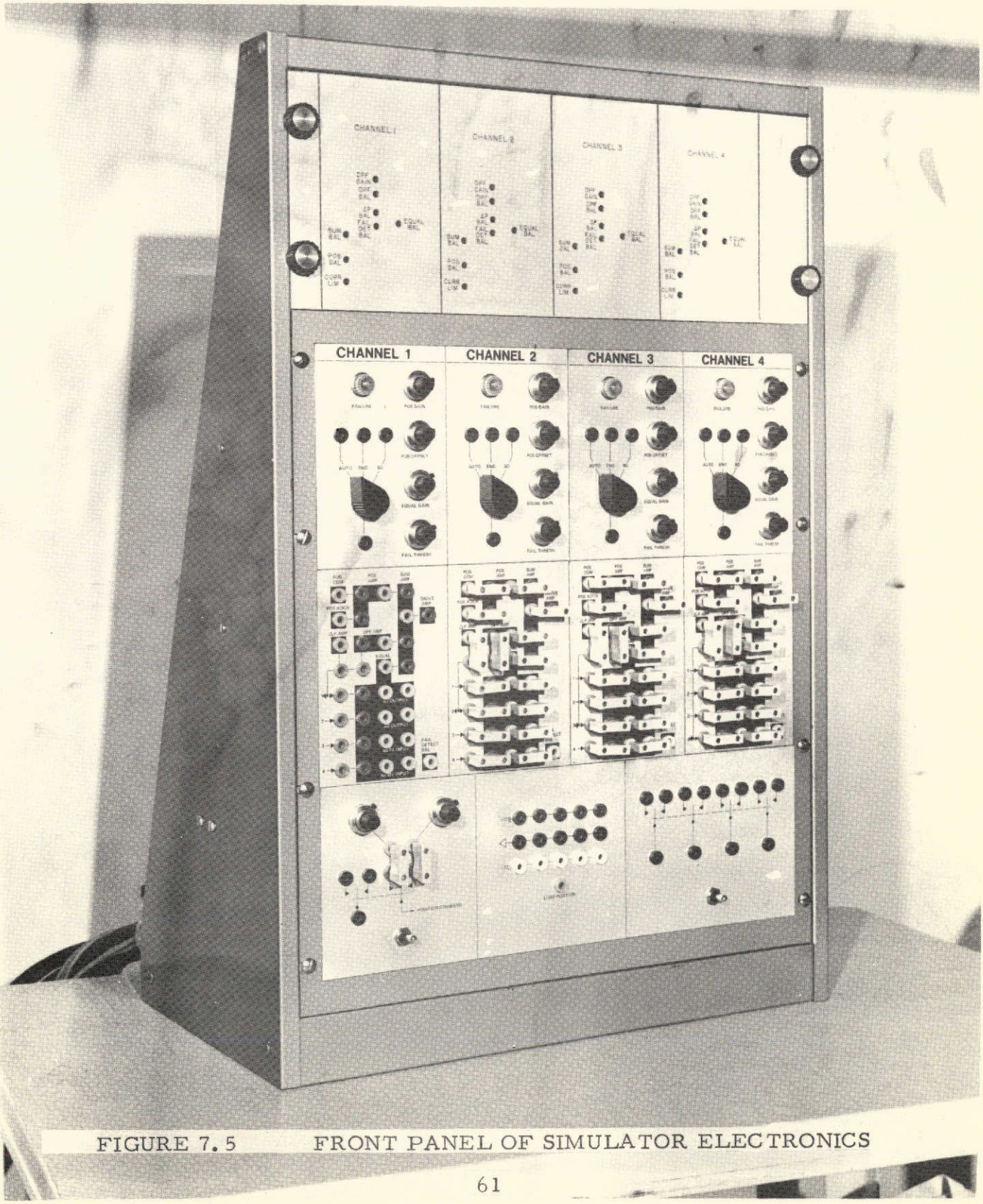

FIGURE 7.5 FRONT PANEL OF SIMULATOR ELECTRONICS

4 Channels Operating

Channels 1 and 2 Bypassed

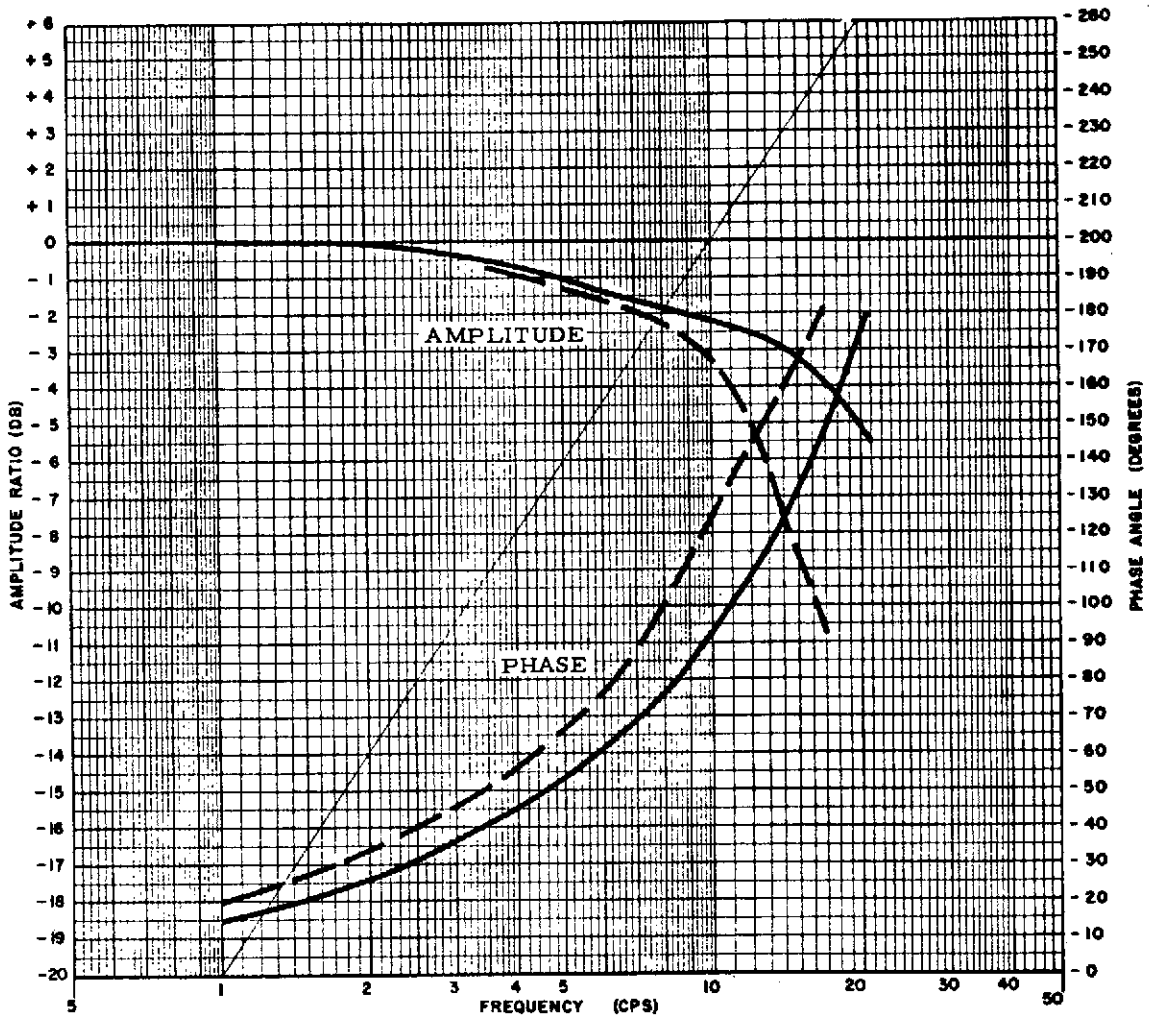

FIGURE 7.6 FREQUENCY RESPONSE OF CRANKSHAFT TO 1° P-P COMMAND SIGNALS

MOOG
MOOG INC., EAST AURORA, NEW YORK

Number Of Operating Channels	Analog	Simulator
4	15 Hz	10 Hz
2	11 Hz	7 Hz

For the 4-channel case, the primary sources of additional lag are the servovalve dynamics, which were not included in the analog study, and friction in the liquid springs. For example, the servovalve contributes 18 degrees of phase lag at 10 Hz (out of a total difference of about 25 degrees). With only two channels operating, the phase difference at 10 Hz is about 50 degrees. This large difference is due to viscous damping contributed by the bypass solenoid valves in the shutoff channels, which present a finite restriction to the bypass flow, even in the fully open position. The same factors also explain the reduced peaking in the amplitude data. The effects of increased viscous damping in the 2-channel data are particularly apparent.

Figure 7.7 shows the crankshaft response to 1° command steps for comparison with the analog data of Figure 6.5. The servovalve dynamics have caused a longer initial time delay and a somewhat slower rise time. Improved damping due to friction is also apparent in the 4-channel case, as are the effects of solenoid valve viscous damping in the 2- channel case.

The effects of removing the liquid springs are illustrated in Figure 7.8. It is clear that damping has been reduced somewhat, due to reduced friction. To demonstrate the effects of rate limiting, a 2° command step is shown in Figure 7.9, and a series of frequency responses are given in Figure 7.10 (refer to Figures 6.7 and 6.6 for a comparison with corresponding analog results). Crankshaft response data for load disturbance inputs were not taken becuase there is no convenient way to apply external loads to the crankshaft.

7.4 Simulator Equalization - Normal Operation

After the basic servoloops were checked out, the equalization loops were closed. As the equalization gain pots were opened up, the servovalve torque motors would start to buzz at K_{VE} on the order of 600 sec^{-1}. This is a problem because the desired value of K_{VE} is 710 sec^{-1}. The fundamental frequency of the buzzing would abruptly change from approximately 650 Hz

4 Channels Operating

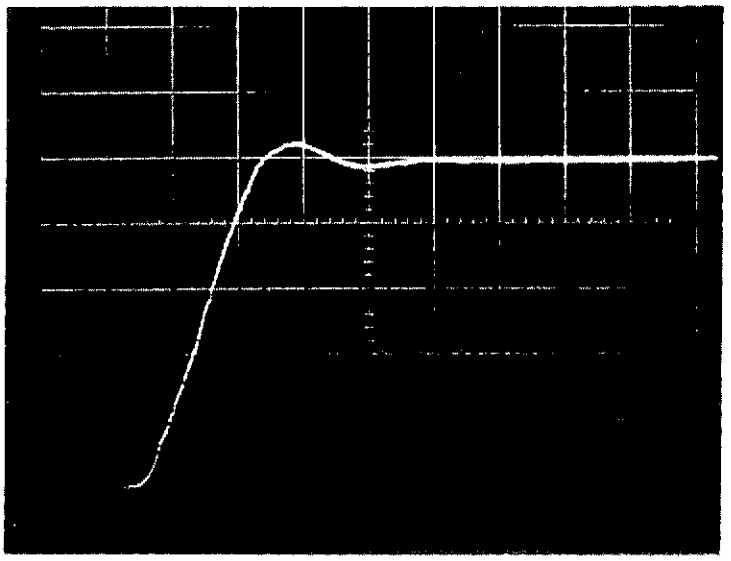

Scales :

0.2 deg/div (vert)

0.02 sec/div (hor)

Channels 1 and 2 Bypassed

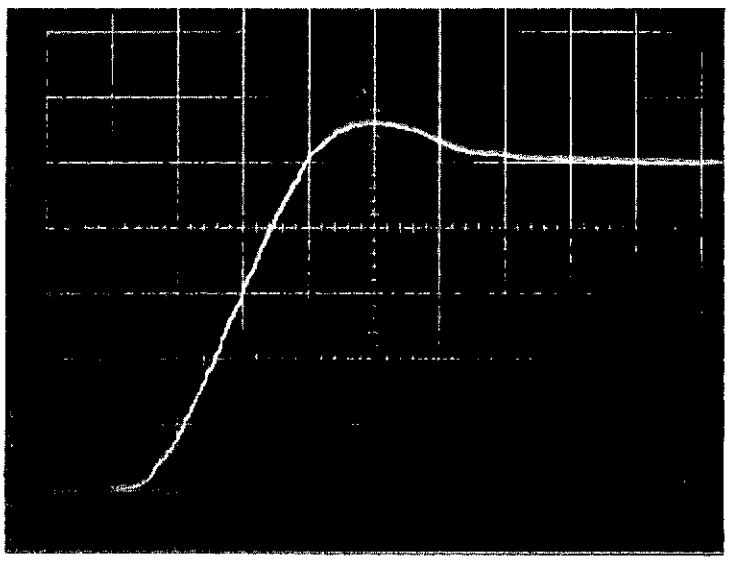

FIGURE 7.7 CRANKSHAFT RESPONSE TO + 1° COMMAND STEP

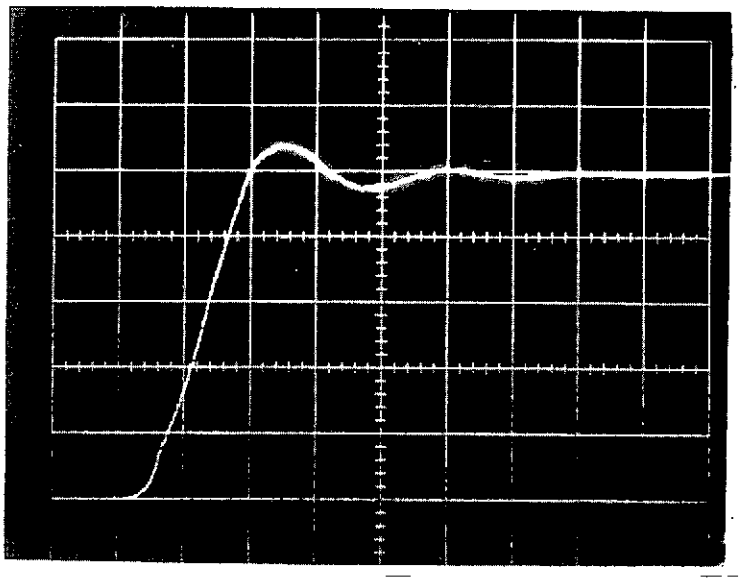

Scales :

0.2 deg/div (vert)

0.02 sec/div (hor)

FIGURE 7.8 +1° COMMAND STEP - LIQUID SPRINGS REMOVED

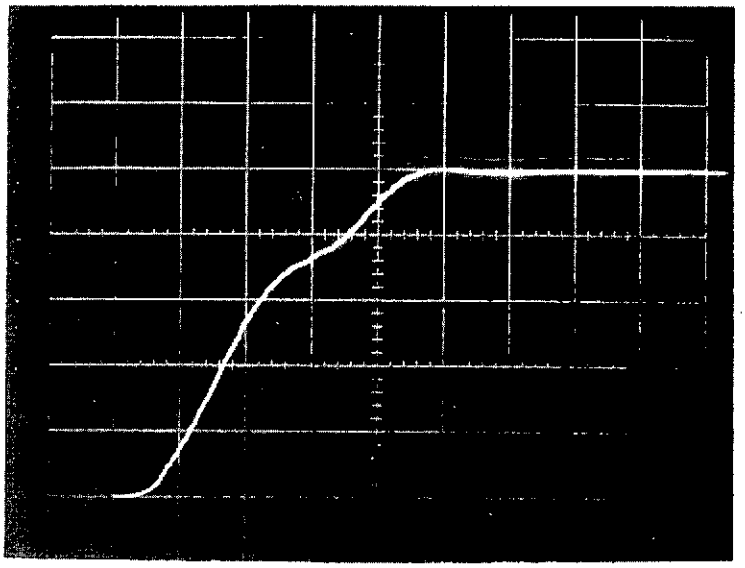

Scales :

0.4 deg/div (vert)

0.02 sec/div (hor)

FIGURE 7.9 CRANKSHAFT RESPONSE TO + 2° COMMAND STEP

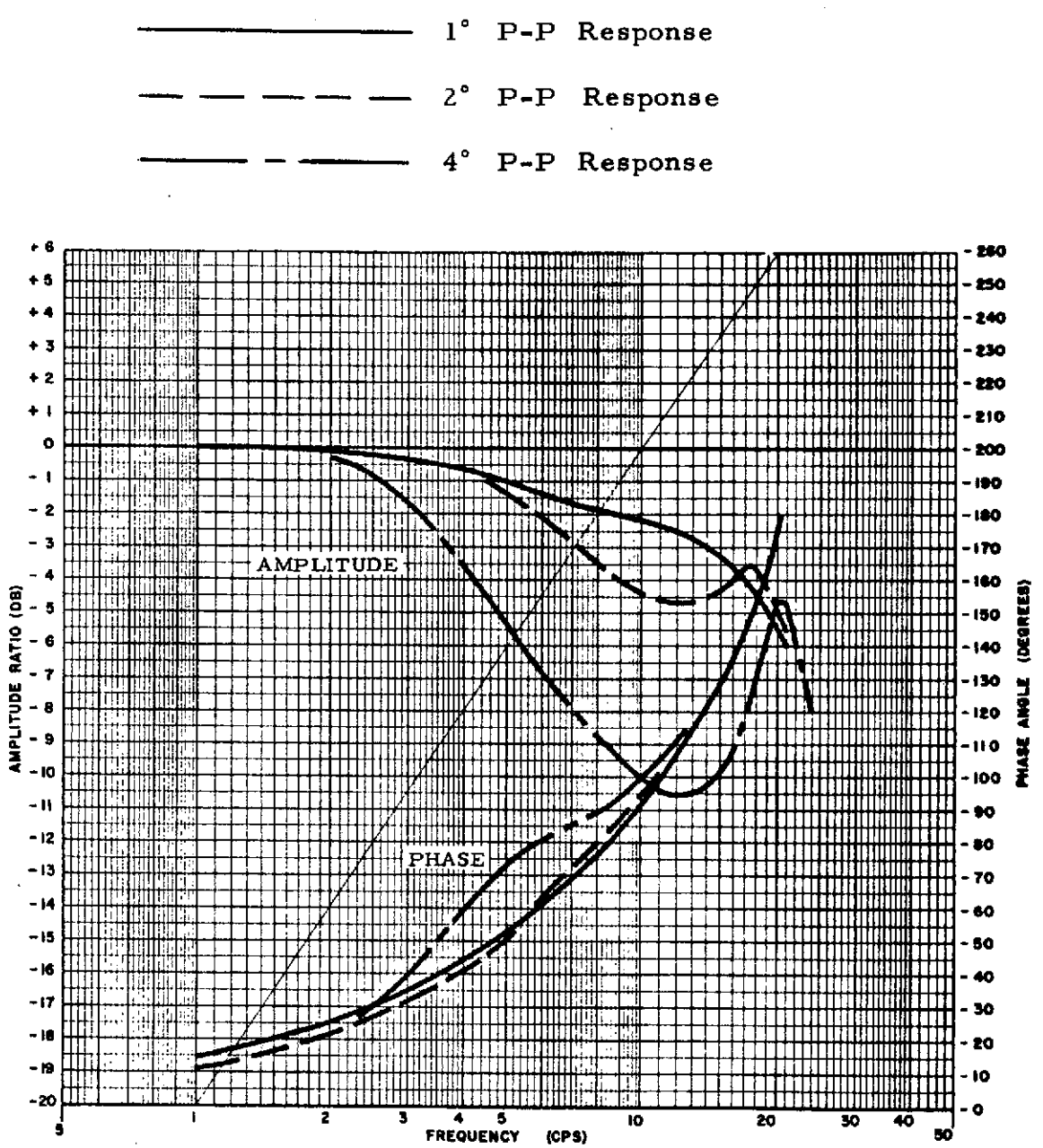

FIGURE 7.10 EFFECTS OF RATE LIMITING ON CRANKSHAFT FREQUENCY RESPONSE

to approximately 350 Hz as gain was changed slightly. The buzzing could be measured as a load-pressure limit cycle with a peak-to-peak amplitude of about 100 psi. Of course, this limit cycle would never show up on the crankshaft pot output, but it was certainly not doing the servovalve torque motors any good.

The first attempt at a fix was to assume that the instability was simply caused by the torque motor resonance. Therefore, a first-order low-pass filter was applied to the equalization output (break frequency at 40 Hz). The system would then oscillate at a loop gain of about 200 sec^{-1}, at a frequency of about 40 Hz. A quick look at pressure loop dynamics confirmed that this behavior should not be possible. Finally, a combination of pressure loop measurements and analytical work uncovered a rather complex stability problem at frequencies well above the load resonance. The problem encountered on the simulator is believed to be typical of high-gain pressure loops in general, and a detailed analysis is therefore given in Appendix A. The outcome of this analysis was that the only practical solution, in the present application, is to filter the equalization output with a first-order breakpoint at 1 Hz. Actually, it may be desirable to filter the equalization even further to obtain smoother failure transients, but the 1 Hz breakpoint certainly constitutes an upper limit.

With the equalization stability problem resolved, K_{VE} was set at 710 sec^{-1}, and the "worst case" offset conditions defined in Section 2.0 were applied. The nulls of channels 1 and 3 were offset + 10% of full stroke, while channels 2 and 4 were not offset. As defined in Section 7.1, positive values of X and δ require a negative command voltage. Therefore, the command voltage to channels 1 and 3 was biased $(-.10\, S_P\, K_X) = -1.65$ v. The choice of channels 1 and 3 as the offset channels was made to minimize side loads on the crankshaft bearings. Since channels 1 and 2 were offset in the analog study, the reader is reminded to compare channel 2 data (analog) with channel 3 data (simulator), and channel 3 data (analog) with channel 2 data (simulator).

When the equalization loops and offset conditions were finally set up, the following static data were obtained for zero command input.

Measured Output	No Equalization	MVE
δ ~ deg	+ 3.1	+ 6.2
ΔP_1 ~psi	+ 2950	+ 300
ΔP_3 ~psi	+ 3000	+ 300
ΔP_2 ~psi	- 2880	0
ΔP_4 ~psi	- 2690	- 20
ΔP_{av}	+ 95	+ 145
$Max(\Delta P_n - \Delta P_{av})$	2975	165
ΔP_{mid}	—	+ 300

As in the analog study, these data show that the mid-value equalization has reduced the force fight form nearly 100% to about 5%. This degree of force sharing is maintained over the full output range of the system. (When interpreting load pressure data from the simulator, the reader should bear in mind that the absolute accuracy of the measurements is on the order of ± 50 psi.)

Figure 7.11 shows the crankshaft response to small command steps (channel 1 and 3 nulls still offset + 10%). Without equalization, the response is quite sluggish. The equalization removes the effects of interchannel mismatch effectively enough that the step response is virtually identical to the response with all channels perfectly synchronized (Figure 7.7). The load pressure responses for these same step inputs are given in Figure 7.12.

7.5 Simulator Equalization-Hardover Failures

Numerous combinations of hardover failures, followed by manual shut offs, were examined to determine the most cirtical sequence. The most critical sequence is the same as determined in the analog study: channel No. 1 hardover (-), No. 1 shutdown, No. 2 hardover (+), No. 2 shutdown (remember that the operational states of channels 2 and 3 were traded

With Equalization (MVE)

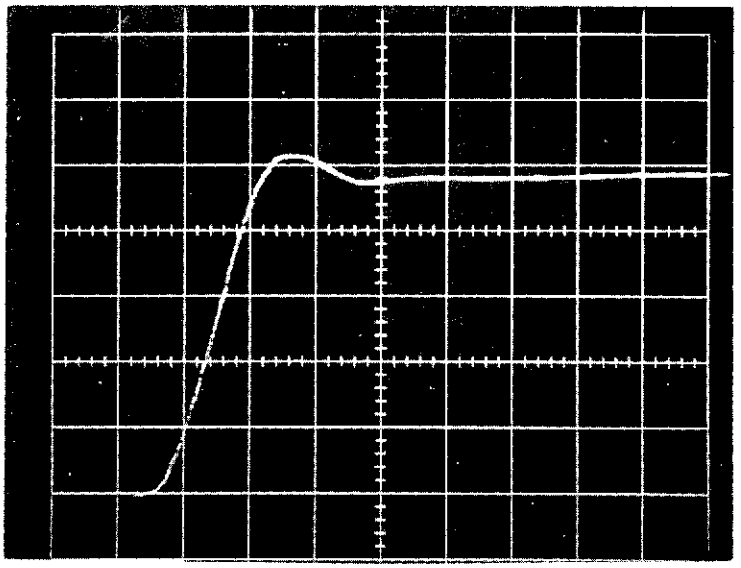

Scales :

0.2 deg/div (vert)

0.02 sec/div (hor)

No Equalization

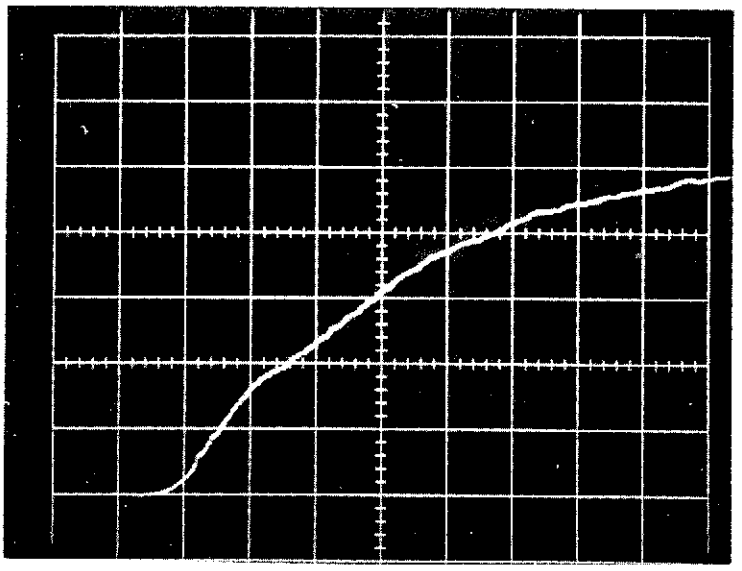

FIGURE 7.11 EFFECT OF EQUALIZATION ON CRANKSHAFT RESPONSE TO + 1° STEP COMMAND

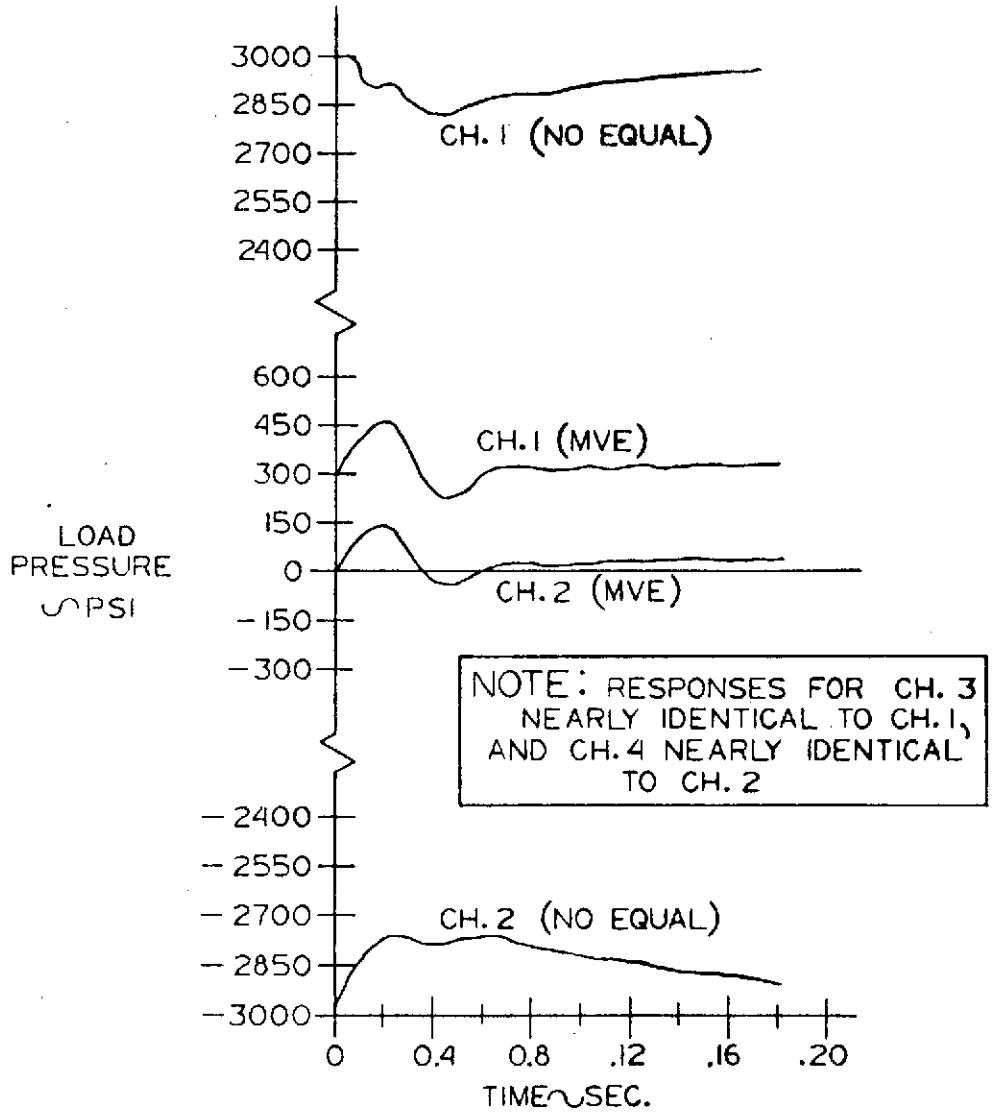

FIGURE 7. 12 EFFECT OF EQUALIZATION ON LOAD PRESSURE RESPONSE TO + 1° CRANKSHAFT STEP COMMAND

MOOG
MOOG INC., EAST AURORA, NEW YORK

in going from the analog study to the simulator). The hardover failures were simulated by patching a large voltage directly into the drive amplifier, thereby forcing the servovalve wide open in the appropriate direction. Shutdown of a channel was accomplished manually with the appropriate mode selector switch. The resulting steady-state crankshaft deflections are presented in the following table.

	Crankshaft Deflection ~ Deg.				
Equalization	Before Failures	$\Delta P_1 \rightarrow$ -3000	No. 1 Shutoff	$\Delta P_2 \rightarrow$ + 3000	No. 2 Shutoff
None	+ 3.1	0	+ 1.5	+ 6.1	+ 3.1
MVE	+ 6.2	- 0.7	+ 0.2	+ 8.0	+ 0.3

This data is very similar to the analog data of Section 6.3.

The steady-state load pressure changes for this hardover sequence were also measured, and are as follows. Note that the mid-value pressures given are the values computed by the mid-value logic.

Change	Equal.	ΔP_1	ΔP_3	ΔP_2	ΔP_4	ΔP_{mid}*
None	None	+2950	+3000	-2880	-2690	—
"	MVE	+300	+300	0	- 20	+300
$\Delta P_1 \rightarrow$ -3000	None	-3000	+3000	- 20	+ 70	—
"	MVE	-3000	+1140	+820	+850	+850
No. 1 Shutoff	None	0	+3000	-1470	-1300	—
"	MVE		+240	- 70	- 50	- 50
$\Delta P_2 \rightarrow$ +3000	None		+600	+3000	-2950	—
"	MVE		-890	+3000	-1240	-890
No. 2 Shutoff	None		+3000	0	-2620	—
"	MVE		+200	0	- 90	- 90

* Computed by MVE logic

As with the analog results, this table shows that the equalization continues to hold force fight to minimum, even after failed channels are shut down. During the sequence, the failure detection thresholds were set at 500 psi. The failure indicator light in the appropriate channel came on promptly as each failure occurred, and it stayed lit. Throughout the sequence, there was not even a momentary failure indication in the unfailed channels. Of course, this failure detection behavior could be predicted by the foregoing load pressure data.

The crankshaft transient responses for the foregoing failure sequence are given in Figure 7.13. There are a number of differences between these transients and the analog transients of Figure 6.13. First, all the transients exhibit fewer oscillatory tendencies; this is due to friction and additional viscous damping, as discussed in Section 7.3. The other difference is that the hardover transients are much slower on the simulator than on the analog. After studying the data, it became apparent that the difference was due to incorrect mechanization of hardover failures on the analog computer. The analog failures were mechanized by suddenly sending a channel's load pressure to plus or minus 3000 psi. In real life, however, it takes a finite time for the load pressure to change because oil must first flow to wind up K_S. This effect could have been accounted for if the analog hardovers were mechanized in the same way that they were mechanized on the simulator, i.e. introduction of a large current into the servovalve. The shutoff transient data for the analog compares reasonably well with the simulator because sending a channel's load pressure to zero is a fairly accurate reproduction of the bypass solenoid valve's function (the time delay in the simulator data is the response time of the solenoid valve).

Transient data for the same hardover sequence, but using the automatic shutoff feature, is given in Figure 7.14. The small-signal crankshaft response to command inputs, after both channels are shut off, is shown in Figure 7.15. With equalization, the response is nearly the same as when the two operating channels are perfectly synchronized (see Figure 7.7). However, with no equalization, the response is very sluggish.

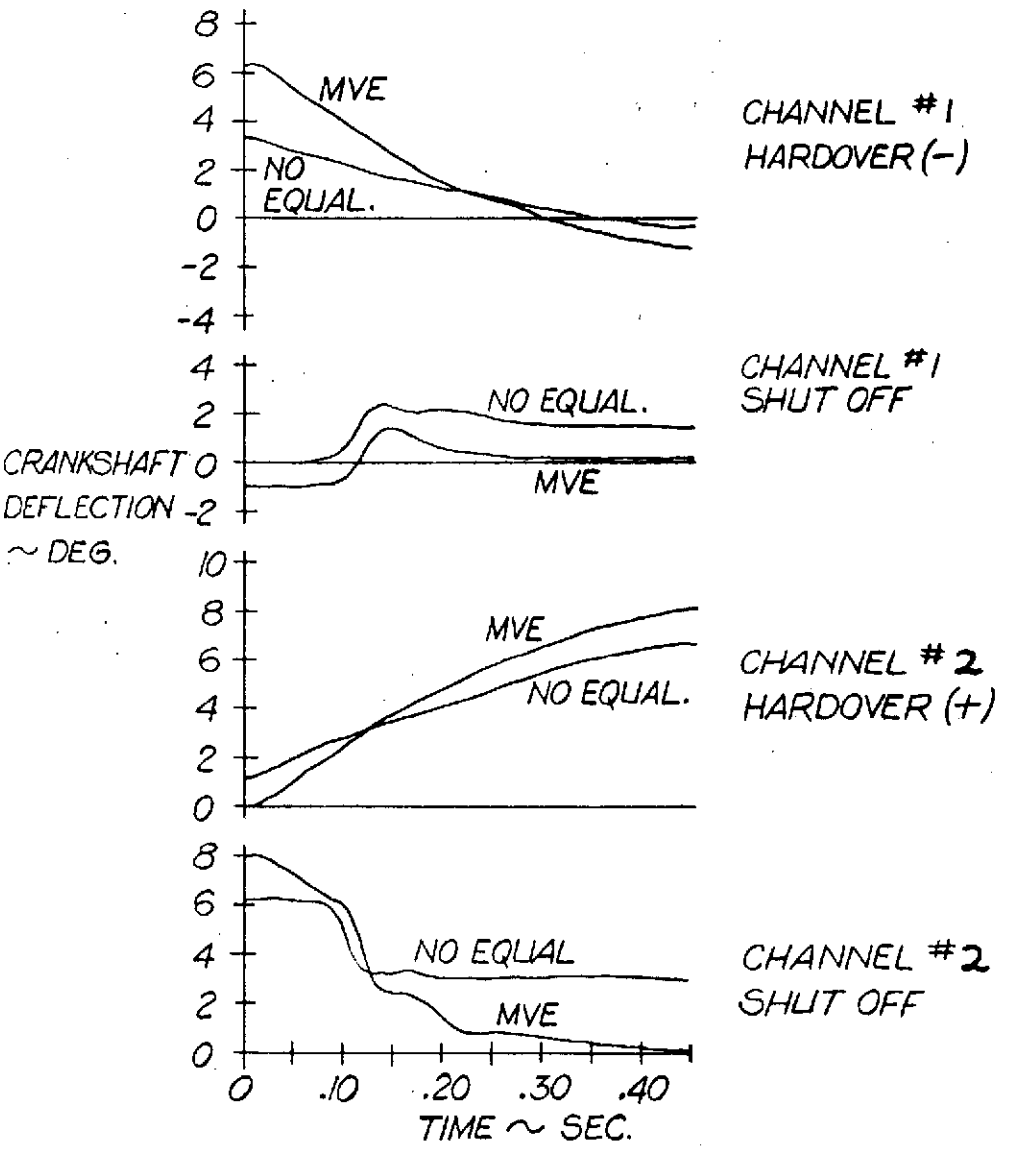

FIGURE 7.13 EFFECT OF EQUALIZATION ON RESPONSE TO A SERIES OF HARDOVER FAILURES AND SHUTDOWNS

Channel # 1 Hardover (-)

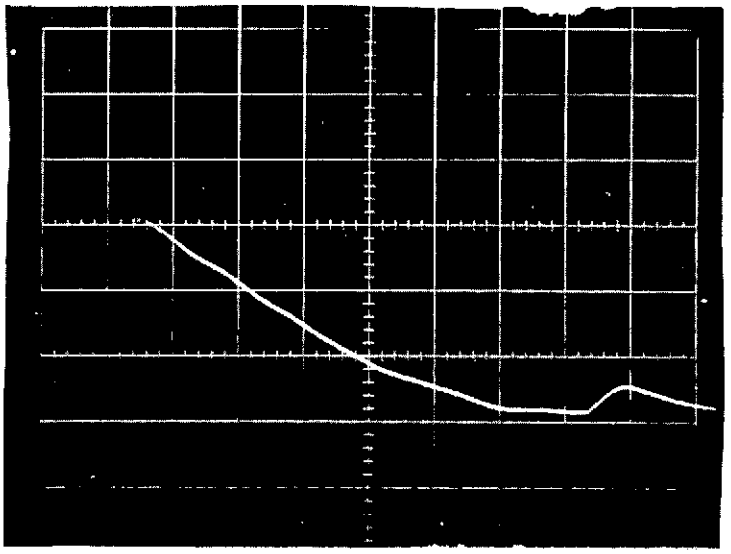

Scales :
2.0 deg/div (vert)
(middle line is +4°)
0.05 sec/div (hor)

Channel # 2 Hardover (+)

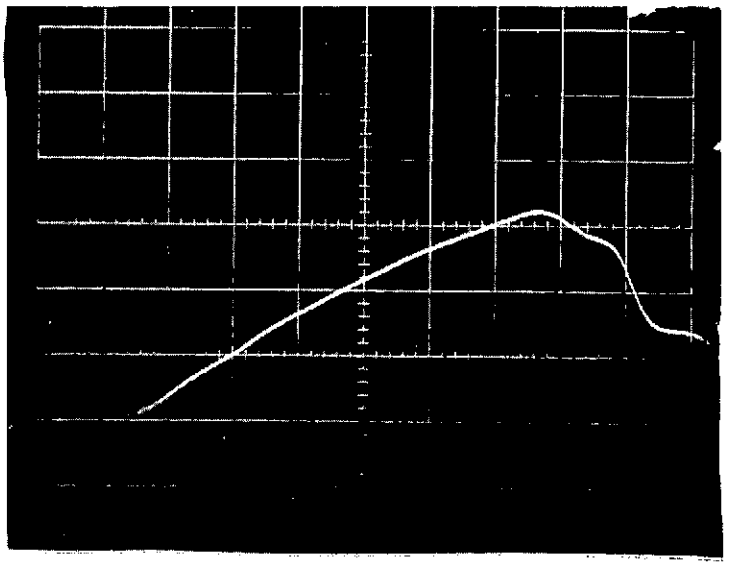

FIGURE 7.14 CRANKSHAFT RESPONSE TO A SERIES OF HARDOVER FAILURES WITH AUTOMATIC SHUTDOWNS

With Equalization (MVE)

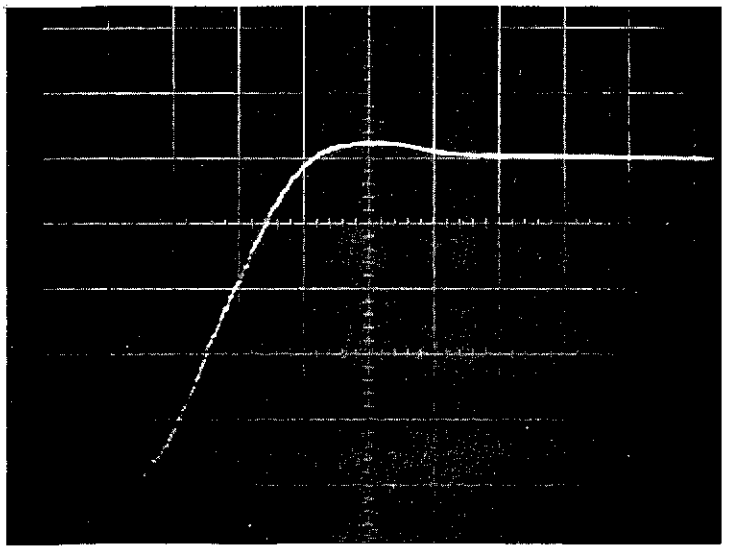

Scales :

0.2 deg/div (vert)

0.02 sec/div (hor)

No Equalization

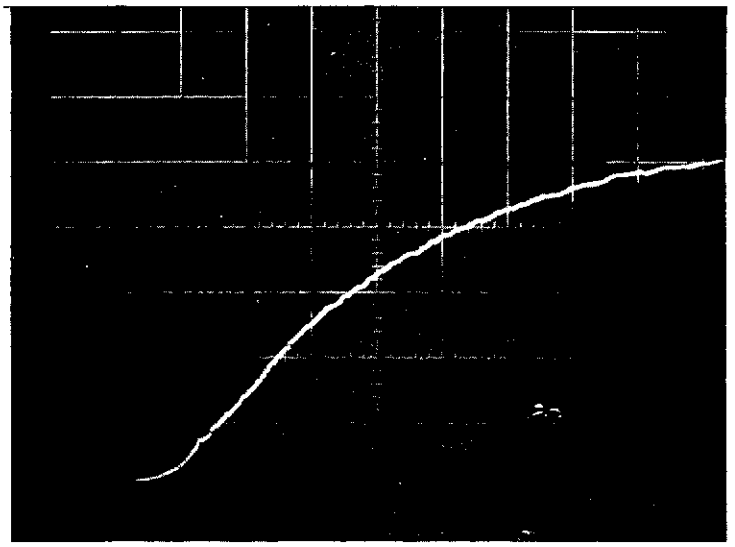

FIGURE 7.15 EFFECT OF EQUALIZATION ON CRANKSHAFT RESPONSE TO + 1° STEP COMMAND (CHANNELS 1 AND 2 SHUTOFF)

7.6 Simulator Failure Detection

As mentioned in Section 7.5, the failure detection logic functioned very satisfactorily during all hardover failures and shutdowns. However to more completely evaluate the logic, it was deemed necessary to also investigate the detectability of various failures in the equalization logic itself. The static crankshaft deflections for various equalization failures in channel 1 are shown below, for various pre-failure offsets in channels 1 and 3.

Failure	Crankshaft Deflection ~ Deg.		
	+10% Offset	Zero Offset	-10% Offset
None	+ 6.2	0	- 0.3
Equal. output open	+ 6.4	0	- 1.4
Equal output hardover *	- 0.7	- 0.8	+ 1.0
ΔP amp. output open	+ 1.2	+ 1.0	+ 0.7
ΔP amp. output hardover *	+ 1.1	- 0.8	+ 0.6
ΔP_{mid} output open	- 1.0	- 1.3	- 1.4
ΔP_{mid} output hardover *	- 0.7	- 1.3	+ 1.0
ΔP negative feedback open	+ 7.5	+ 1.3	+ 1.0

* Hardover in most critical direction

These transients are comparable with those obtained for hydraulic hardovers. Notice that the values given are considerably different than the values obtained for similar failures on the analog computer (see Section 6.4). This is due to the fact that the various equalization voltages which are being failed are based on ΔP_n for the analog computer, while the corresponding simulator voltages are based on $(\Delta P_n + P_s)$.

With the failure detection thresholds set at 500 psi, none of the foregoing equalization failures generate a false failure indication in an operating channel, even momentarily. The failure indicator light in the faulty channel (No. 1) came on promptly with most of the failures, and it stayed

lit. However, there are two types of failures which do not result in a positive failure indication. The first is when the equalization output goes open. With the offsets of channels 1 and 3 initially + 10% or zero, no failure indication occurs at all. This is no great problem since the failure is passive in these cases (the equalization output was near zero to begin with). As soon as equalization is required in the failed channel, a failure indication results. The second problem occurs when the ΔP_{mid} output goes open. In this case, no failure indication is given statically, but a momentary indication occurs during the failure transient, which is sufficient to shut off the channel if the mode selector switch is in the AUTO position. Also, any subsequent rapid command input will generate a momentary failure indication in the faulty channel.

On the basis of the failures examined to date, it appears that the MVE provides a simple and reasonably positive method for identifying failures.

8.0 CONCLUDING REMARKS

The feasibility of obtaining a high degree of force sharing in parallel high-stiffness servoactuators, without the use of secondary actuators, has been clearly demonstrated. The major advantages of the equalization scheme described in this report are as follows.

- A very high degree of force sharing is attainable, without degrading system response or output stiffness.
- It is not necessary that the individual channels be physically located close together.
- Because the system is an all-active type, it is inherently fail-operative after the first failure, even in the absence of detection/correction logic.
- The failure detection/correction logic is relatively simple and gives positive indications for a wide range of failure types, including transducer failures.
- Since the equalization is mechanized electronically, the mechanical hardware is of minimal complexity. The additional electronics required by the equalization are quite straightforward.

The primary disadvantage of the system is that the main pistons must be oversized unless reduced force output capability is acceptable when failed channels are shut off. In contrast, a system employing secondary actuators retains full force output capability as channels are shut off. The oversized pistons may more than offset the weight saved by deleting the secondary actuators.

With regard to the possibility of common failure modes, it is not clear to the author whether the interchannel mechanical connections of the secondary actuator approach or the electrical interchannel connections of the proposed approach are inherently more reliable. What is clear is that arguments on the subject could easily go on forever. As is usually the case, the relative merits of the available approaches must be evaluated for each specific application.

REFERENCES

1. Anon., Redundant Electrohydraulic Servoactuators, Moog Report MR-1275A, Feb. 1970.

2. Robert H. Hurlow, Multiple-Channel Actuation System for the Boeing 2707 SST Horizontal Tail, AIAA Paper no. 70-915, July 1970.

3. L.R. Tomlinson and R.L. Schoenman (Boeing), Control Systems Mechanizations for the USA Supersonic Transport, Presented at the SAE Control and Guidance Systems Committee, Philadelphia, Pa., 23September 1971.

4. Gordon D. Smith, Servoactuator Study for Space Shuttle Applications, General Dynamics/Convair Report no. GDC-DCB70-014, September 1970.

5. Anon., Horizontal Tail Design Status Review, Bertea Corp. Informal Brochure, November 1969.

6. J.R. Horsnell, The SST Flight Control System Concept, AIAA Paper no. 67-570, August 1967.

7. Jack E. Emfinger, Fly-By-Wire Redundant Actuator, Sperry-Rand magazine, date not known.

8. Jack E. Emfinger, A Prototype Fly-By-Wire Flight Control System, USAF Report AFFDL-TR-69-9, August 1969.

9. F.L. Miller and J.E. Emfinger, Fly-By-Wire Techniques, USAF Report AFFDL-TR-67-53, June 1967.

10. O.D. Branson and R.K. VanAusdal, Study of Load Pressure Synchronization of 3 Channel Hydraulic Actuators, Bendix/Electrodynamics Report no 7-2045, April 1966.

11. Gordon D. Smith, Servoactuator Configuration Study for Booster Flight Controls (WBS Element 0.3.3.5), General Dynamic/Convair Report no. 76-549-1-048, May 1971.

REFERENCES (CONT'D)

12. N. Saslove, Space Shuttle Servoactuator Study: an Annotated Bibliography, General Dynamics/Convair Report no GDC-DCB70-013, July 1970

13. G. E. Amies, Cecil Clark, et. al. , Survivable Flight Control System; Interim Report No. 1, Studies, Analyses, and Approach, USAF Report AFFDL-TR-71-20 (Supplement - 3), May 1971.

14. Anon. , Preliminary Presentation of a Survivable Flight Control System for the Stabilator Surface Using a Passive Synchronization Technique, Bendix/Electrodynamics (no report no. , no date).

15. J. E. Rinde, P. S. Coppola, et. al. , Investigation and Development of Redundancy Techniques to Achieve Dual Fault Corrective Capability in Flight Control Actuators, USAF Report AFFDL-TR-67-17, June 1967.

APPENDIX A: ANALYSIS OF PRESSURE LOOP STABILITY

The equalization stability problem described in Section 7.4 was first attacked by looking at basic pressure loop dynamics. To simplify both analysis and measurements, it is convenient to consider the case of only one actuator connected to the load (the other 3 actuators and the liquid springs disconnected from the crankshaft). Since the stability problem occurs at frequencies well above the load resonance, this simplification should not appreciably affect the results.

The basic pressure loop dynamics can be readily obtained from Figure 5.2 by neglecting K_{PQ}, B_L, K_L, F_2, F_3, F_4, F_D, and non-linearities. Considering the equalization as a simple proportional feedback, the equalization loop of Figure 5.2 can be rearranged as in Figure A-1.

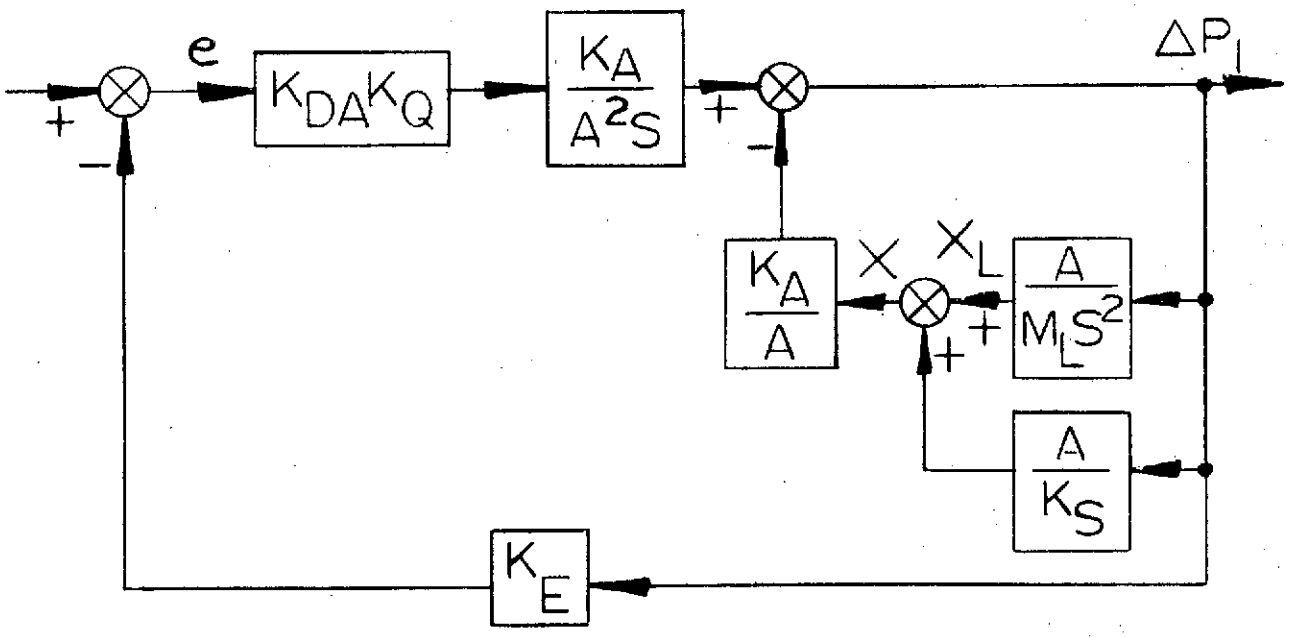

FIGURE A-1 BASIC PRESSURE LOOP DYNAMICS

Closing the inner loops, the forward loop becomes:

$$\frac{\Delta P_1}{e} = \left[\frac{\left(K_{DA}K_Q\right)\left(\frac{M_L}{A^2}\right) S}{\left(\frac{M_L}{K_T}\right) S^2 + 1}\right] \quad , \quad \frac{K_T}{M_L} = \omega_L{}^2$$

Actually, the poles have some damping due to K_{PQ} and friction, but the high frequency behavior is of primary interest. At frequencies well above ω_L, the pressure loop transfer function looks like an integrator.

$$G_{OL} = K_E \left(\frac{K_{DA}\, K_Q\, K_T}{A^2}\right)\left(\frac{1}{S}\right) = \left(\frac{K_{VE}}{S}\right)$$

This loop cannot be driven unstable, even at infinite gain. Even if the servovalve dynamics are considered, loop gains (K_{VE}) in excess of 4000 sec^{-1} should be possible.

At this point, detailed frequency response measurements were made for each actuator (with the others disconnected from the crankshaft) by putting a signal into the drive amplifier and looking at the output of the ΔP amplifier. The oscilloscope patterns were rather poor, especially for small input signals. However, by using an oscilloscope and a frequency analyzer, credible data was obtained for a drive signal equivalent to 5.0 ma (P-P). The data showed much higher amplitude at high frequencies than was expected. This suggested the possibility of structural modes.

The most obvious structural mode is the mass of the actuator body suspended between K_A and K_S. This can be modelled as in Figure A-2.

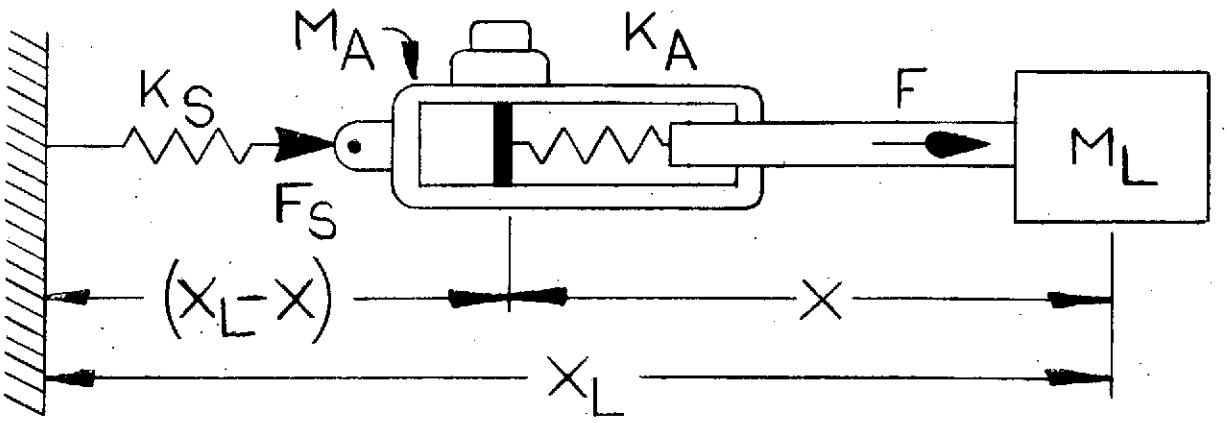

FIGURE A-2 DYNAMIC MODEL - - STRUCTURAL MODES

MOOG
MOOG INC., EAST AURORA, NEW YORK

Developing the dynamic equations for this model, as was done for the simpler model in Section 5.2, it is seen that the only change is in the relationship between X, X_L, and ΔP.

$$F_S = -(X_L - X)\,K_S$$

$$A\Delta P = F = F_S - M_A S^2 (X_L - X) = (M_A S^2 + K_S)(X - X_L)$$

$$X = X_L + \left(\frac{A\Delta P}{M_A S^2 + K_S}\right)$$

Thus, the block diagram of Figure A-1 is modified by replacing the (A/K_S) term with $\left[A/(M_A S^2 + K_S)\right]$. When this is done and the inner loops are closed, the forward-loop transfer function becomes fourth-order. Making the assumption that the poles are well-separated, the transfer function can be approximately factored, with the following result:

$$\frac{\Delta P_1}{e} = \frac{(K_{DA}K_Q)\left(\frac{M_L}{A^2}\right) S \left[\left(\frac{M_A}{K_S}\right) S^2 + 1\right]}{\left[\left(\frac{M'_L}{K_T}\right) S^2 + 1\right]\left[\left(\frac{M_A}{K'_A}\right) S^2 + 1\right]}$$

Where $$M'_L = M_L \left(1 + \frac{M_A}{M_L}\right)$$

$$K'_A = K_A \left(1 + \frac{K_S}{K_A}\right)\left(1 + \frac{M_A}{M_L}\right)$$

At frequencies above the load resonance, the pressure loop characteristics are:

$$G_{OL} = \left(\frac{K_{VE}}{1 + \frac{M_A}{M_L}}\right) \frac{\left[\left(\frac{M_A}{K_S}\right) S^2 + 1\right]}{\left[\left(\frac{M_A}{K'_S}\right) S^2 + 1\right]}$$

Thus, the primary effect of the actuator mass is to add a complex pole-zero combination. Of course, these terms will actually have finite damping.

MOOG

The value of M_A was determined from the natural frequency of the complex zeros, which show up very clearly in the data as a sharp inverted peak. The natural frequency is 40 Hz, which yields $M_A = K_S/(2\pi\ 40)^2 = 0.69$ lb-sec^2/in. This is approximately ten times the mass of the actuators themselves. The reason for this is that the leaf springs themselves contribute considerable effective mass to M_A, and a rough calculation confirms that 0.69 is the correct order of magnitude. With M_A determined, the calculated natural frequency of the structural poles is 97 Hz. (Notice also that the presence of M_A reduces the calculated value of ω_L to 10.6 Hz, which is exactly the value measured in Section 7.1.) Recognizing that the expression used to calculate the pole natural frequency is crude at best, the frequency was varied to obtain a curve fit to the measured frequency response data. In addition, at least one other structural mode is clearly evident in the data. Without trying to ascertain the exact source of this mode, another complex pole-zero combination was added to the transfer function. By including servovalve dynamics and adjusting the natural frequencies and damping ratios of the structural modes, the following complete transfer function was obtained.

$$G_{OL} = G_L\ G_1\ G_2\ G_{SV}$$

$$G_L = \left[\frac{\left(\frac{K_{VE}}{4920}\right) S}{\left(\frac{S}{2\pi(10.6)}\right)^2 + \frac{2(0.03)}{2\pi(10.6)} S + 1}\right]$$

Load Dynamics

$$G_1 = \left[\frac{\left(\frac{S}{2\pi(40)}\right)^2 + \frac{2(0.20)}{2\pi(40)} S + 1}{\left(\frac{S}{2\pi(120)}\right)^2 + \frac{2(0.40)}{2\pi(120)} S + 1}\right]$$

First Structural Mode

$$G_2 = \left[\frac{\left(\frac{S}{2\pi(160)}\right)^2 + \frac{2(0.30)}{2\pi(160)} S + 1}{\left(\frac{S}{2\pi(300)}\right)^2 + \frac{2(0.30)}{2\pi(300)} S + 1}\right]$$

Second Structural Mode

$$G_{SV} = \left[\frac{1}{\left[\frac{S}{2\pi(45)} + 1 \right] \left[\left(\frac{S}{2\pi(1000)} \right)^2 + \frac{2(0.50)}{2\pi(1000)} S + 1 \right]} \right]$$

Servovalve Dynamics

A Bode plot of this open-loop transfer function is shown in Figure A-3 for a loop gain of 100 sec^{-1}. Also shown in the figure are the measured data from the most representative actuator (channel 3). It is apparent that the curve fit is quite good for frequencies up to about 400 Hz. Above this value, the data is of questionable accuracy and servovalve resonant modes begin to appear (the latter are not adequately accounted for in G_{SV}).

Figure A-3 makes it clear why there is a pressure loop stability problem. As mentioned in Section 7.4, a limit cycle appeared at loop gains of about 600 sec^{-1}, with a frequency which abruptly changed from approximately 650 Hz to 350 Hz as gain was changed slightly. The computed curves of Figure A-3 show 180 degrees of phase lag at 500 Hz and a gain margin of 18 dB, thereby predicting instability at K_{VE} = 800 sec^{-1}. The experimental data suggest that instabilities could occur at either 400 Hz or 650 Hz at K_{VE} between 500 and 800 sec^{-1} (data from Channel 2 shows that the phase lag actually reaches 180 degrees at 400 Hz).

Since the trends indicated by Figure A-3 seemed well supported both analytically and experimentally, a cure for the problem was obvious: roll off the high-frequency amplitude with a low-pass filter. Accordingly, a first-order lag at 40 Hz was added to the feedback. Unfortunately, this change caused instability to occur at loop gains as low as 200 sec^{-1}. The only possible explanation for this behavior is that the pressure loop characteristics must be substantially different at very low amplitudes than those shown in Figure A-3. An attempt was made to repeat the data of Figure A-3 at drive signal amplitudes comparable to those observed during the 40 Hz limit cycles (i = 0.7 ma P-P). The oscilloscope patterns are terrible at this amplitude, but there is a tendency for the phase lag to steadily increase from 90 degrees near 25 Hz to 180 degrees near 100 Hz. This is a marked contrast to the higher amplitude data.

The most likely explanation for the low-emplitude characteristics is that the load pressures are insufficient to overcome actuator seal friction, and the piston is virtually locked in its bore. With X = 0, Figure A-1 indicates that the pressure-loop transfer function changes to:

$$G_{OL} = K_E \left(\frac{K_{DA} K_Q K_A}{A^2} \right) \left(\frac{1}{S} \right) = \left(\frac{K_A}{K_T} \right) \left(\frac{K_{VE}}{S} \right)$$

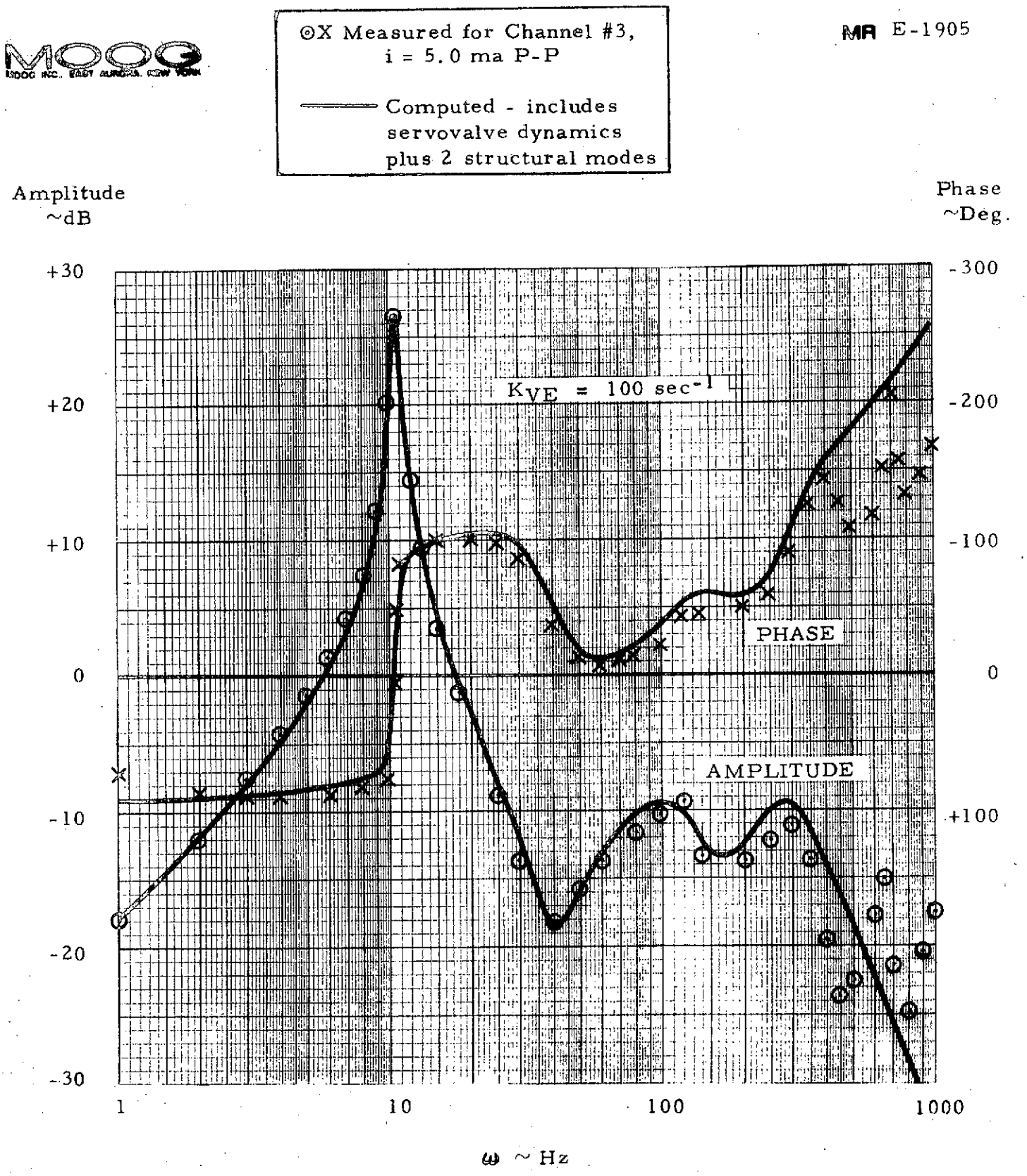

FIGURE A-3 - PRESSURE LOOP CHARACTERISTICS FOR A SINGLE ACTUATOR

A Bode plot of this transfer function, with servovalve dynamics added, is shown in Figure A-4 for K_{VE} = 100 sec^{-1}. Note that the plot only applies for frequencies appreciably above the load resonance, because frequencies near the load resonance cause the piston to break free, even at low drive amplitudes. The Bode plot of Figure A-3 is reproduced for comparison. The comparison shows that the piston-locked case has a larger gain margin than the piston-free case. This means that instability will first occur at the larger amplitudes. However, the 40 Hz lag which improves piston-free stability, substantially degrades piston-locked stability, as is shown in Figure A-5. This figure shows that piston-locked instability can occur for K_{VE} = 100 sec^{-1} at a frequency of 40 Hz. Considering the fact that the servovalve is operating near its null region, this represents reasonable correlation with the measured values of 200 sec^{-1} and 40 Hz.

The foregoing discussion makes it clear that the use of electronic compensation to achieve higher loop gain is of limited value. The dilemma is that lag compensation is needed to improve piston-free stability, while lead compensation is needed in the piston-locked case. The entire situation is complicated by the fact that the foregoing analysis applies to stability near zero crankshaft deflection. As the crankshaft is deflected to large angles, instability occurs at much lower loop gains (350 sec^{-1} or lower in some cases). This is probably due to the fact that the oil spring is greatly stiffened with the piston nearly bottomed, causing the piston-locked Bode amplitude to be increased.

In view of the complex stability situation at high frequencies, the only practical solution to the problem seemed to be the use of lag filtering at frequencies substantially below the load resonance, so that high static loop gains could be achieved with modest high-frequency gains. Using a first-order lag, the highest corner frequency, for which K_{VE} = 710 sec^{-1} could be comfortably obtained, was 1.0 Hz.

The use of low-frequency lag filtering in an equalization loop is very satisfactory, because the primary purpose of the loop is to equalize interchannel mismatch, which generally developes over a period of time. For other high-gain pressure loop applications, this type of filtering may not be satisfactory. In some cases, high-frequency compensation may help considerably. Thus, it would appear that both piston-free and piston-locked stability should be analyzed in any high-gain pressure loop application.

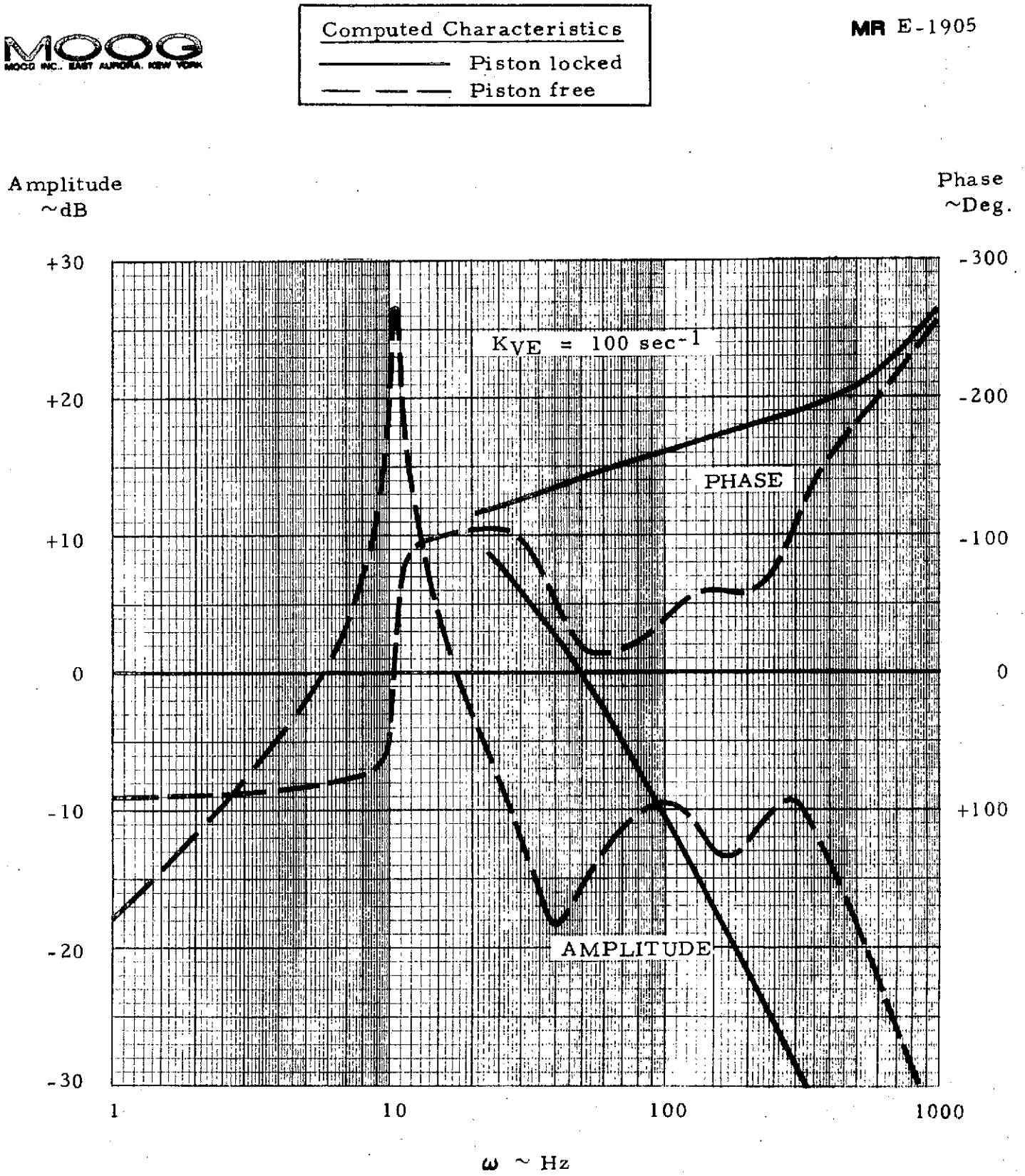

FIGURE A-4 - COMPARISON OF PRESSURE LOOP CHARACTERISTICS - PISTON LOCKED VERSUS FREE

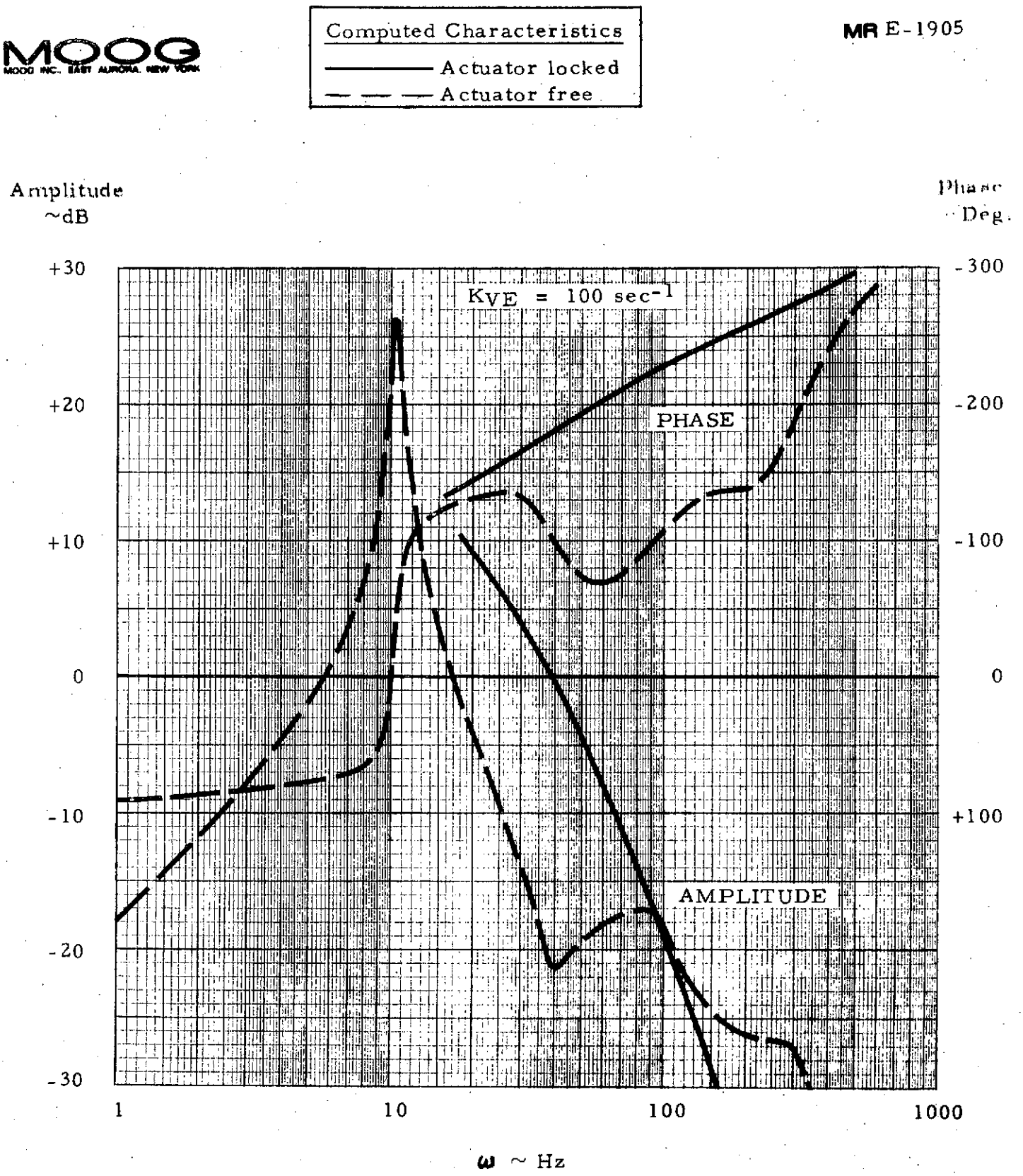

FIGURE A-5 - EFFECTS OF A FIRST ORDER LAG AT 40 HZ

APPENDIX B: OPERATING INSTRUCTIONS FOR THE SIMULATOR

The purpose of this appendix is to acquaint the reader with the basic operation of the simulator, as well as provide adjustment and calibration procedures.

B-1 Mechanical and Hydraulic Adjustments

There are two basic adjustments which can be made to the liquid springs. The sliding collars should be adjusted so that they are barely snug against the crankshaft fittings, and so that the pendulum hangs straight down. This should be done with all four actuators bypassed (or disconnected), and the spring charge pressures should be at least 100 psi to ensure that both rods are fully extended. The second adjustment is the charge pressure itself, which should be checked on a daily basis unless the room temperature is uniform 24 hours a day. The recommended charge pressure is 180 psi, which represents about 250 pounds of breakout force reflected to the actuator crank arm. This can be indirectly measured by observing the ΔP amplifier output required for a single actuator to break out the liquid spring (roughly 50 psi or 50 mv recommended). If the preload needs adjustment, it can be accomplished by applying a grease gun to the fitting at the base of each spring. The proper fluid is Dow-Corning 200 (1000 C.S.). Note that the spring rates can be cut in half by interconnecting the springs with a length of hydraulic hose, or an arbitrary reduction in rate can be accomplished by using accumulators.

The leaf springs also have two basic adjustments. The spring rate is adjusted by moving the actuator attach fitting in the slot (the proper bolt torque is 70 foot-pounds, after lubricating the threads and bearing surfaces with Molycote). The rate varies inversely as the cube of the spring length. The spring attach bolts can then be loosened to move the springs so that the actuator centerlines remain perpendicular to the springs (bolt torque is critical here; 300 foot-pounds after lubrication).

Both crankshaft bearings should be greased and adjusted periodically. One bearing is an expansion type, the other is not. Adjustment instructions are printed on each bearing. It is also important to keep Molycote on all bolts carrying bearing loads (both ends of actuators and liquid springs), so that fretting corrosion does not occur.

The cross-port relief valves should ideally be set so that they crack at 3200 psi and reseal at 2900 psi. In practice, however, this is rather difficult to achieve. The procedure is to give each servovalve a hard-over signal, then vary the supply pressure until the valves crack and reseal (repeat with servovalves hardover in opposite direction). Determination of when a valve is cracked is usually made by listening for valve chatter, but this is not dependable. Monitoring the ΔP amplifier output is helpful.

Physical dimensions and assembly details of the simulator fixture can be obtained from Moog Drawing T-18324 (12 sheets).

B-2 Electronic Functional Details

A brief functional description of the simulator electronics was given in Section 7.2, using the functional schematic of Figure 7.4. To provide a more complete description of the electronics, the schematics of Figures B-1 through B-4 were generated. Figures B-2 through B-4 show the circuits for each printed circuit card. Figure B-1 gives detailed interconnect wiring, including all connections to the various jacks, pots, switches, and lights on the front panel.

All operator controls and adjustments are on the front panel of the electronics rack, as shown in Figure 7.5. The top section of the panel covers the front of the card rack, and the holes are for screwdriver adjustment of trim pots mounted on the printed circuit cards. These pots are used for balancing the various operational amplifiers, setting the DPF gain, and setting the maximum servovalve current for each channel. Four calibrated pots for each channel are mounted in the section immediately below. These are for setting parameters which are more frequently changed, namely position loop gain, position null offset (for introduction of interchannel mismatch), equalization loop gain, and failure detection threshold. Adjustment procedures for all the pots are given in Section B-3.

Adjacent to the four calibrated pots are a mode selector switch and a failure indicator, the operation of which is explained in section 7.2. The banana jacks around the mode switch are simply connected to an uncommitted set of mode switch contacts. These can be patched so that an auxiliary function is switched when a channel is shut off or engaged, e.g. to trigger an oscilloscope.

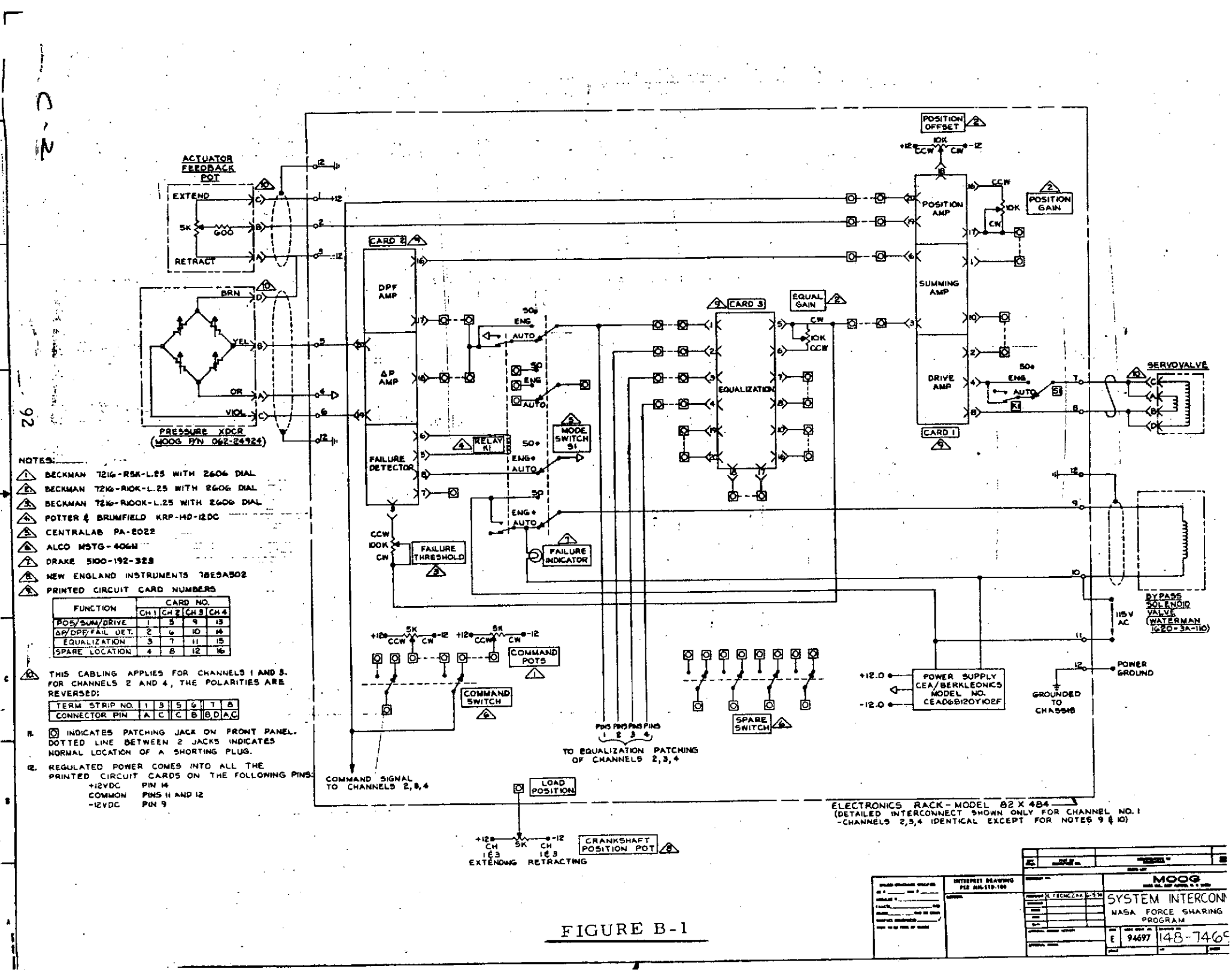

NOTES:

1. BECKMAN 7216-R5K-L.25 WITH 2606 DIAL
2. BECKMAN 7216-R10K-L.25 WITH 2606 DIAL
3. BECKMAN 7216-R100K-L.25 WITH 2606 DIAL
4. POTTER & BRUMFIELD KRP-11D-12DC
5. CENTRALAB PA-2022
6. ALCO MSTG-406N
7. DRAKE 5100-192-328
8. NEW ENGLAND INSTRUMENTS 18E3A502
9. PRINTED CIRCUIT CARD NUMBERS

FUNCTION	CARD NO.			
	CH 1	CH 2	CH 3	CH 4
POS/SUM/DRIVE	1	5	9	13
ΔP/DPF/FAIL DET.	2	6	10	14
EQUALIZATION	3	7	11	15
SPARE LOCATION	4	8	12	16

10. THIS CABLING APPLIES FOR CHANNELS 1 AND 3. FOR CHANNELS 2 AND 4, THE POLARITIES ARE REVERSED:

TERM STRIP NO.	1	3	5	6	7	8
CONNECTOR PIN	A	C	C	B	B,D	A,C

11. ⊙ INDICATES PATCHING JACK ON FRONT PANEL. DOTTED LINE BETWEEN 2 JACKS INDICATES NORMAL LOCATION OF A SHORTING PLUG.
12. REGULATED POWER COMES INTO ALL THE PRINTED CIRCUIT CARDS ON THE FOLLOWING PINS:
    +12VDC PIN 14
    COMMON PINS 11 AND 12
    -12VDC PIN 9

ELECTRONICS RACK - MODEL 82 X 484
(DETAILED INTERCONNECT SHOWN ONLY FOR CHANNEL NO. 1 -CHANNELS 2,3,4 IDENTICAL EXCEPT FOR NOTES 9 & 10)

FIGURE B-1

MOOG
SYSTEM INTERCONN
NASA FORCE SHARING PROGRAM
E 94697 148-746

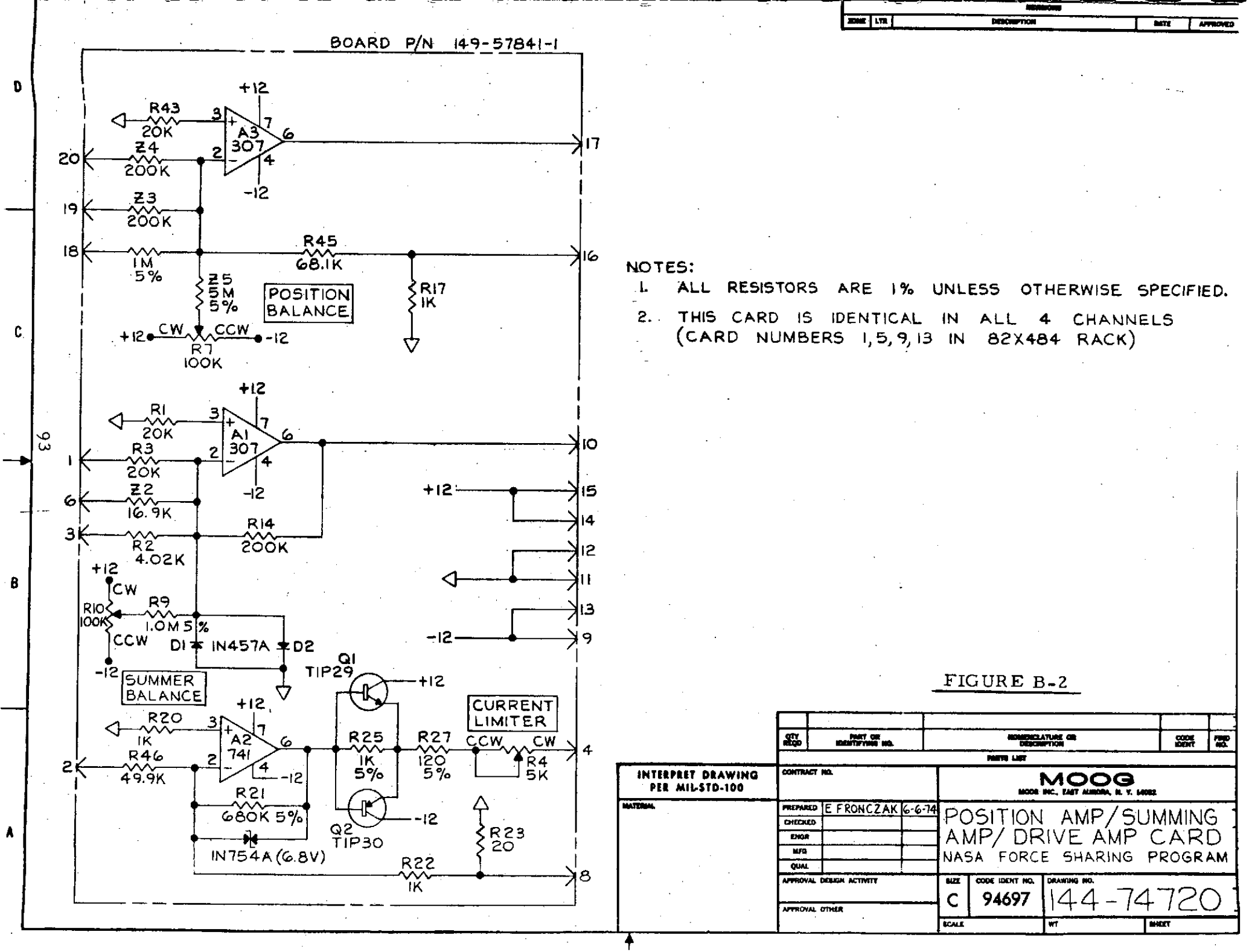

NOTES:

1. ALL RESISTORS ARE 1% UNLESS OTHERWISE SPECIFIED.
2. THIS CARD IS IDENTICAL IN ALL 4 CHANNELS (CARD NUMBERS 1, 5, 9, 13 IN 82X484 RACK)

FIGURE B-2

QTY REQD	PART OR IDENTIFYING NO.	NOMENCLATURE OR DESCRIPTION	CODE IDENT	FIND NO.

PARTS LIST

INTERPRET DRAWING PER MIL-STD-100

MATERIAL

CONTRACT NO.

MOOG
MOOG INC., EAST AURORA, N. Y. 14052

PREPARED	E FRONCZAK	6-6-74
CHECKED		
ENGR		
MFG		
QUAL		

APPROVAL DESIGN ACTIVITY

APPROVAL OTHER

POSITION AMP/SUMMING AMP/ DRIVE AMP CARD
NASA FORCE SHARING PROGRAM

SIZE	CODE IDENT NO.	DRAWING NO.
C	94697	144-74720

SCALE | WT | SHEET

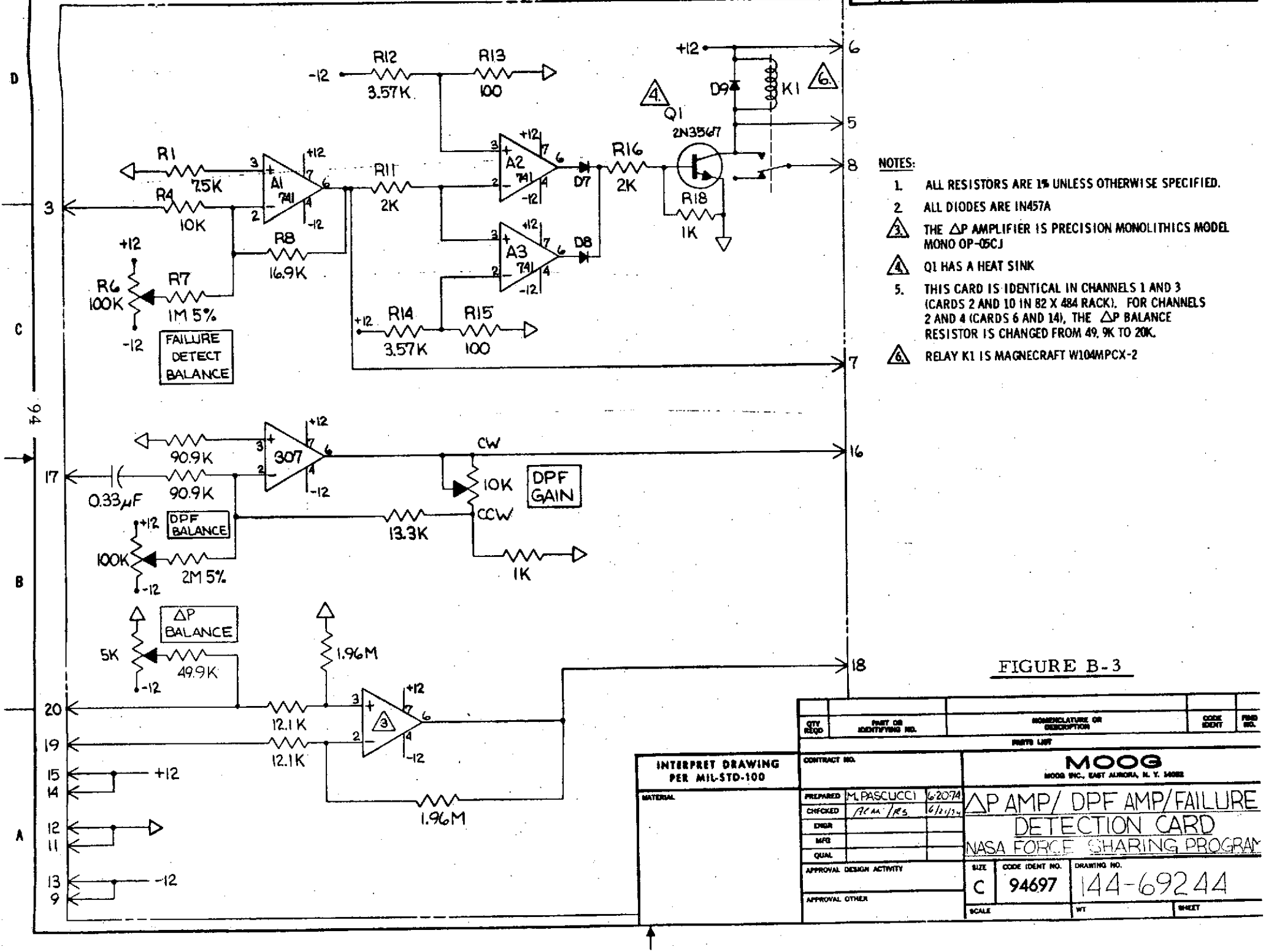

FIGURE B-3

QTY REQD	PART OR IDENTIFYING NO.	NOMENCLATURE OR DESCRIPTION	CODE IDENT	FSCM NO.

PARTS LIST

INTERPRET DRAWING PER MIL-STD-100

MATERIAL

CONTRACT NO.

MOOG
MOOG INC., EAST AURORA, N. Y. 14052

PREPARED	M. PASCUCCI	6-20-74
CHECKED	ACM / RS	6/21/74
ENGR		
M/E		
QUAL		

APPROVAL DESIGN ACTIVITY

APPROVAL OTHER

ΔP AMP/ DPF AMP/FAILURE DETECTION CARD
NASA FORCE SHARING PROGRAM

SIZE	CODE IDENT NO.	DRAWING NO.
C	94697	144-69244

SCALE | WT | SHEET

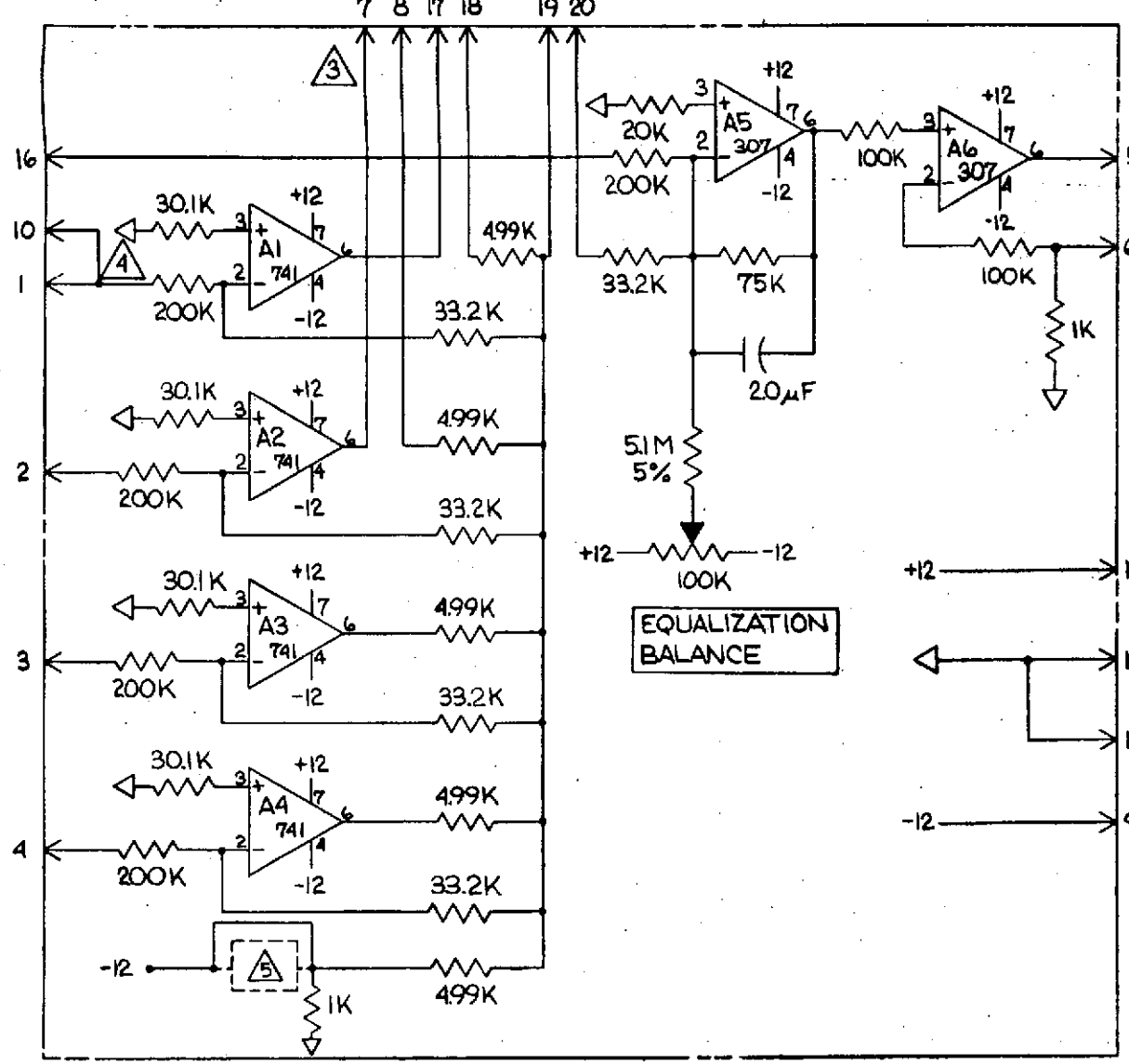

NOTES:

1. ALL RESISTORS ARE 1% UNLESS OTHERWISE SPECIFIED.
2. THIS IS THE SCHEMATIC FOR CHANNEL NO. 1 (CARD NO. 3 IN THE 82 X 484 ELECTRONICS RACK). CHANNELS 2, 3, 4 (CARDS 7, 11, 15) ARE IDENTICAL, EXCEPT FOR NOTES 3 AND 4.
3. PINS 7, 8, 17, 18 ARE CONNECTED AS SHOWN FOR CHANNELS 1 AND 2 (CARDS 3 AND 7). ON CHANNELS 3 AND 4 (CARDS 11 AND 15), PINS 7/8 TIE INTO A3 INSTEAD OF A1, AND PINS 17/18 TIE INTO A4 INSTEAD OF A2.
4. PIN 10 IS SHOWN JUMPERED TO PIN 1 FOR CHANNEL NO. 1 (CARD 3). FOR CHANNEL 2 (CARD 7), PIN 10 IS JUMPERED TO PIN 2, INSTEAD OF PIN 1. FOR CHANNEL 3, (CARD 11), PIN 10 IS JUMPERED TO PIN 3. FOR CHANNEL 4 (CARD 15), PIN 10 IS JUMPERED TO PIN 4.
5. A RESISTOR CAN BE PLACED HERE (AND THE JUMPER CUT) TO REDUCE THE REFERENCE VOLTAGE FROM 12 VOLTS.

FIGURE B-4

QTY REQD	PART OR IDENTIFYING NO.	NOMENCLATURE OR DESCRIPTION	CODE IDENT	REF NO.

PARTS LIST

INTERPRET DRAWING PER MIL-STD-100

MATERIAL

CONTRACT NO.

MOOG
MOOG INC., EAST AURORA, N. Y. 14052

PREPARED	M. PASCUCCI	6-20-74
CHECKED	ACM /RS	6/21/74
ENGR		
MFG		
QUAL		

APPROVAL DESIGN ACTIVITY

APPROVAL OTHER

EQUALIZATION CARD

NASA FORCE SHARING PROGRAM

SIZE	CODE IDENT NO.	DRAWING NO.
C	94697	144-69243

SCALE NONE WT SHEET

The patch panel for each channel should be relatively self-explanatory, with amplifier outputs generally blue and inputs generally green. Care should be taken to ensure that amplifier outputs are never patched to a stiff source, such as ± 12 volts or ground. All equalization interconnect jacks are orange, and the yellow jacks provide internal access to the mid-value logic (MVL). The jack labelled "FAIL DETECT BAL" can be monitored while the failure detection balance pot is adjusted. Exactly how each jack is connected into the electronics can be ascertained from Figure B-1. The jacks labelled "POS COM" on all four channels are tied together and connected to the wiper of the switch labelled "POSITION COMMAND". When the switch poles are patched to the two command pots with shorting plugs, a common position command signal can be sent to all four channels and rapidly switched between two values. An auxiliary set of switch contacts can be used to trigger an oscilloscope. By removing the command shorting plugs, a common external command signal can be introduced, e. g. from a function generator. Of course, the command pots can also be used to generate arbitrary reference voltages for other purposes.

The +12, common, and -12 jacks are directly connected to the regulated power supply. The jack labelled "LOAD POSITION" is directly connected to the wiper of the crankshaft position pot. At the extreme lower right of the front panel is a spare switch, which can be patched for functions such as abruptly switching from normal operation to a hardover failure condition at any point in the electronics.

B-3 Electronic Calibration Procedures

The most fundamental electronic adjustment is to set the various balance pots. Because many of the amplifiers to be balanced are in series, it is usually wise to adjust all the balance pots at one time, following an orderly procedure. The appropriate initial conditions are as follows.

(1) Turn on the hydraulic power supply and exercise the actuators to remove trapped air.

(2) Turn all mode switches to "SO", making sure that the crankshaft has stopped in the desired "zero" position. If the liquid springs are connected, they will probably drive the crankshaft to a repeatable "zero" position when all actuators are bypassed. The crankshaft pot can then be mechanically nulled.

MOOG
MOOG INC. EAST AURORA, NEW YORK

(3) Disconnect the position command pots and ground the position command input.

(4) The primary patch panel for each channel should have shorting plugs in their normal locations, except the three plugs which supply the inputs to the summing amplifier. These three inputs should be grounded.

(5) The DPF gains, position gains, equalization gains, current limits, and failure thresholds should all be set at their maximum values (fully clockwise), or at the settings to actually be used during the simulation.

(6) The position offset pots should all be set at 500 (mid range).

Now the following balance adjustments can be made.

(1) Position Balance: outputs of all position amplifiers set to zero.

(2) ΔP Balance: outputs of all ΔP amplifiers set to + 3.24 volts.

(3) DPF Balance: outputs of all DPF amplifiers set to zero.

(4) Equalization Balance: outputs of all equalization logic modules set to zero.

(5) Failure Detect Balance: "FAIL DETECT BAL" outputs all set to zero.

(6) Summing Amplifier Balance: all servovalve drive currents set to zero. Zero servovalve current is achieved when the voltages on pin 8 of the drive amplifier cards are zero (cards 1, 5, 9, 13).

Calibration data for the various transducers were obtained and the following relationships developed.

- Crankshaft pot output: 0.07 v/deg, positive for positive crankshaft deflection, zero adjusted mechanically.
- Actuator pot output: 2.15 v/in, positive for positive crankshaft deflection, zero adjusted with position amplifier balance.
- ΔP amplifier output: $e = .00108 (\Delta P + 3000)$, zero set by adjusting ΔP amplifier balance for $e = + 3.24$ v at $\Delta P = 0$.

MOOG
MOOG INC., EAST AURORA, NEW YORK

In addition, the velocity gain of each actuator was measured by disconnecting the actuators from the crankshaft and removing the shorting plug between the summing amplifier and drive amplifier. Step voltages of ±2.0 volts were then put into the drive amplifier, and the output of the actuator feedback pot was recorded on an X-Y plotter(this input represents about 1.7 ma of valve current, out of a maximum limit of 3.0 ma). The average combined velocity gain of the actuator and drive amplifier was measured to be 0.90 in/sec per volt.

The various loop gains were set by using the above measurements and K_T = 34,900 lb/in (based on K_A = 193,000 and K_S measured to be 42,600). The appropriate amplifier gains can then be computed from the following equations. Note that the summing amplifier gain is different for each loop (10.0 for position, 11.8 for DPF, and 49.8 for equalization).

$$K_{VX} = K_{POT}\, K_{POS}\, K_{SUM} (K_{DRIVE}\, K_Q / A) = 19.3\, K_{POS}$$

$$K_{VD} = K_{\Delta P}\, K_{DPF}\, K_{SUM} (K_{DRIVE}\, K_Q / A) (K_T / A) = 80\, K_{DPF}$$

$$K_{VE} = K_{\Delta P}\, K_{EQ}\, K_{SUM} (K_{DRIVE}\, K_Q / A) (K_T / A) = 340\, K_{EQ}$$

For the position loop gain of 40 sec^{-1} used in the simulation, the required position amplifier gain was 2.09 v/v (gain pot setting of 515 required-scale is 000 to 1000). For the DPF gain of 72 sec^{-1} used, the DPF amplifier gain was 0.90 v/v (note that this is the high frequency gain - the 0.33μF DPF capacitor must be shorted when setting the gain). The equalization amplifier gain was 2.08 v/v to obtain an equalization loop gain of 710 sec^{-1} (gain pot setting of 450 required).

The failure threshold can be set by removing the shorting plugs on the yellow jacks labelled "A5 P_n INPUT" and "A5 MV INPUT". If the right-hand "A5 MV INPUT" jack is grounded in each channel and the appropriate voltage is applied to the right-hand "A5 P_n INPUT" jack, the threshold pot can be adjusted until the failure indicator just barely lights. The appropriate input voltage is 1.08 volts to achieve a threshold of (ΔP_n - ΔP_{mid}) = 1000psi. For the present simulation, the threshold pots were set at 475 to achieve a threshold of ± 500 psi (with the equalization gain pots set at 450).

The easiest way to obtain a given position null offset in a channel is to input a command voltage of the desired magnitude but opposite sign, and adjust the position offset pot until the output of the position amplifier is zero (transducer input voltage grounded). Full actuator stroke (7.66 inches) requires a command signal change of 16.5 volts.

Changes to the DPF time constant must be made by changing amplifier components. The time constant can be changed by replacing the capacitor, without affecting loop gains. If the resistors are changed instead, the ratio of feedback resistance to input resistance should be preserved if loop gain is not to be affected.

The current limit pots can be set by putting ± 12 volts into the drive amplifiers (after removing the shorting plugs, of course), and measuring the voltage on pin 8 of the drive amplifier cards. The conversion factor is 20 millivolts for 1.0 milliamp.